

V393
.R46

AD 291 418 #1

ARIES



DEPARTMENT OF THE NAVY
DAVID TAYLOR MODEL BASIN

HYDROMECHANICS

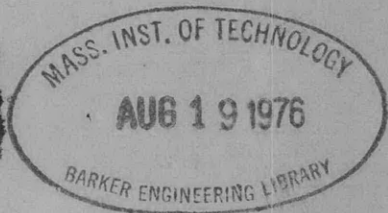
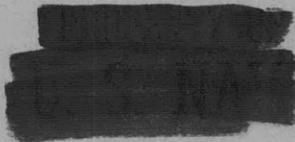
ELASTIC LOBAR BUCKLING OF RING-
SUPPORTED CYLINDRICAL SHELLS
UNDER HYDROSTATIC PRESSURE

by

AERODYNAMICS

Thomas E. Reynolds

STRUCTURAL
MECHANICS

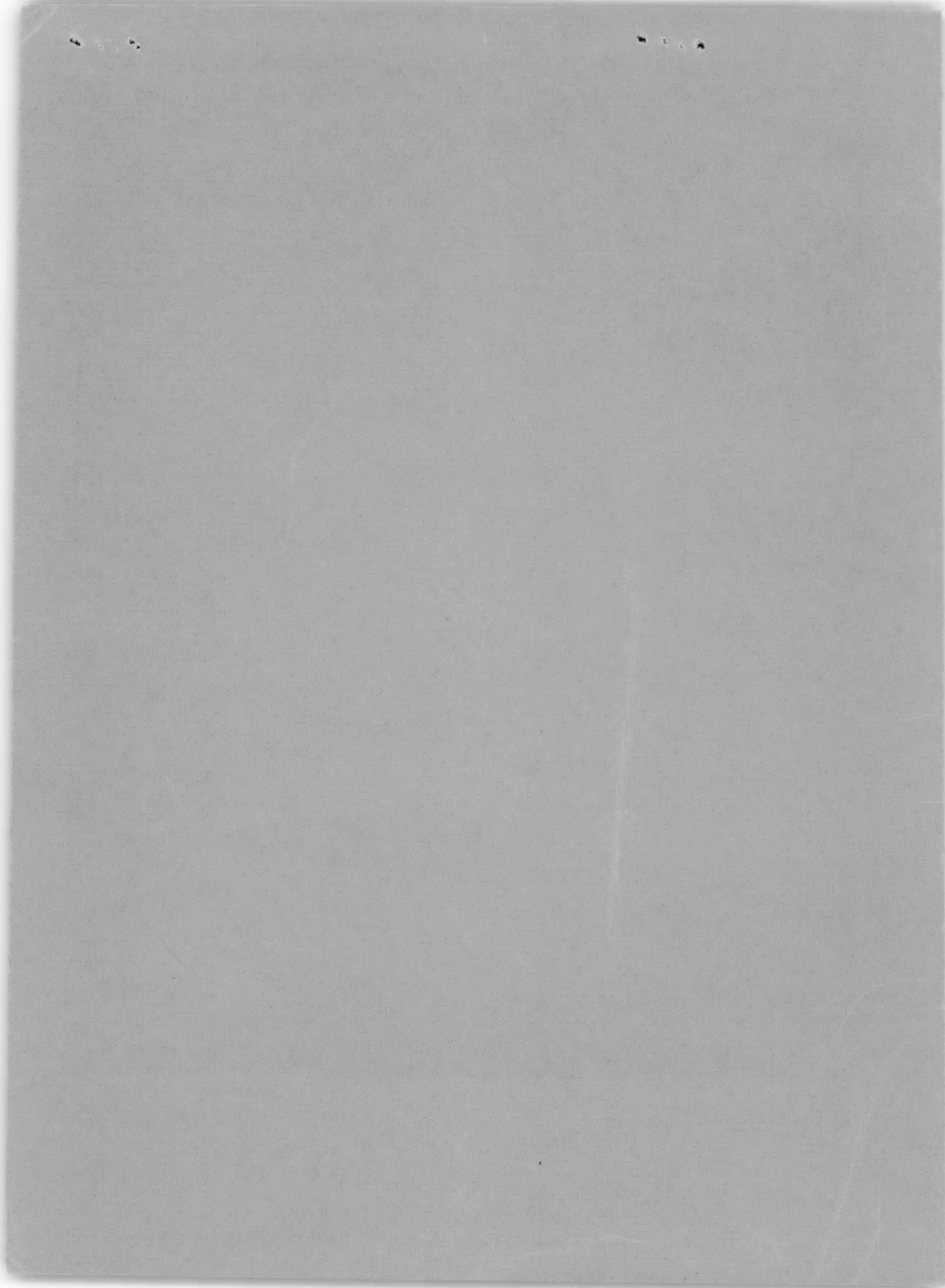


APPLIED
MATHEMATICS

STRUCTURAL MECHANICS LABORATORY
RESEARCH AND DEVELOPMENT REPORT

September 1962

Report 1614



DEPARTMENT OF THE NAVY
DAVID TAYLOR MODEL BASIN
WASHINGTON 7, D. C.

IN REPLY REFER TO

9110/Subs
5605
(733:TER:1kg)
Ser 7-409
28 November 1962

From: Commanding Officer and Director, David Taylor Model Basin
To: Chief, Bureau of Ships (442) (in duplicate)

Subj: Elastic shell buckling of ring-stiffened cylinders;
forwarding of report on

Encl: (1) DTMB Report 1614 entitled, "Elastic Lobar Buckling of
Ring-Supported Cylindrical Shells under Hydrostatic
Pressure" (2 copies)

1. One of the problems relating to the strength of stiffened cylindrical shells under hydrostatic pressure is the local elastic buckling of the shell between stiffeners. Although this problem has received considerable study, the results of analytical and experimental work for shells with closely-spaced stiffeners have not been entirely satisfactory. Theoretical studies have failed to account adequately for the influence of the stiffeners on buckling strength, while elastic buckling failures have seldom been observed experimentally because of fabrication imperfections and inadequate yield strengths of the material used in structural models. As part of a program at the David Taylor Model Basin to investigate the fundamental behavior of shell structures, efforts have been directed toward eliminating these deficiencies. Enclosure (1) presents the results of recent theoretical and experimental studies.

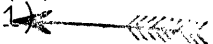
2. In enclosure (1) a small-deflection analysis is developed for elastic interframe buckling which takes into account the influence of the frames on deflections before and during buckling. Tests of a machined, ring-stiffened cylinder are described in which collapse by elastic buckling was observed. The buckling pressures for this and three other cylinders, previously reported are in good agreement with the new solution, but exceed those given by the solution of Von Mises.

E. E. Johnson
E. E. JOHNSON
By direction



9110/Subs
5605
(733:TER:1kg)
Ser 7-409
28 November 1962

Copy to:

BUSHIPS (320) with 1 copy of encl (1)
(335) with 3 copies of encl (1)
(341A) with 1 copy of encl (1)
(420) with 1 copy of encl (1)
(421) with 1 copy of encl (1)
(423) with 1 copy of encl (1)
(440) with 1 copy of encl (1)
(443) with 1 copy of encl (1)
(525) with 2 copies of encl (1)
(633) with 1 copy of encl (1)
(651F) with 1 copy of encl (1)
CHONR (439) with 1 copy of encl (1)
(466) with 1 copy of encl (1)
CNO (Op 07T) with 1 copy of encl (1)
(Op 311) with 1 copy of encl (1)
(Op 713) with 1 copy of encl (1)
(Op 725) with 1 copy of encl (1)
CDR, ASTIA, with 10 copies of encl (1)
CO and DIR, USNEES, with 1 copy of encl (1)
CDR, USNRL (2027), with 1 copy of encl (1)
CO and DIR, USNUSL, with 1 copy of encl (1)
CO and DIR, USNEL, with 1 copy of encl (1)
CDR, USNOTS, China Lake, with 1 copy of encl (1)
CO, USNUOS, with 1 copy of encl (1)
NAVSHIPYD PTSMH, with 2 copies of encl (1)
NAVSHIPYD MARE, with 2 copies of encl (1)
NAVSHIPYD CHASN, with 1 copy of encl (1)
SUPSHIP, Groton, with 1 copy of encl (1)
EB Div, Gen Dyn Corp, with 1 copy of encl (1)
SUPSHIP, Newport News, with 1 copy of encl (1)
NNSB and DD Co, with 1 copy of encl (1)
SUPSHIP, Pascagoula, with 1 copy of encl (1)
Ingalls Shipbldg Corp, with 1 copy of encl (1)
SUPSHIP, Camden, with 1 copy of encl (1)
NY Shipbldg Corp, with 1 copy of encl (1)
SUPSHIP, Quincy, with 1 copy of encl (1)
DIR, DEF R and E, Attn: Tech Lib, with 1 copy of encl (1)
CO, USNROTC and NAVADMINU, MIT, with 1 copy of encl (1) 
O in C, PGSCOL, Webb, with 1 copy of encl (1)
DIR, APL, Univ of Washington, Seattle, with 1 copy of encl (1)
NAS, Attn: Comm on Undersea Warfare, with 1 copy of encl (1)



9110/Subs
5605
(733:TER:1kg)
Ser 7-409
28 November 1962

Copy to:

Prof J. Kempner, Plytech Inst of Bklyn, with 1 copy of encl (1)
Prof G. Gerard, N.Y. Univ, with 1 copy of encl (1)
Dr. E. Wenk, Jr, Technical Assistant, The White House, (with 1
copy of encl (1))
Dr. R. DeHart, SRI, with 1 copy of encl (1)
Mr. L.P. Zick, Chic Bridge and Iron Co, Chicago, with 1 copy
of encl (1)
Dean V.L. Salerno, Fairleigh Dickinson Univ, with 1 copy of
encl (1)
Prof E.O. Waters, Yale Univ, with 1 copy of encl (1)
Mr. C.F. Larson, Sec'y, Welding Research Council, with 1 copy
of encl (1)
Mr. A.F. Kirstein, NBS, with 1 copy of encl (1)
Dr. W.A. Nash, Univ of Florida, with 1 copy of encl (1)
Prof H.L. Langhaar, Univ of Illinois, with 1 copy of encl (1)
Prof P.P. Bijlaard, Cornell University, with 1 copy of encl (1)
Dr. R.G. Sturm, 1245 Scott Ave., Chicago Heights, Ill, with
1 copy of encl (1), with 1 copy of encl (1)
Dr. J. Walsh, WHOI, with 1 copy of encl (1)



ELASTIC LOBAR BUCKLING OF RING-
SUPPORTED CYLINDRICAL SHELLS
UNDER HYDROSTATIC PRESSURE

by

Thomas E. Reynolds

September 1962

Report 1614
S-F013 0302

TABLE OF CONTENTS

	Page
ABSTRACT	1
INTRODUCTION	1
BACKGROUND	2
PART I - THEORY	6
GENERAL ANALYSIS	6
RINGS OF FINITE RIGIDITY	15
SIMPLE SUPPORT CONDITIONS	31
RINGS OF INFINITE RIGIDITY (CLAMPED SUPPORT CONDITIONS)	37
NUMERICAL EXAMPLE	46
Rings of Finite Rigidity	46
Simple Support Conditions	48
Rings of Infinite Rigidity	49
SUMMARY AND CONCLUSIONS	53
PART II - EXPERIMENT	55
EARLIER TESTS	55
DESCRIPTION OF TEST CYLINDER	55
PRELIMINARY TEST	56
FINAL TEST	58
Instrumentation and Test Procedure	58
Results and Discussion	60
COMPARISON WITH PREVIOUS TESTS	67
SUMMARY AND CONCLUSIONS	68
PART III - EVALUATION OF BUCKLING THEORY	69
COMPARISON OF THEORY WITH EXPERIMENT	69
CONCLUSIONS	74
ACKNOWLEDGMENTS	75

TABLE OF CONTENTS (continued)

	Page
APPENDIX A - STRAIN ENERGY OF THE SHELL	77
APPENDIX B - STRAIN ENERGY OF RINGS	83
APPENDIX C - POTENTIAL OF THE EXTERNAL LOADS	87
APPENDIX D - INFINITE SERIES FORMULATION OF THE INITIAL DEFLECTIONS	89
APPENDIX E - STRESS FUNCTION	97
APPENDIX F - DETERMINATION OF THE MODULUS OF ELASTICITY FOR CYLINDER BR-4B	99
REFERENCES	101

LIST OF FIGURES

Figure 1 - Shell Instability	2
Figure 2 - General Instability	3
Figure 3 - Stiffened Cylinder and Coordinate System	7
Figure 4 - Asymmetric Shell Buckling Mode	7
Figure 5 - Buckling Configurations for Three Degrees of Fixity ...	15
Figure 6 - Even Mode Buckling	27
Figure 7 - ϕ_1 as a Function of β for Simple Support ($\nu = 0.3$)	34
Figure 8 - n as a Function of β for Simple Support ($\nu = 0.3$)	34
Figure 9 - Buckling Pressure as a Function of β for Simple Support ($\nu = 0.3$)	35
Figure 10 - Variation in Approximate and Matrix Solutions with J for Cylinder BR-4B	48

LIST OF FIGURES (continued)

	Page
Figure 11 - Test Cylinder BR-4B	56
Figure 12 - Gage Locations for Final Test	59
Figure 13 - Views of Collapsed Cylinder BR-4B	61
Figure 14 - Typical Plots of Circumferential Strains at Midbay versus Pressure (Final Test)	62
Figure 15 - Circumferential Strain Patterns (Run 2, Final Test) ..	63
Figure 16 - Typical Southwell Plots for Exterior Circumferential Strains at Midbay (Run 2, Final Test)	64
Figure 17 - Distribution of Nonlinear Circumferential Strain for Bay 3 at 630 psi along 90-deg Generator	66
Figure 18 - Theoretical and Experimental Distribution of Linear Strain for Bay 3 (Run 2, Final Test)	66
Figure 19 - Experimental and Theoretical Results	73
Figure 20 - Deflected Element of Shell	87
Figure 21 - Determination of Young's Modulus for BR-4B (Response of Ring to Diametral Loading)	100

LIST OF TABLES

	Page
Table 1 - Coefficients of the Initial Deflections for Cylinder BR-4B	47
Table 2 - Comparison of Approximate and Matrix Solutions for Cylinder BR-4B with Finite Rings	47
Table 3 - Relative Amplitudes of Buckling Modes for Cylinder BR-4B with Finite Rings	49
Table 4 - Buckling Pressures for Cylinder BR-4B with Simple Supports	49
Table 5 - Buckling Pressures for Cylinder BR-4B with Infinitely Rigid Rings	50
Table 6 - Comparison of Buckling Configurations for Cylinder BR-4B with Infinitely Rigid Rings	54
Table 7 - Circumferential Strain Sensitivities (Exterior) at Midbay, Preliminary Test	58
Table 8 - Loading Schedule for Final Test	60
Table 9 - Southwell Results from Circumferential Strains at Midbay (Run 2, Final Test)	64
Table 10 - Maximum Stresses Measured during Final Run (Bay 4 at 110 deg, 630 psi)	65
Table 11 - Experimental Results Compared with Previous Tests ...	68
Table 12 - Properties of Steel Test Cylinders	71
Table 13 - Comparison of Theory and Experiment	72

NOTATION

A_f	Area of frame cross section
a_m	$\left[1 + 4 \left(\frac{m\pi}{\beta} \right)^4 + 2 \frac{pR}{Eh} \lambda_m^2 \right]^{-1} = \frac{1}{\left[1 + 4 \left(\frac{m\pi}{\beta} \right)^4 \right] \left(1 - \frac{p}{p_m} \right)}$
b	Frame width
d	Frame depth
E	Young's modulus
e	Distance between median surface of shell and centroid of frame
$e_x, e_\theta, e_{x\theta}$	Axial, circumferential, and shear strains
$F(x, \theta)$	Stress function
h	Shell thickness
I_{xG}, I_{zG}	Moments of inertia of frame about x- and z-axes, respectively, through frame centroid
i, j, J, k, m	Integers referring to number of axial waves
K	Frame torsion constant
L	Inner (unsupported) frame spacing
L_f	Center-to-center frame spacing
n	Integer, number of circumferential waves
p	Pressure, positive when internal
R	Mean radius of shell
r	Radius to any point in cylinder

u, v, w	Axial, tangential, and radial buckling displacements
\bar{u}, \bar{w}	Axisymmetric prebuckling displacements
x, θ, z	Axial coordinate, central angle, thickness coordinate
β	$L_f \sqrt{\frac{3(1-\nu^2)}{R^2 h^2}}$
ϵ^*	Nonlinear component of measured strain
$\epsilon_{xx}, \epsilon_{\theta\theta}, \epsilon_{x\theta}$	Axial, circumferential, and shear strain components
η	$\left[\frac{L_f h}{A_f} \left(1 + \frac{e}{R} \right) + \sum_{m=-\infty}^{\infty} a_m \right]^{-1}$
λ_j	$\frac{j\pi R}{L_f}$
ν	Poisson's ratio
$\sigma_x, \sigma_\theta, \sigma_{x\theta}$	Axial, circumferential, and shear stresses
ϕ_m	$\frac{\lambda_m^2}{n^2 + \lambda_m^2}$
ψ	pR/Eh
∇_l^4	Operator, $\frac{\partial^4}{\partial x^4} + \frac{2\partial^4}{R^2 \partial \theta^2 \partial x^2} + \frac{\partial^4}{R^4 \partial \theta^4}$
$u_x, u_\theta,$ $M_x \dots$ etc.	Subscripts x and θ on $u, v, w, \bar{u}, \bar{w}, M$ and N indicate differentiation with respect to x and θ

ABSTRACT

A small-deflection analysis is developed for the elastic interbay buckling of ring-stiffened cylindrical shells in which the influence of the rings on deformations before and during buckling is considered.

Tests were carried out with a machined, ring-stiffened cylinder (BR-4B) subjected to external hydrostatic pressure. Collapse was initiated by elastic asymmetric buckling of the shell. Strain measurements taken during the test demonstrated that the Southwell method of determining buckling strength nondestructively is applicable in the case of interbay buckling.

The results of this and three other tests of machined cylinders are in good agreement with the theory. While the Von Mises theory is inaccurate for closely spaced rings, its continued application for estimating elastic buckling strength is probably justified since it is always conservative and can be represented in a simple form.

INTRODUCTION

One problem in the field of pressure-vessel design that has been of particular interest for many years is the elastic instability of thin cylindrical shells under hydrostatic pressure. In practice, it is the buckling which occurs between closely spaced ring stiffeners as shown in Figure 1. Despite the considerable study which this problem has received, some additional investigation appeared needed in at least two areas. One of these concerned experimental work with short shells since a thorough evaluation of theory was still lacking. The other involved the analytical study of the influence of the rings on the buckling strength. Several investigators have considered this effect, but in each case it seemed that the treatment has been either approximate or incomplete.

As part of a continuing program at the Model Basin to study the phenomenon of shell instability, effort has been directed toward eliminating some of these deficiencies. The present report, which gives the results of this effort, is divided into three sections.

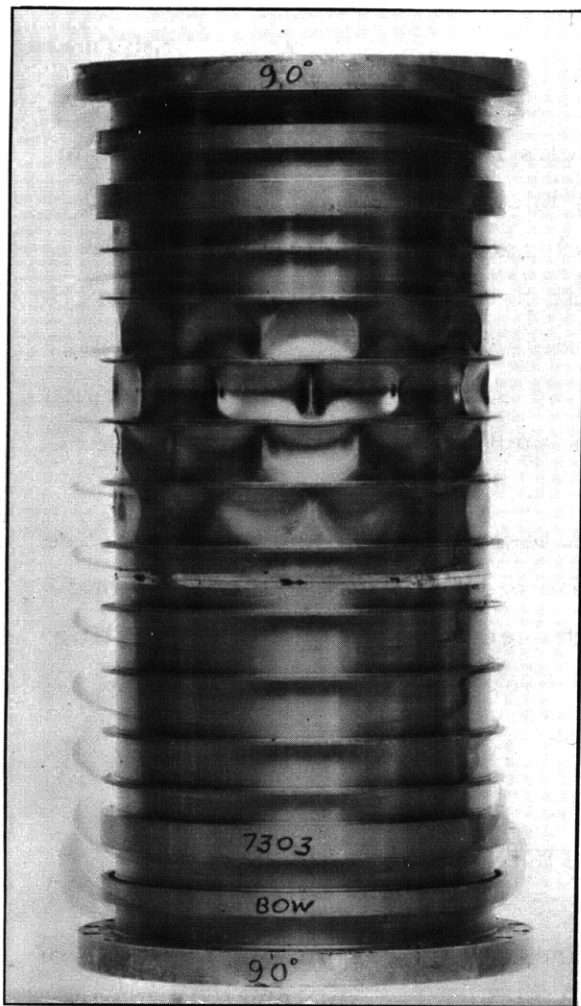


Figure 1 - Shell Instability

The first deals with the development of a small deflection analysis which accounts for the restraint provided by the rings. This is done by expressing the deflection both before and during buckling in trigonometric series form and obtaining a solution through the use of energy methods. The special cases of simple and clamped support are also treated. In addition, the significance of including the energy associated with bending stresses developed prior to buckling is examined. Much of the work is based on relations derived in appendixes.

The second section describes tests of a machined cylinder designated Model BR-4B. This includes a discussion of strain data, buckling strength, and mode of collapse. The applicability of the Southwell method for determining shell buckling strength is also examined.

In the third section, the present analysis and others are evaluated on the basis of the test results of Model BR-4B and of recent tests of three other machined cylinders.

BACKGROUND

In view of all the effort that has been devoted to the study of the elastic instability of cylindrical shells, it is rather curious that there has yet to be a thorough confirmation of theory by experiment, at least where closely spaced stiffeners are concerned. Surprisingly enough, this has

not been the case with the problem of general instability wherein both rings and shell undergo extensive deformations (Figure 2). It is due largely to the theoretical work of Kendrick^{1, 2, 3} among others, and a rather extensive experimental program conducted at the Model Basin^{4, 5, 6} that the elastic general instability problem has for all practical purposes been solved. This progress is even more striking when it is realized that no rigorous analytical solution was undertaken prior to the work of Salerno and Levine⁷ in 1951.

What then, accounts for the slower progress on a problem which would appear the simpler of the two and which has been studied over a much longer period? Basically it is the disparity which has persisted in varying degree between the physical conditions prevailing in the experiments and those which have received theoretical consideration.

First, let it be said that theoretical development has lacked neither variety nor distinction. The case of a simply supported shell of finite length under radial pressure was first treated by Southwell in 1913.⁸ The next year Von Mises presented a more exact analysis,⁹ which he extended in 1929 to include end pressure.¹⁰ In that same year, Tokugawa¹¹ published almost identical results to those of Von Mises. While rightly regarded as classics today, these analyses are not completely rigorous

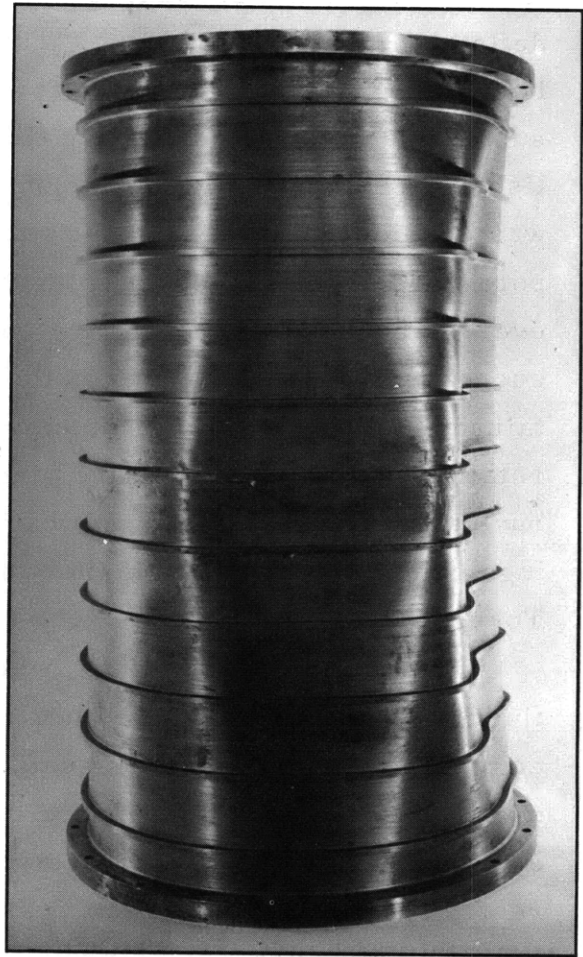


Figure 2 - General Instability

¹References are listed on page 101.

in that they do not account for the influence of the boundary conditions on deflections prior to buckling. This influence is unimportant for relatively long shells, but it may not be for short shells such as are embodied in submarine hulls. Recognizing this, Von Sanden and Tölke¹² in 1932 published a comprehensive paper on the buckling of shells wherein the effect was considered. Their results included not only the case of simple support but that for finite stiffening rings as well. In this latter case, however, they assumed that during buckling, the rings merely provide simple support. Using a different mathematical approach, Kendrick² also obtained a solution to this problem. While neither analysis included the rotational restraint which the rings presumably would provide during buckling, the results showed that buckling pressures for short ring spacings can be significantly higher than those given by either Von Mises or Tokugawa.

Salerno and Levine^{13, 14} were apparently the first to include the influence of stiffeners on the buckling deformations. Unfortunately, in computing the buckling pressure, they neglected the prebuckling deformations altogether. Because of this shortcoming and because of certain errors in their energy expressions, the analysis is not considered correct. Others, notably Sturm¹⁵ and Nash,¹⁶ investigated the consequences of having stiffeners which provide full fixity. The resulting buckling pressures were much higher for closely spaced stiffeners than for the case of simple support, even though the effect of the boundary conditions on the prebuckling deformations was neglected.

Still others have studied the possibility of "snap-through" buckling at pressures much lower than the small deflection analyses just mentioned might predict. Notable contributions to this development of large deflection theory include the work of Donnell,^{17, 18} Langhaar and Boresi,¹⁹ and Kempner and Crouzet-Pascal.²⁰ These studies have shown generally that the phenomenon of "snap-through" in cylindrical shells under hydrostatic pressure is possible and that the associated buckling pressure is somewhat influenced by geometrical imperfections. Experimental studies by Kirstein and Wenk²¹ have borne out these conclusions. So far, however, it has been difficult to assess quantitatively the imperfections present in test structures. It has also been recognized that such imperfections can

have an important influence on the stresses existing in the shell prior to buckling. Sturm,¹⁵ Bodner and Berks,²² and Galletly and Bart,²³ for example, have shown that as a result of irregularities in circularity, the stresses can be so greatly increased that inelastic collapse can occur at a pressure well below that which elastic buckling theory would predict.

Inelastic buckling, which is frequently the mode of collapse for efficiently designed shells, has also received some attention in recent years. For example, the work of Gerard,^{24,25} Lunchick,²⁶ Nott,²⁷ and Reynolds²⁸ have shown that inelastic buckling strength can often be predicted with reasonable accuracy even though the complexity of the problem virtually precludes a rigorous analysis. These investigators, it should be noted, have had the benefit of much more experimental data than has been available for the study of elastic buckling.

It is because of this lack of data that a thorough evaluation of elastic buckling theory has not been possible. Most of the elastic data from Windenburg's studies,²⁹ for example, have been in the long-shell range, whereas data for short shells, i. e., those with closely spaced stiffeners, are extremely limited. This results from the fact that the source of much of the available data for short shells has been proof tests of pressure vessels designed for structural efficiency rather than for the study of elastic buckling. Such structures are so designed that collapse rarely occurs before stresses have exceeded the elastic limit of the material. Consequently, tests of this nature seldom provide pertinent data for the evaluation of elastic buckling theory, although they have sometimes been used for that purpose. On the other hand, some cylinders specifically designed to buckle elastically have apparently suffered premature failure by reason of geometric imperfections, residual fabrication stresses, and other uncontrollable factors. Tests of Models BR-1³⁰ and BR-5³¹ conducted at the Model Basin are examples in which this problem was encountered. However, even if all these experimental difficulties had not existed, the various theories then available still have not considered realistically the actual conditions existing at the shell boundaries.

Nearly all the available data have come from tests of ring-stiffened cylinders, yet most analytical solutions are based on arbitrary assumptions regarding the boundary conditions which the stiffeners impose on

the shell. One remedy would be to attempt to duplicate in the laboratory a set of idealized conditions as assumed for the theory. However, the best one could do with such a procedure would be to establish the applicability of a certain formula in the special case, for instance, of simple support. The question of what formula is reliable for the case actually encountered in practice would still be unanswered.

The recent successes in the studies of general instability using machined cylinders of high-strength steel^{4,5,6} strongly indicate that the problems associated with imperfections, insufficient yield strength, etc., could be overcome and that elastic instability in short, ring-stiffened shells would be experimentally possible. It seemed reasonable, therefore, to undertake an experimental study using a machined, ring-stiffened cylinder designed to collapse by elastic instability. At the same time, it appeared worthwhile to explore the possibilities of an analytical approach whereby the boundary conditions imposed by the rings could be treated more realistically.

PART I - THEORY

GENERAL ANALYSIS

The structure under consideration is a circular cylindrical shell of infinite length reinforced by regularly spaced uniform ring frames, as shown in Figure 3. The shell is assumed to be isotropic, and its thickness is small compared to its radius so that the problem is restricted to two dimensions.

There is ample experimental evidence (e. g., Figure 1) that under hydrostatic pressure, asymmetric (lobar) buckling occurs in the mode shown schematically in Figure 4. Such a pattern, it will be seen, repeats itself at every other frame. Consequently, in computing the total potential of the cylinder in its buckled state, it is convenient to carry out the calculation over any two adjacent frame spaces.

The total potential U_T of the system is defined by

$$U_T = U_s + U_f - W \quad [1]$$

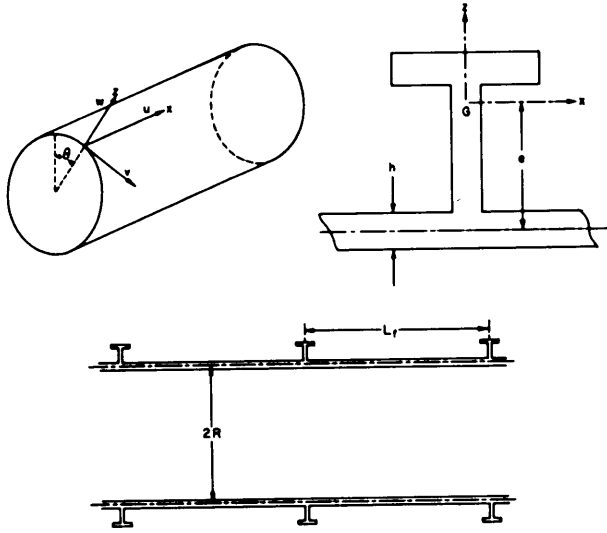


Figure 3 - Stiffened Cylinder and Coordinate System

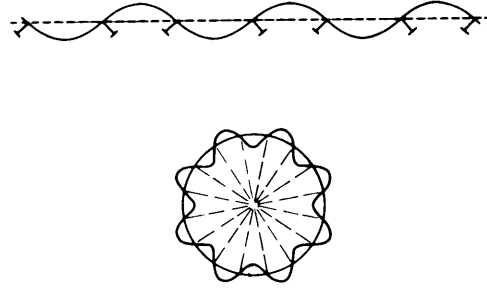


Figure 4 - Asymmetric Shell Buckling Mode

where U_s is the strain energy of the shell,

U_f is the strain energy of the frames, and

W is the work done by the external pressure.

Referring to Appendixes A, B, and C, where these three quantities are derived, we have for the total potential

$$\begin{aligned}
 U_T = \frac{EhR}{2(1-\nu^2)} \int_0^{2L_f} \int_0^{2\pi} \left\{ u_x^2 + u_x (v_x^2 + w_x^2) + M^2 + M \left(\frac{u_\theta^2}{R^2} + N^2 \right) + 2\nu \left[u_x M \right. \right. \\
 \left. \left. + \frac{u_x}{2} \left(\frac{u_\theta^2}{R^2} + N^2 \right) + \frac{M}{2} (v_x^2 + w_x^2) \right] + \left(\frac{1-\nu}{2} \right) \left[\left(v_x + \frac{u_\theta}{R} \right)^2 \right. \right. \\
 \left. \left. + 2 \left(v_x + \frac{u_\theta}{R} \right) \left(w_x N - u_x v_x - \frac{u_\theta M}{R} \right) \right] \right\} dx d\theta
 \end{aligned}$$

[2]

$$\begin{aligned}
& + \frac{Eh^3}{24R(1-\nu^2)} \int_0^{2L_f} \int_0^{2\pi} \left\{ R^2 \left[w_{xx}^2 + u_x N_x^2 - 2w_{xx} (Nv_{xx} + u_{xx} w_x + u_x w_{xx}) \right] \right. \\
& \quad + N_\theta^2 + Mw_{x\theta}^2 - 2N_\theta \left(u_{\theta\theta} \frac{w_x}{R} + M_\theta N + MN_\theta - \frac{w_x^2}{2} \right) \\
& \quad + 2\nu \left[Rw_{xx} N_\theta + u_\theta \frac{w_{x\theta}^2}{2} - Rw_{xx} \left(u_{\theta\theta} \frac{w_x}{R} + M_\theta N + MN_\theta - \frac{w_x^2}{2} \right) \right. \\
& \quad \left. - RN_\theta (Nv_{xx} + u_{xx} w_x + u_x w_{xx}) + R^2 N_x^2 \frac{M}{2} \right] \\
& \quad + \left(\frac{1-\nu}{2} \right) \left[(RN_x + w_{x\theta})^2 - 2 \left(v_x + \frac{u_\theta}{R} \right) (R^2 w_{xx} N_x + w_{x\theta} N_\theta) \right. \\
& \quad \left. - 2(RN_x + w_{x\theta})(2u_{x\theta} w_x + u_\theta w_{xx} + u_x w_{x\theta} + RM_x N + RMN_x \right. \\
& \quad \left. + Rv_x w_{xx} + N_\theta v_x + Nv_{x\theta} + Ru_x N_x + u_\theta \frac{N_\theta}{R} + w_{x\theta} M) \right] \left. \right\} dx d\theta \\
& + \frac{ER^2 A_f}{2(R+e)} \sum_{i=0}^1 \int_0^{2\pi} \left[M^2 + \frac{MR}{R+e} \left(\frac{u_\theta^2}{R^2} + N^2 \right) - 2 \frac{e}{R} M \left[N_\theta - u_{\theta\theta} \frac{w_x}{R} \right. \right. \\
& \quad \left. \left. - \frac{e}{R+e} u_\theta \frac{w_{x\theta}}{R} - MN_\theta - M_\theta N + \frac{w_x^2}{2} - \frac{N^2}{2} \left(\frac{R-e}{R+e} \right) \right] \right. \\
& \quad \left. - \frac{eN_\theta}{R+e} \left(\frac{u_\theta^2}{R^2} + N^2 \right) + \left(\frac{I_{xG}}{A_f R^2} + \frac{e^2}{R^2} \right) \left\{ N_\theta^2 + \frac{R}{R+e} M (w_{x\theta}^2 + N^2) \right. \right. \\
& \quad \left. \left. - 2N_\theta \left[u_{\theta\theta} \frac{w_x}{R} + \frac{e}{R+e} u_\theta \frac{w_{x\theta}}{R} + M_\theta N + MN_\theta - \frac{w_x^2}{2} \right. \right. \right. \\
& \quad \left. \left. \left. + \frac{N^2}{2} \left(\frac{R-e}{R+e} \right) \right] \right\} \right] \frac{d\theta}{x=iL_f}
\end{aligned}$$

[2]
continued

$$\begin{aligned}
& + \frac{EI_{zG}}{2(R+e)} \sum_{i=0}^1 \int_0^{2\pi} \left\{ \left[w_x - \frac{u_{\theta\theta}}{R+e} + \frac{e}{R+e} w_{x\theta\theta} \right]^2 - 2 \left[w_x - \frac{u_{\theta\theta}}{R+e} \right. \right. \\
& \quad \left. \left. + \frac{e}{R+e} w_{x\theta} \right] \left[v_x N + \frac{e}{R+e} (v_{x\theta\theta} N + 2v_{x\theta} N_\theta + v_x N_{\theta\theta}) \right] \right\} d\theta \Big|_{x=iL_f} \\
& + \frac{EK}{4(1+\nu)(R+e)^3} \sum_{i=0}^1 \int_0^{2\pi} \left[(Rw_{x\theta} + u_\theta)^2 - 2R(Rw_{x\theta} + u_\theta)(v_{x\theta} N \right. \\
& \quad \left. + v_x N_\theta) \right] d\theta \Big|_{x=iL_f} \qquad \qquad \qquad [2] \\
& \qquad \qquad \qquad \qquad \qquad \qquad \qquad \qquad \qquad \qquad \qquad \qquad \qquad \text{continued} \\
& - \frac{pR^2}{2} \int_0^{2L_f} \int_0^{2\pi} \left[\frac{2w}{R} + u_x + u_x \left(M + \frac{w}{R} \right) + \frac{1}{R^2} (w^2 + v^2) \right] dx d\theta
\end{aligned}$$

where

$$\begin{aligned}
M &= \frac{v_\theta + w}{R} \\
N &= \frac{w_\theta - v}{R}
\end{aligned}$$

and all terms beyond the third order in the displacements have been discarded. The quantities appearing in Equation [2] are defined as follows:

- E is Young's Modulus,
- h is the shell thickness,
- R is the radius to the shell middle surface,
- L_f is the frame spacing,
- ν is Poisson's ratio,
- A_f is the area of the frame cross section,
- I_{xG} is the moment of inertia of a frame about the centroid in its plane of curvature (Figure 3),

- I_{zG} is the moment of inertia of a frame about the centroid out of its plane of curvature (Figure 3),
- e is the distance from the frame centroid to the neutral axis of shell (Figure 3),
- K is the torsion constant of the frame (Appendix B),
- p is the hydrostatic pressure (positive outward),
- θ and x are the angular and axial coordinates (x positive to the right), and
- u, v and w are the axial, tangential and radial displacements, respectively (u positive to the right, w positive outward).

The subscripts indicate differentiation.

During buckling, the system passes from an initial or prebuckling equilibrium state, in which all deformations are axisymmetric, to the buckled or asymmetric state. The change in total potential accompanying this process may be called ΔU_T . The final buckled state will be described by the deflections u_F, v_F and w_F which are the total of the displacements developed from the initial application of pressure and are given by

$$\begin{aligned} u_F &= \bar{u}(x) + u(x, \theta) \\ v_F &= v(x, \theta) \\ w_F &= \bar{w}(x) + w(x, \theta) \end{aligned} \quad [3]$$

where u, v, w are the buckling displacements and \bar{u}, \bar{w} are the initial or prebuckling displacements, being axisymmetric in form for the case of hydrostatic pressure, and satisfying the conditions

$$\begin{aligned} (\bar{u}_x)_{x=0} &= (\bar{u}_x)_{x=L_f} \\ (\bar{w})_{x=0} &= (\bar{w})_{x=L_f} \\ (\bar{w}_x)_{x=0} &= (\bar{w}_x)_{x=L_f} = 0 \end{aligned} \quad [4]$$

To find the change in total potential, we replace u , v , w in Equation [2] by u_F , v_F , w_F and subtract the total potential for the initial equilibrium state. With only linear and quadratic terms retained, the result is

$$\begin{aligned}
\Delta U_T = & \frac{EhR}{2(1-\nu^2)} \int_0^{2L_f} \int_0^{2\pi} \left\{ u_x^2 + M^2 + 2\nu u_x M + \left(\frac{1-\nu}{2}\right) \left(v_x + \frac{u_\theta}{R}\right)^2 \right. \\
& + \frac{\bar{w}}{R} \left[\frac{u_\theta^2}{R^2} + N^2 + \nu(w_x^2 + v_x^2) - (1-\nu) \frac{u_\theta}{R} \left(v_x + \frac{u_\theta}{R}\right) \right] \\
& + \bar{w}_x \left[2\nu w_x M + (1-\nu) N \left(v_x + \frac{u_\theta}{R}\right) + 2u_x w_x \right] + \bar{u}_x \left[v_x^2 + w_x^2 \right. \\
& \left. \left. + \nu \left(\frac{u_\theta^2}{R^2} + N^2\right) - (1-\nu) v_x \left(v_x + \frac{u_\theta}{R}\right) \right] \right\} dx d\theta \\
& + \frac{Eh^3}{24R(1-\nu^2)} \int_0^{2L_f} \int_0^{2\pi} \left\{ R^2 w_{xx}^2 + N_\theta^2 + 2\nu R w_{xx} N_\theta + \left(\frac{1-\nu}{2}\right) (RN_x + w_{x\theta})^2 \right. \\
& + \frac{\bar{w}}{R} \left[w_{x\theta}^2 - 2N_\theta^2 + 2\nu \left(R^2 \frac{N_x^2}{2} - R w_{xx} N_\theta\right) - (1-\nu)(RN_x + w_{x\theta})^2 \right] \\
& + 2\bar{w}_x \left[w_x N_\theta - u_{\theta\theta} \frac{N_\theta}{R} - R^2 u_{xx} w_{xx} + \nu(Rw_x w_{xx} - w_{xx} u_{\theta\theta} \right. \\
& \left. - RN_\theta u_{xx}) - \left(\frac{1-\nu}{2}\right) (RN_x + w_{x\theta})(2u_{x\theta} + N) \right] - 2R \bar{w}_{xx} \left[2u_x w_{xx} \right. \\
& + Nv_{xx} + u_{xx} w_x + \nu \left(u_{\theta\theta} \frac{w_x}{R} + M_\theta N + MN_\theta - \frac{w_x^2}{2} + N_\theta u_x \right) \\
& + \left(\frac{1-\nu}{2}\right) \left(v_x + \frac{u_\theta}{R}\right) (2RN_x + w_{x\theta}) \left. \right] - 2\bar{u}_x \left[R^2 \left(w_{xx}^2 - \frac{N_x^2}{2}\right) \right. \\
& \left. - \nu \left(\frac{w_{x\theta}^2}{2} - RN_\theta w_{xx}\right) + \left(\frac{1-\nu}{2}\right) (RN_x + w_{x\theta})^2 \right] \\
& \left. - 2\bar{u}_{xx} \left[R w_x w_{xx} + \nu N_\theta w_x \right] \right\} dx d\theta
\end{aligned} \tag{5}$$

$$\begin{aligned}
& + \frac{ER^2A_f}{2(R+e)} \sum_{i=0}^1 \int_0^{2\pi} \left\{ M^2 - \frac{2e}{R} MN_\theta + \frac{\bar{w}}{R+e} \left(\frac{u_\theta^2}{R^2} + N^2 \right) + \frac{2e\bar{w}}{R^2} \left[2MN_\theta \right. \right. \\
& \quad \left. \left. + \frac{u_{\theta\theta} w_x}{R} + \frac{e}{R+e} u_\theta \frac{w_{x\theta}}{R} + M_\theta N - \frac{w_x^2}{2} + \frac{N^2}{2} \left(\frac{R-e}{R+e} \right) \right] \right\} d\theta_{x=iL_f} \\
& + \frac{E(I_{xG} + A_f e^2)}{2(R+e)} \sum_{i=0}^1 \int_0^{2\pi} \left\{ N_\theta^2 + \frac{\bar{w}}{R} \left[\frac{R}{R+e} (w_{x\theta}^2 + N^2) - 2N_\theta^2 \right] \right\} d\theta_{x=iL_f} \\
& + \frac{EI_{zG}}{2(R+e)} \sum_{i=0}^1 \int_0^{2\pi} \left[w_x - \frac{1}{R+e} (u_{\theta\theta} - e w_{x\theta\theta}) \right]^2 d\theta_{x=iL_f} \\
& + \frac{EK}{4(1+\nu)(R+e)^3} \sum_{i=0}^1 \int_0^{2\pi} (Rw_{x\theta} + u_\theta)^2 d\theta_{x=iL_f} \\
& - \frac{pR^2}{2} \int_0^{2L_f} \int_0^{2\pi} \left[\frac{2w}{R} + u_x \left(\frac{w}{R} + M \right) + \frac{w^2 + v^2}{R^2} + u_x \right] dx d\theta \quad [5] \text{ continued}
\end{aligned}$$

where M and N now involve only the buckling displacements v and w .

As explained in Appendix D, \bar{u} and \bar{w} can be expressed by the closed form solution of Von Sanden and Günther³² for the linear case, or by the more exact nonlinear solution of Pulos and Salerno.³³ However, as can be seen from Appendix D, manipulation of either of these solutions could be extremely cumbersome. Kendrick² provides convincing evidence of this in an analysis of the same buckling problem.

A simpler approach is to express \bar{u} and \bar{w} in terms of infinite trigonometric series, as indicated by Von Sanden and Tölke.¹² This has been carried out in Appendix D with the following results:

$$\bar{w} = \frac{pR^2}{2Eh} (2 - \nu) \left[1 - \eta \sum_{m=-\infty}^{\infty} a_m \cos \left(\frac{2\lambda_m x}{R} \right) \right] \quad [6]$$

$$\bar{u}_x = \frac{pR}{2Eh} \left[1 - 2\nu + \nu(2 - \nu) \eta \sum_{m=-\infty}^{\infty} a_m \cos\left(\frac{2\lambda_m x}{R}\right) \right] \text{ continued} \quad [6]$$

where, for the equivalent of the Salerno and Pulos solution,

$$\begin{aligned} \lambda_m &= \frac{m\pi R}{L_f} \\ \eta &= \frac{1}{\frac{L_f h}{A_f} \left(1 + \frac{e}{R}\right) + \sum_{m=-\infty}^{\infty} a_m} \\ a_m &= \frac{1}{1 + 4\left(\frac{m\pi}{\beta}\right)^4 + 2\frac{pR}{Eh}\lambda_m^2} = \frac{1}{\left[1 + 4\left(\frac{m\pi}{\beta}\right)^4\right] \left(1 - \frac{p}{P_m}\right)} \\ \beta &= \left[\frac{3(1 - \nu^2)}{R^2 h^2} \right]^{\frac{1}{4}} L_f \end{aligned} \quad [7]$$

If the pressure term in the denominator of a_m is neglected, we have the equivalent of the Von Sanden and Günther solution:*

$$a_m = \frac{1}{1 + 4\left(\frac{m\pi}{\beta}\right)^4} \quad [8]$$

This approximate form is found to be sufficiently accurate for the range of geometry to be considered, particularly since this analysis is not concerned with an examination of stresses and deflections at discrete points. Appendix D also gives an alternative means of computing $\sum_{m=-\infty}^{\infty} a_m$ for the approximate form:

$$\sum_{m=-\infty}^{\infty} a_m = \frac{\beta}{2} \left(\frac{\sinh \beta + \sin \beta}{\cosh \beta - \cos \beta} \right) \quad [9]$$

*A small discrepancy between the series and closed form solutions results from neglecting the faying width of the frame, as explained in Appendix D.

Except for very large values of β , however, the convergence is so rapid that the series form is often the more convenient.

Having the necessary Equations [5] and [6], it is possible at this point to apply the principle of stationary potential and, through the methods of variational calculus, proceed to a solution of the problem. The most rigorous procedure would be to formulate the partial differential equations of equilibrium and then attempt to solve them. This approach is rejected here primarily because of the lengthy task which would be involved in obtaining the differential equations. The work of Von Sanden and Tölke¹² indicates that an exact solution to the differential equations may be entirely possible, provided the initial deflections are expressed in their trigonometric series form. A simpler procedure which will be followed here is to apply the Ritz method whereby displacement functions having arbitrary coefficients are assumed and the problem of satisfying the condition for stationary potential is reduced to the solution of a system of algebraic equations.

Since the success of this method depends upon the degree to which the assumed functions approximate the exact buckling shape, it is important to choose a set of functions which permit a wide variation in shape. Accordingly, the displacements are assumed as follows:

$$\begin{aligned}
 u &= \cos n\theta \sum_{m=1}^{\infty} u_m \cos\left(\frac{\lambda_m x}{R}\right) \\
 v &= \sin n\theta \sum_{m=1}^{\infty} v_m \sin\left(\frac{\lambda_m x}{R}\right) \\
 w &= \cos n\theta \sum_{m=1}^{\infty} w_m \sin\left(\frac{\lambda_m x}{R}\right)
 \end{aligned}
 \tag{10}$$

where m and n are positive integers and u_m , v_m , w_m are the arbitrary coefficients.

It can be seen from Figure 5 that with appropriate adjustment of the coefficients, buckling configurations satisfying simple support, partial fixity, or full fixity can be generated. It should be recognized

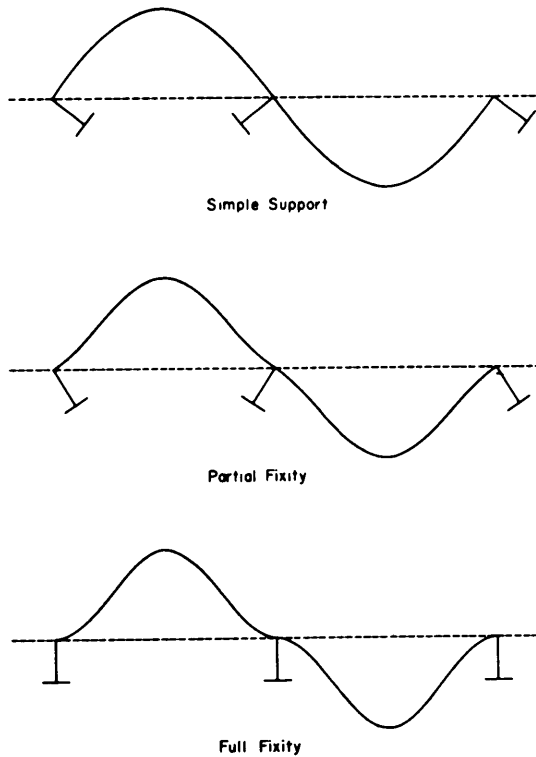


Figure 5 - Buckling Configurations for Three Degrees of Fixity

simple support and complete fixity (infinite rings). Certain approximations and methods peculiar to each case are developed which lead to simplified results.

RINGS OF FINITE RIGIDITY

In this case, rings of practical size are considered. The basic assumption is that the various ring properties are of the same order of magnitude as comparable quantities for the shell. The basic approximation is to eliminate the unknown deflections u and v through the use of a stress function, as explained in Appendix E. The complexity of the buckling equations is thereby reduced by a factor of 3. Since this procedure constrains u and v , it leads inherently to a higher buckling pressure than

although v and w vanish at each frame for any set of coefficients, no generality is lost, since this is one of the conditions which define the present buckling problem. Buckling configurations involving radial and tangential deflections of the rings properly belong to the category of overall buckling or general instability which is outside the scope of this analysis.

While the procedure for solving the problem in this general form is straightforward, considerable effort would be involved, and the results would probably be unmanageable. It is desirable, therefore, to introduce simplifying approximations where possible before proceeding further. The sections that follow consider separately three cases of interest: partial fixity (finite rings),

would result if complete generality were preserved. However, other investigators have found that the error thus introduced is extremely small for the case of a simply supported shell under hydrostatic loading. The assumption in this analysis is that the error will also be small in the case of ring support where the rings are of practical size. In the case of a fully clamped shell (corresponding to a ring of infinite rigidity), the assumption is not valid for the assumed buckling configuration, Equation [10], as will be discussed in a later section.

From Appendix E, the equations defining the stress function $F(x, \theta)$ and the deflections are

$$\begin{aligned} \nabla^4 F - \frac{Ew_{xx}}{R} &= 0 \\ u_x &= \frac{1}{E} \left(\frac{F_{\theta\theta}}{R^2} - \nu F_{xx} \right) \\ v_\theta &= \frac{R}{E} \left(F_{xx} - \nu \frac{F_{\theta\theta}}{R^2} \right) - w \\ v_x + \frac{u_\theta}{R} &= \frac{-2(1+\nu)}{ER} F_{x\theta} \end{aligned} \quad [11]$$

where the operator $\nabla^4 = \frac{\partial^4}{\partial x^4} + \frac{2\partial^4}{R^2 \partial \theta^2 \partial x^2} + \frac{\partial^4}{R^4 \partial \theta^4}$

The remaining unknown deflection w is still assumed to have the trigonometric series form (Equation [10]). If this series is now substituted in Equations [11], the result is

$$\begin{aligned} u &= \cos n\theta \sum_{m=1}^{\infty} U_m w_m \cos \left(\frac{\lambda_m x}{R} \right) \\ v &= \sin n\theta \sum_{m=1}^{\infty} V_m w_m \sin \left(\frac{\lambda_m x}{R} \right) \end{aligned} \quad [12]$$

$$w = \cos n\theta \sum_{m=1}^{\infty} w_m \sin\left(\frac{\lambda_m x}{R}\right)$$

$$F = \cos n\theta \sum_{m=1}^{\infty} f_m \sin\left(\frac{\lambda_m x}{R}\right)$$

$$f_m = -\frac{ER}{\lambda_m^2} \phi_m^2 w_m$$

$$U_m = -\frac{\phi_m}{\lambda_m} [1 - (1 + \nu) \phi_m]$$

[12]
continued

$$V_m = -\frac{n \phi_m}{\lambda_m^2} [1 + (1 + \nu) \phi_m]$$

$$\phi_m = \frac{\lambda_m^2}{n^2 + \lambda_m^2}$$

When these quantities are introduced in Equation [5], certain simplifications arise. It can be seen that

$$\begin{aligned} & \frac{EhR}{2(1-\nu^2)} \int_0^{2L_f} \int_0^{2\pi} \left[u_x^2 + M^2 + 2\nu u_x M + \left(\frac{1-\nu}{2}\right) \left(v_x + \frac{u_\theta}{R} \right)^2 \right] dx d\theta \\ & = \frac{hR}{2E} \int_0^{2L_f} \int_0^{2\pi} \left\{ (\nabla^2 F)^2 + 2(1+\nu) \left[\left(\frac{F_{x\theta}}{R} \right)^2 - \frac{F_{xx} F_{\theta\theta}}{R^2} \right] \right\} dx d\theta \end{aligned} \quad [13]$$

when substitutions are made from Equation [11]. Furthermore,

$$\begin{aligned} \int_0^{2L_f} \int_0^{2\pi} [F_{x\theta}^2 - F_{xx} F_{\theta\theta}] dx d\theta &= \int_0^{2L_f} [F_x F_{x\theta}]_{\theta=0}^{\theta=2\pi} dx \\ &\quad - \int_0^{2\pi} [F_x F_{\theta\theta}]_{x=0}^{x=2L_f} d\theta = 0 \end{aligned} \quad [14]$$

because of the periodicity of F in both the x and θ directions, as indicated by Equation [12]. Hence Equation [13] becomes

$$\begin{aligned} \frac{EhR}{2(1-\nu^2)} \int_0^{2L_f} \int_0^{2\pi} \left[u_x^2 + M^2 + 2\nu u_x M + \left(\frac{1-\nu}{2}\right) \left(v_x + \frac{u_\theta}{R} \right)^2 \right] dx d\theta \\ = \frac{hR}{2E} \int_0^{2L_f} \int_0^{2\pi} (\nabla^2 F)^2 dx d\theta \end{aligned} \quad [15]$$

Equations [12] also provide a useful approximation which is valid for short shells. The quantity N , which appears repeatedly in Equation [5], can be written:

$$N = \frac{w_\theta - \nu}{R} = -n \sin n\theta \sum_{m=1}^{\infty} w_m \left\{ 1 - \frac{\phi_m}{\lambda_m^2} \left[1 + (1+\nu)\phi_m \right] \right\} \sin\left(\frac{\lambda_m x}{R}\right) \quad [16]$$

Since $\phi_m \leq 1$ and, for short shells, $\lambda_m^2 \gg 1$, little accuracy will be lost if one makes the approximation*

$$N = \frac{w_\theta}{R} = -n \sin n\theta \sum_{m=1}^{\infty} w_m \sin\left(\frac{\lambda_m x}{R}\right) \quad [17]$$

In addition, it will be seen that several terms in the frame energy integrals vanish at the frames according to Equations [10] and [12].

Accordingly, the simplified form of Equation [5] is

$$\begin{aligned} \Delta U_T = \frac{hR}{2E} \int_0^{2L_f} \int_0^{2\pi} (\nabla^2 F)^2 dx d\theta + \frac{Eh^3}{24R(1-\nu^2)} \int_0^{2L_f} \int_0^{2\pi} \left[R^2 w_{xx}^2 \right. \\ \left. + \frac{w_{\theta\theta}^2}{R^2} + 2\nu w_{xx} w_{\theta\theta} + 2(1-\nu) w_{x\theta}^2 \right] dx d\theta \end{aligned} \quad [18]$$

*The accuracy of this approximation depends not on the size of n but only on the size of λ_m . Its range of validity, therefore, includes the case of axisymmetric buckling of a short shell ($n=0$, $\phi_m=1$) but not that of asymmetric buckling of a long shell where λ_m may not be large.

$$\begin{aligned}
& + \frac{EI_{zG}}{2(R+e)} \sum_{i=0}^1 \int_0^{2\pi} \left[w_x - \frac{1}{R+e} (u_{\theta\theta} - ew_{x\theta\theta}) \right]_{x=iL_f}^2 d\theta \\
& + \frac{EK}{4(1+\nu)(R+e)^3} \sum_{i=0}^1 \int_0^{2\pi} (Rw_{x\theta} + u_\theta)_{x=iL_f}^2 d\theta \\
& + \frac{EhR}{2(1-\nu^2)} \int_0^{2L_f} \int_0^{2\pi} \left\{ \bar{w} \left[\frac{u_\theta^2 + w_\theta^2}{R^2} + \nu(w_x^2 + v_x^2) - (1-\nu) \frac{u_\theta}{R} \left(v_x + \frac{u_\theta}{R} \right) \right] \right. \\
& \quad + \bar{w}_x \left[2\nu w_x \left(\frac{w + v_\theta}{R} \right) + 2u_x w_x + (1-\nu) \frac{w_\theta}{R} \left(v_x + \frac{u_\theta}{R} \right) \right] \\
& \quad \left. + \bar{u}_x \left[\nu \left(\frac{u_\theta^2 + w_\theta^2}{R} \right) + w_x^2 + v_x^2 - (1-\nu) v_x \left(v_x + \frac{u_\theta}{R} \right) \right] \right\} dx d\theta \\
& - \frac{pR}{2} \int_0^{2L_f} \int_0^{2\pi} \left[u_x (2w + v_\theta) + \frac{w^2 + v^2}{R} \right] dx d\theta \\
& + \frac{E(I_{xG} + A_f e^2)}{2(R+e)^2} \sum_{i=0}^1 \int_0^{2\pi} \bar{w} w_{x\theta}^2_{x=iL_f} d\theta \quad [18] \text{ continued} \\
& + \frac{ER^2 A_f}{2(R+e)} \sum_{i=0}^1 \int_0^{2\pi} \frac{\bar{w}}{R} \left\{ \frac{u_\theta^2}{R(R+e)} + \frac{2e}{R} \left[\frac{u_{\theta\theta} w_x}{R} + \frac{eu_\theta w_{x\theta}}{R(R+e)} - \frac{w_x^2}{2} \right] \right\}_{x=iL_f} d\theta + \Delta U_b
\end{aligned}$$

where ΔU_b is the portion of the bending strain energy which involves the initial deflections.* It is given by

* ΔU_b can be simplified further since $\int_0^{2\pi} \left[\frac{w_{\theta\theta}}{R} \left(\frac{v_\theta + w}{R} \right) + \frac{w_\theta}{R} \left(\frac{v_{\theta\theta} + w_\theta}{R} \right) \right] d\theta$ will vanish on integration.

$$\begin{aligned}
\Delta U_b = & -\frac{Eh^3}{24R(1-\nu^2)} \int_0^{2L_f} \int_0^{2\pi} \left\{ \frac{\bar{w}}{R} \left[(3-5\nu)w_{x\theta}^2 + \frac{2w_{\theta\theta}^2}{R^2} + 2\nu w_{xx} w_{\theta\theta} \right] \right. \\
& + 2\bar{w}_x \left[R^2 u_{xx} w_{xx} + \nu u_{xx} w_{\theta\theta} - \left(w_x - \frac{u_{\theta\theta}}{R} \right) \left(\frac{w_{\theta\theta}}{R} + 2\nu R w_{xx} \right) \right. \\
& + (1-\nu)w_{x\theta} \left(u_{x\theta} + \frac{w_{\theta}}{R} \right) \left. \right] + R\bar{w}_{xx} \left[2R \left(2u_x w_{xx} + \frac{w_{\theta} v_{xx}}{R} + u_{xx} w_x \right) \right. \\
& + 3(1-\nu)w_{x\theta} \left(v_x + \frac{u_{\theta}}{R} \right) + 2\nu \left\{ \frac{u_{\theta\theta} w_x}{R} - \frac{w_x^2}{2} + \frac{w_{\theta\theta}}{R} \left(\frac{v_{\theta} + w}{R} + u_x \right) \right. \\
& \left. \left. + \frac{w_{\theta}}{R} \left(\frac{v_{\theta\theta} + w_{\theta}}{R} \right) \right\} \right] + \bar{u}_x \left[2R^2 w_{xx}^2 + (3-5\nu)w_{x\theta}^2 + 2\nu w_{\theta\theta} w_{xx} \right] \\
& \left. + 2R\bar{u}_{xx} \left[R w_x w_{xx} + \frac{\nu w_x w_{\theta\theta}}{R} \right] \right\} dx d\theta \tag{19}
\end{aligned}$$

After the series expressions, Equations [6] and [12], are introduced, Equation [18] can be integrated. In so doing, it should be noted that because the functions of Equation [12] are orthogonal in the interval $0 \leq x \leq 2L_f$, coupling of different buckling modes (i, j) will arise only from the frame energy and from shell energy terms involving products of the buckling modes with the initial deflections. The resulting integrated form of Equation [18] is

$$\begin{aligned}
\Delta U_T = & \frac{\pi E L_f h}{2R} \sum_{m=1}^{\infty} w_m^2 \left[\phi_m^2 + \frac{h^2 \lambda_m^4}{12R^2(1-\nu^2)\phi_m^2} \right] \\
& + \frac{\pi E I_{zG}}{2R^2(R+e)} \sum_{i=1}^{\infty} \sum_{j=1}^{\infty} w_i w_j \delta_{ij} \left[\lambda_i + \frac{n^2 R}{R+e} \left(U_i - \frac{e\lambda_i}{R} \right) \right] \left[\lambda_j + \frac{n^2 R}{R+e} \left(U_j - \frac{e\lambda_j}{R} \right) \right] \\
& + \frac{\pi EK}{4(1+\nu)(R+e)^3} \sum_{i=1}^{\infty} \sum_{j=1}^{\infty} w_i w_j \delta_{ij} n^2 (U_i + \lambda_i)(U_j + \lambda_j) \tag{20}
\end{aligned}$$

$$\begin{aligned}
& + \frac{\pi p L_f}{4} (2 - \nu) \eta \sum_{i=1}^{\infty} \sum_{j=1}^{\infty} w_i w_j \delta_{ij} \left[\frac{n^2 R}{R+e} U_i U_j - \frac{2e}{R} \lambda_i \left(\frac{n^2 R U_j}{R+e} + \frac{\lambda_j}{2} \right) \right] \\
& + \frac{\pi p L_f}{4} (2 - \nu) \eta \left(\frac{I_{xG} + A_f e^2}{R^2 A_f} \right) \sum_{i=1}^{\infty} \sum_{j=1}^{\infty} w_i w_j \delta_{ij} \frac{n^2 R}{R+e} \lambda_i \lambda_j \\
& + \frac{\pi p L_f}{2} \sum_{m=1}^{\infty} w_m^2 \left(n^2 + \frac{\lambda_m^2}{2} + \frac{3q_{mm}}{2} - r_m \right) \quad [20] \text{ continued} \\
& - \frac{\pi p L_f}{4} (2 - \nu) \eta \sum_{i=1}^{\infty} \sum_{j=1}^{\infty} w_i w_j \left\{ a_{\frac{1}{2}(i-j)} \left[n^2 - 2\lambda_j (\lambda_i - \lambda_j) \ell_{ij} + q_{ij} \right] \right. \\
& \quad \left. - a_{\frac{1}{2}(i+j)} \left[n^2 + 2\lambda_j (\lambda_i + \lambda_j) \ell_{ij} - q_{ij} \right] \right\} + \Delta U_b
\end{aligned}$$

where:

$$\delta_{ij} = 1 + (-1)^{i+j}$$

$$\begin{aligned}
r_m &= 1 + \phi_m + \phi_m^2 \left[\phi_m (1 - \phi_m) (1 + \nu)^2 - (1 + 2\nu) \right] \\
& \quad + \phi_m \left(\frac{1 - \phi_m}{\lambda_m^2} \right) \left[1 + (1 + \nu) \phi_m \right]^2
\end{aligned}$$

$$\ell_{ij} = \phi_i (1 - \phi_i) + \phi_j (1 - \phi_j)$$

$$q_{ij} = \frac{i}{j} \phi_j (1 - \phi_i) \left[1 - (1 - \nu)(\phi_i - \phi_j) - \phi_i \phi_j (1 - 3\nu) \right]$$

$$a_{\frac{1}{2}(i-j)} = \frac{1}{\left\{ 1 + 4 \left[\frac{(i-j)\pi}{2\beta} \right]^4 \right\} \left[1 - \frac{p}{P_{\frac{1}{2}(i-j)}} \right]}$$

$$a_{\frac{1}{2}(i+j)} = \frac{1}{\left\{ 1 + 4 \left[\frac{(i+j)\pi}{2\beta} \right]^4 \right\} \left[1 - \frac{p}{P_{\frac{1}{2}(i+j)}} \right]}$$

ΔU_b has not been given explicitly at this point since it will be necessary to examine only a few of its characteristic terms. For example, we find

$$I_1 = -\frac{Eh^3}{24R(1-\nu^2)} \int_0^{2L_f} \int_0^{2\pi} \frac{2\bar{w} w_{\theta\theta}^2}{R^3} dx d\theta \quad [21]$$

$$= \frac{\pi p L_f (2-\nu)}{4} \left[\frac{h^2 n^2}{6R^2(1-\nu^2)} \right] \left[\sum_{m=1}^{\infty} n^2 w_m^2 - \eta \sum_{i=1}^{\infty} \sum_{j=1}^{\infty} n^2 w_i w_j [a_{\frac{1}{2}(i-j)} - a_{\frac{1}{2}(i+j)}] \right]$$

This can be compared with other terms, designated by Z, appearing in ΔU_T :

$$Z = \frac{\pi p L_f}{4} \left[\sum_{m=1}^{\infty} 2n^2 w_m^2 - (2-\nu) \eta \sum_{i=1}^{\infty} \sum_{j=1}^{\infty} n^2 w_i w_j [a_{\frac{1}{2}(i-j)} - a_{\frac{1}{2}(i+j)}] \right] \quad [22]$$

It is immediately seen that if $\frac{h^2 n^2}{6R^2} \ll 1$, which is a reasonable approximation for thin shells, I_1 is negligible compared with Z.

Another characteristic term appearing in ΔU_b is

$$I_2 = -\frac{Eh^3}{24R(1-\nu^2)} \int_0^{2L_f} \int_0^{2\pi} 2(1-\nu) \frac{\bar{w}_x w_{x\theta} w_{\theta}}{R} dx d\theta$$

$$= -\frac{\pi p L_f}{4} (2-\nu) \eta \left[\frac{h^2 (1-\nu)}{6R^2(1-\nu^2)} \right] \sum_{i=1}^{\infty} \sum_{j=1}^{\infty} n^2 w_i w_j \lambda_i [a_{\frac{1}{2}(i+j)} (\lambda_i + \lambda_j)$$

$$+ a_{\frac{1}{2}(i-j)} (\lambda_i - \lambda_j)] \quad [23]$$

Comparing I_2 with Z, we find that I_2 is negligible if $\frac{h^2}{6R^2} (\lambda_i + \lambda_j) \lambda_i$ and $\frac{h^2}{6R^2} (\lambda_i - \lambda_j) \lambda_i$ are negligible compared with unity. This will hold for short thin shells except when i or j are large. In such cases, however, it will be seen from Equation [20] that $a_{\frac{1}{2}(i+j)}$ or $a_{\frac{1}{2}(i-j)}$ will be extremely

small so that all terms in which either appears as a multiple will be negligible.

A third term is

$$\begin{aligned}
I_3 &= \frac{Eh^3}{24R(1-\nu^2)} \int_0^{2L_f} \int_0^{2\pi} \nu R \bar{w}_{xx} w_x^2 dx d\theta \\
&= \frac{\nu\pi p L_f}{4} (2-\nu)\eta \left[\frac{h^2}{12R^2(1-\nu^2)} \right] \sum_{i=1}^{\infty} \sum_{j=1}^{\infty} w_i w_j \lambda_i \lambda_j \left[a_{\frac{1}{2}(i-j)} (\lambda_i - \lambda_j)^2 \right. \\
&\quad \left. + a_{\frac{1}{2}(i+j)} (\lambda_i + \lambda_j)^2 \right] \tag{24}
\end{aligned}$$

A comparison with Z reveals that I_3 will also be negligible so long as

$$\frac{h^2 \lambda_i \lambda_j}{12R^2(1-\nu^2)} (\lambda_i - \lambda_j)^2 \text{ and } \frac{h^2 \lambda_i \lambda_j}{12R^2(1-\nu^2)} (\lambda_i + \lambda_j)^2$$

are negligible compared with n^2 . As in the case of I_2 , when this does not hold, the question no longer has importance.

It can be shown further that each term appearing in ΔU_b will be one of these three general types. Hence, the entire integral ΔU_b is negligible. In other words, the bending stresses associated with the prebuckling deformations can be neglected.

Inspection of Equation [20] reveals some additional approximations which can be made. It will be seen from Equation [12] that U_m is negligible compared with λ_m since ϕ_m is always less than unity and λ_m is much greater than unity. Hence,

$$w_m (U_m + \lambda_m) \approx w_m \lambda_m \tag{25}$$

It also follows that

$$w_m^2 \left(n^2 + \frac{\lambda_m^2}{2} + \frac{3q_{mm}}{2} - r_m \right) \approx w_m^2 \left(n^2 + \frac{\lambda_m^2}{2} \right) \tag{26}$$

If $n^2 \gg 1$,* we can also neglect q_{ij} , so that

$$\begin{aligned} & a_{\frac{1}{2}(i-j)} [n^2 - 2\lambda_j(\lambda_i - \lambda_j) \ell_{ij} + q_{ij}] - a_{\frac{1}{2}(i+j)} [n^2 + 2\lambda_j(\lambda_i + \lambda_j) \ell_{ij} - q_{ij}] \\ & \approx a_{\frac{1}{2}(i-j)} [n^2 - 2\lambda_j(\lambda_i - \lambda_j) \ell_{ij}] - a_{\frac{1}{2}(i+j)} [n^2 + 2\lambda_j(\lambda_i + \lambda_j) \ell_{ij}] \end{aligned} \quad [27]$$

When $i \gg j$, this approximation will not hold. However, as explained for I_2 and I_3 , the entire expression (Equation [27]) in such cases is negligible.

We have then for the approximate form of Equation [20]:

$$\begin{aligned} \Delta U_T = & \frac{\pi E L_f h}{2R} \sum_{m=1}^{\infty} w_m^2 \left[\phi_m^2 + \frac{h^2 \lambda_m^4}{12R^2(1-\nu^2)\phi_m^2} \right] \\ & + \frac{\pi E I_{xG}}{2R^2(R+e)} \sum_{i=1}^{\infty} \sum_{j=1}^{\infty} w_i w_j \delta_{ij} \left[\lambda_i + \frac{n^2 R}{R+e} \left(U_i - \frac{e\lambda_i}{R} \right) \right] \left[\lambda_j + \frac{n^2 R}{R+e} \left(U_j - \frac{e\lambda_j}{R} \right) \right] \\ & + \frac{\pi EK}{4(1+\nu)(R+e)^3} \sum_{i=1}^{\infty} \sum_{j=1}^{\infty} w_i w_j \delta_{ij} \lambda_i \lambda_j n^2 \\ & + \frac{\pi p L_f}{4} (2-\nu) \eta \sum_{i=1}^{\infty} \sum_{j=1}^{\infty} w_i w_j \delta_{ij} \left[\frac{n^2 R}{R+e} U_i U_j - \frac{2e\lambda_i}{R} \left(\frac{n^2 R}{R+e} U_j + \frac{\lambda_j}{2} \right) \right] \\ & + \frac{\pi p L_f}{4} (2-\nu) \eta \left(\frac{I_{xG} + A_f e^2}{R^2 A_f} \right) \sum_{i=1}^{\infty} \sum_{j=1}^{\infty} w_i w_j \delta_{ij} \frac{n^2 R}{R+e} \lambda_i \lambda_j \\ & + \frac{\pi p L_f}{2} \sum_{m=1}^{\infty} w_m^2 \left(n^2 + \frac{\lambda_m^2}{2} \right) \end{aligned} \quad [28]$$

*This is generally a valid assumption for asymmetric buckling of short shells; for axisymmetric buckling, q_{ij} is identically zero.

$$\begin{aligned}
- \frac{\pi p L_f}{4} (2-\nu) \eta \sum_{i=1}^{\infty} \sum_{j=1}^{\infty} w_i w_j \left\{ a_{\frac{1}{2}(i-j)} \left[n^2 - 2\lambda_j (\lambda_i - \lambda_j) \ell_{ij} \right] \right. \\
\left. - a_{\frac{1}{2}(i+j)} \left[n^2 + 2\lambda_j (\lambda_i + \lambda_j) \ell_{ij} \right] \right\} \quad [28] \\
\text{continued}
\end{aligned}$$

The buckling condition is now obtained using the principle of stationary potential. Minimizing ΔU_T with respect to the w_j and multiplying the resulting equations by $\frac{R}{\pi E L_f h}$, one obtains the simultaneous equations:

$$\begin{aligned}
\frac{\partial(\Delta U_T)}{\partial w_j} = 0 = w_j \left[\phi_j^2 + \frac{h^2 \lambda_j^4}{12 R^2 (1-\nu^2) \phi_j^2} \right] \\
+ \frac{I_z G}{R(R+e) L_f h} \left[\lambda_j + \frac{n^2 R}{R+e} \left(U_j - \frac{e \lambda_j}{R} \right) \right] \sum_{i=1}^{\infty} w_i \delta_{ij} \left[\lambda_i + \frac{n^2 R}{R+e} \left(U_i - \frac{e \lambda_i}{R} \right) \right] \\
+ \frac{K R n^2 \lambda_j}{2(1+\nu)(R+e)^3 L_f h} \sum_{i=1}^{\infty} w_i \delta_{ji} \lambda_i \\
+ \frac{\psi(2-\nu) \eta}{2} \sum_{i=1}^{\infty} w_i \delta_{ji} \left\{ \frac{n^2 R}{R+e} U_i U_j - \frac{e}{R} \left[\lambda_i \left(\frac{n^2 R}{R+e} U_j + \frac{\lambda_j}{2} \right) \right. \right. \\
\left. \left. + \lambda_j \left(\frac{n^2 R}{R+e} U_i + \frac{\lambda_i}{2} \right) \right] \right\} \\
+ \frac{\psi(2-\nu) \eta}{2} \left(\frac{I_{xG} + A_f e^2}{R^2 A_f} \right) \left(\frac{R}{R+e} \right) n^2 \lambda_j \sum_{i=1}^{\infty} w_i \delta_{ji} \lambda_i \\
+ \psi w_j \left(n^2 + \frac{\lambda_j^2}{2} \right) \quad [29] \\
- \frac{\psi(2-\nu) \eta}{2} \sum_{i=1}^{\infty} w_i \left\{ a_{\frac{1}{2}(i-j)} \left[n^2 + \ell_{ji} (\lambda_i - \lambda_j)^2 \right] \right. \\
\left. - a_{\frac{1}{2}(i+j)} \left[n^2 + \ell_{ji} (\lambda_i + \lambda_j)^2 \right] \right\}
\end{aligned}$$

where ψ is $\frac{pR}{Eh}$.

It is an interesting consequence of Equations [29] that all modes corresponding to odd values of i and j are coupled and the same is true of all even modes, but that no coupling exists between odd and even modes. This arises from the two consistent definitions

$$\left. \begin{aligned} \delta_{ji} &= 1 + (-1)^{i+j} = 0 \\ a_{\frac{1}{2}(i-j)} &= a_{\frac{1}{2}(i+j)} = 0 \end{aligned} \right\} \text{ unless } i, j \text{ odd or } i, j \text{ even} \quad [30]$$

The problem thus can be grouped into two sets of equations corresponding to the odd and the even modes, respectively. It is clear that only the odd modes need be considered here since the even modes lead to buckling configurations of the type (shown in Figure 6) which repeats itself at each frame and is of no practical significance. When the problem is restricted to the odd modes, Equations [29] become:

$$\begin{aligned} 0 = w_j & \left[\phi_j^2 + \frac{h^2 \lambda_j^4}{12R^2(1-\nu^2)\phi_j^2} + \psi \left(n^2 + \frac{\lambda_j^2}{2} \right) \right] + \frac{2I_{zG}}{R(R+e)L_f h} \left[\lambda_j + \frac{n^2}{1+\frac{e}{R}} \left(U_j \right. \right. \\ & \left. \left. - \frac{e\lambda_j}{R} \right) \right] \sum_{i=1}^{\infty} w_i \left[\lambda_i + \frac{n^2}{1+\frac{e}{R}} \left(U_i - \frac{e\lambda_i}{R} \right) \right] + \frac{Kn^2 \lambda_j}{(1+\nu)R^2(1+\frac{e}{R})^3 L_f h} \sum_{i=1}^{\infty} w_i \lambda_i \\ & + \psi (2-\nu) \eta \left[\sum_{i=1}^{\infty} w_i \left\{ \frac{n^2 U_i U_j}{1+\frac{e}{R}} - \frac{e}{R} \left[\lambda_i \left(\frac{n^2 U_j}{1+\frac{e}{R}} + \frac{\lambda_j}{2} \right) + \lambda_j \left(\frac{n^2 U_i}{1+\frac{e}{R}} + \frac{\lambda_i}{2} \right) \right] \right\} \right. \\ & + \left(\frac{I_{xG} + A_f e^2}{R^2 A_f} \right) \frac{n^2 \lambda_j}{1+\frac{e}{R}} \sum_{i=1}^{\infty} w_i \lambda_i - \frac{1}{2} \sum_{i=1}^{\infty} w_i \left\{ a_{\frac{1}{2}(i-j)} [n^2 + \ell_{ji} (\lambda_i - \lambda_j)^2] \right. \\ & \left. \left. - a_{\frac{1}{2}(i+j)} [n^2 + \ell_{ji} (\lambda_i + \lambda_j)^2] \right\} \right] \quad i, j = 1, 3, 5 \dots \quad [31] \end{aligned}$$



Figure 6 - Even Mode Buckling

If j is given an upper limit J , Equations [31] can be written in the form

$$B_j w_j + \sum_{i=1}^J b_{ji} w_i + \psi \left[C_j w_j + \sum_{i=1}^J c_{ji} w_i \right] = 0 \quad [32]$$

where:

$$B_j = \phi_j^2 + \frac{h^2 \lambda_j^4}{12R^2(1-\nu^2)\phi_j^2}$$

$$b_{ji} = \frac{2I_{zG}}{R^2(1+\frac{e}{R})L_f h} \left[\lambda_j + \frac{n^2}{1+\frac{e}{R}} \left(U_j - \frac{e\lambda_j}{R} \right) \right] \left[\lambda_i + \frac{n^2}{1+\frac{e}{R}} \left(U_i - \frac{e\lambda_i}{R} \right) \right]$$

$$+ \frac{Kn^2 \lambda_j \lambda_i}{(1+\nu)R^2(1+\frac{e}{R})^3 L_f h}$$

$$C_j = n^2 + \frac{\lambda_j^2}{2}$$

$$c_{ji} = (2-\nu)\eta \left[\frac{n^2 U_i U_j}{1+\frac{e}{R}} - \frac{e}{R} \left\{ \lambda_i \left(\frac{n^2 U_j}{1+\frac{e}{R}} + \frac{\lambda_j}{2} \right) + \lambda_j \left(\frac{n^2 U_i}{1+\frac{e}{R}} + \frac{\lambda_i}{2} \right) \right\} \right]$$

$$+ \left(\frac{I_{xG} + A_f e^2}{R^2 A_f} \right) \frac{n^2 \lambda_j \lambda_i}{1+\frac{e}{R}}$$

$$+ \frac{1}{2} \left\{ a_{\frac{1}{2}(i+j)} [n^2 + l_{ji} (\lambda_i + \lambda_j)^2] - a_{\frac{1}{2}(i-j)} [n^2 + l_{ji} (\lambda_i - \lambda_j)^2] \right\}$$

$$i, j = 1, 3, 5 \dots J \cdot$$

A requirement for the existence of a nontrivial solution to these equations is that the determinant formed from the coefficients of the w_j must vanish. This condition can be written in matrix notation as follows:

$$\{[B] + [C] \psi\} [X] = 0 \quad [33]$$

where:

$$[B] = \begin{bmatrix} B_1 + b_{11}, & b_{13}, & b_{15}, & \dots & b_{1J} \\ b_{31}, & B_3 + b_{33}, & & & \\ b_{51}, & & B_5 + b_{55}, & & \\ \vdots & & & \ddots & \\ b_{J1}, & & & & B_J + b_{JJ} \end{bmatrix}$$

$$[C] = \begin{bmatrix} C_1 + c_{11}, & c_{13}, & c_{15}, & \dots & c_{1J} \\ c_{31}, & C_3 + c_{33}, & & & \\ c_{51}, & & C_5 + c_{55}, & & \\ \vdots & & & \ddots & \\ c_{J1}, & & & & C_J + c_{JJ} \end{bmatrix}$$

$$[X] = \begin{bmatrix} w_1 \\ w_3 \\ w_5 \\ \vdots \\ w_J \end{bmatrix}$$

Both [B] and [C] are symmetrical matrixes. The equation has $\frac{J+1}{2}$ real roots, all of which are negative, since pressure was defined positive when external. Of these roots, the one (ψ_n) whose absolute value is least defines p_n , the buckling pressure for n circumferential lobes. Since n is an arbitrary integer, it is necessary to obtain p_n for several values of n until the minimum, or critical pressure, p_c is determined. The degree of accuracy depends, of course, on the magnitude of J. As J increases, p_c should converge toward a limiting value.

While the solution of Equation [33] appears reasonably adaptable to a high-speed digital computer, it becomes unmanageable for desk calculation if J is much greater than 5. To overcome this difficulty, an approximate form has been found whereby the computational task is considerably reduced. With suitable rearrangement, Equation [32] can be put in the form:

$$(B_j + \psi C_j) w_j + G_j \sum_{i=1}^J w_i \lambda_i + H_j \sum_{i=1}^J w_i U_i + \psi \sum_{i=1}^J w_i d_{ji} = 0 \quad [34]$$

where B_j and C_j are as before defined for Equation [32] and

$$G_j = \frac{2I_{zG}}{R^2(1+\frac{e}{R})^3 L_f h} \left[1 - \frac{e}{R} (n^2 - 1) \right] \left\{ \lambda_j \left[1 - \frac{e}{R} (n^2 - 1) \right] + n^2 U_j \right\}$$

$$+ \frac{K n^2 \lambda_j}{(1+\nu) R^2 (1+\frac{e}{R})^3 L_f h} + \frac{\psi(2-\nu)\eta}{1+\frac{e}{R}} \left\{ \lambda_j \left[\left(\frac{I_{xG} + A_f e^2}{R^2 A_f} \right) n^2 - \frac{e}{R} \left(1 + \frac{e}{R} \right) \right] - n^2 \frac{e}{R} U_j \right\}$$

$$H_j = \frac{2I_{zG} n^2}{R^2 (1+\frac{e}{R})^3 L_f h} \left\{ \lambda_j \left[1 - \frac{e}{R} (n^2 - 1) \right] + n^2 U_j \right\} + \frac{\psi(2-\nu)\eta}{1+\frac{e}{R}} n^2 \left(U_j - \frac{e \lambda_j}{R} \right)$$

$$d_{ji} = \frac{(2-\nu)\eta}{2} \left\{ a_{\frac{1}{2}(i+j)} [n^2 + \ell_{ji} (\lambda_i + \lambda_j)^2] - a_{\frac{1}{2}(i-j)} [n^2 + \ell_{ji} (\lambda_i - \lambda_j)^2] \right\}$$

To simplify the equations, we neglect all the d_{ji} for which j and i are unequal, so that Equation [34] becomes

$$D_j w_j + G_j \sum_{i=1}^J w_i \lambda_i + H_j \sum_{i=1}^J w_i U_i = 0 \quad j, i = 1, 3, 5 \dots J \quad [35]$$

where:

$$D_j = B_j + \psi(C_j + d_{jj})$$

$$d_{jj} = \frac{(2-\nu)\eta}{2} [a_j(n^2 + 4\ell_{jj}\lambda_j^2) - n^2]$$

It can be seen from Equation [8] that the approximation is not unreasonable. Because a_m decreases rapidly with increasing m , most of the a_m will be negligible. In many cases, it would, in fact, be necessary to retain a_0 only. A more conclusive test of the approximation, however, is a comparison of numerical results. Since a_m approaches zero more slowly as β is increased, a demonstration that the approximation is valid for a large value of β should be sufficient proof of its validity for smaller values. This point is discussed in a later section dealing with a numerical example.

With ℓ_{jj} expressed by Equation [20] and n^2 replaced by $\lambda_j^2 \left(\frac{1-\phi_j}{\phi_j} \right)$, a more concise expression for D_j is obtained:

$$D_j = B_j + \frac{\psi}{2} \left[\lambda_j^2 + n^2 \left\{ 2 - (2-\nu)\eta [1 - a_j(1 + 8\phi_j^2)] \right\} \right] \quad [36]$$

The advantage of the form of Equations [35] over that of Equations [32] can now be demonstrated. With the stipulation that ψ is such that all D_j are different from zero, one can multiply Equation [34] by λ_j/D_j and carry out a summation on j from 1 to J :

$$\sum_{i=1}^J w_i \lambda_i \left[1 + \sum_{i=1}^J \frac{G_i \lambda_i}{D_i} \right] + \sum_{i=1}^J \frac{H_i \lambda_i}{D_i} \sum_{i=1}^J w_i U_i = 0 \quad [37]$$

A second equation is obtained by multiplying Equation [35] by U_j/D_j and performing the same summation:

$$\sum_{i=1}^J w_i U_i \left[1 + \sum_{i=1}^J \frac{H_i U_i}{D_i} \right] + \sum_{i=1}^J \frac{G_i U_i}{D_i} \sum_{i=1}^J w_i \lambda_i = 0 \quad [38]$$

The unknown coefficients w_i are eliminated by combining Equations [37] and [38], and the result is a single equation,

$$\left[1 + \sum_{i=1}^J \frac{H_i U_i}{D_i} \right] \left[1 + \sum_{i=1}^J \frac{G_i \lambda_i}{D_i} \right] - \sum_{i=1}^J \frac{G_i U_i}{D_i} \sum_{i=1}^J \frac{H_i \lambda_i}{D_i} = 0 \quad [39]$$

which can be solved by plotting the left-hand side versus ψ . Such a plot will have $\frac{J+1}{2}$ zero-intercepts, one for each root of the equation, and an equal number of asymptotes corresponding to the vanishing of each of the D_i . The root whose absolute value is a minimum will lie between the first two asymptotes ($i = 1, 3$). As in the case of Equation [33], it is necessary to try several values of n until the critical pressure p_c is determined. The accuracy of the result will, of course, improve as J is increased. In the case where an initial value of J has been found to be insufficient, one can proceed to the next succeeding J (i.e., increase the order of the equations by one) with far less labor than would be involved when working with the matrix, Equation [33].

SIMPLE SUPPORT CONDITIONS

The special case of a shell having regularly spaced simple supports instead of finite rings can be obtained quite easily from the general equations. For this case, the conditions are

$$\begin{aligned} I_{zG} &= I_{xG} = K = 0 \\ A_f &= \infty \\ \bar{w} &= w = 0 \quad \text{at } x = 0, L_f \end{aligned} \quad [40]$$

$$\eta_j = \eta_\infty = \frac{1}{\sum_{m=-\infty}^{\infty} a_m} \quad [40]$$

continued

$$= \frac{2}{\beta} \left(\frac{\cosh \beta - \cos \beta}{\sinh \beta + \sin \beta} \right), \quad \text{if pressure term in } a_m \text{ can be neglected}$$

Substitution of these relations directly into Equation [32] will not lead to the correct result since some of the terms in that equation have been multiplied by A_f , and this would be equivalent to dividing by zero. Instead we return to Equation [18] and note that because of the relations in Equation [40], all frame integrals in which \bar{w} appears as a multiplier as well as those multiplied by I_{zG} , K and I_{xG} will now be zero. It is then evident that Equation [34] for this case will reduce to

$$B_j w_j + \psi \left[C_j w_j + \sum_{i=1}^J d_{ji} w_i \right] = 0 \quad [41]$$

where the B_j , C_j , and d_{ji} are defined in Equations [32] and [34]. This equation can, of course, be solved in exactly the same manner as Equation [32]. However, by making the same approximation as was done to obtain Equation [35], one arrives at a simple linear equation for this case. That is, if all d_{ji} are neglected where j and i are unequal, the resulting equation has the uncoupled form:

$$P_n = -\frac{Eh}{R} \left(\frac{B_j}{C_j + d_{jj}} \right) = \frac{-\frac{Eh}{R} \left[\phi_j^2 + \frac{h^2 \lambda_j^4}{12R^2(1-\nu^2) \phi_j^2} \right]}{\frac{\lambda_j^2}{2} + n^2 \left\{ 1 - \left(\frac{2-\nu}{2} \right) \eta_\infty [1 - a_j (1 + 8\phi_j^2)] \right\}} \quad [42]$$

This solution* gives a minimum buckling pressure for $j=1$, which is the

*It may be of some interest to compare Equation [42] with the equivalent solution of Von Mises (Equation [8] of Reference 29), which in the terminology of this report is:

first asymptote of Equation [39] with η set equal to η_∞ .

It is now possible to find the value of n for which p_n will be a minimum. If n^2 is replaced by $\lambda_1^2 \left(\frac{1 - \phi_1}{\phi_1} \right)$ in Equation [42], p_n will be effectively minimized by setting $\partial p_n / \partial \phi_1$ equal to zero. The resulting equation is

*(Footnote continued from preceding page)

$$p_n = \frac{-\frac{Eh}{R} \left[\phi_1^2 + \frac{h^2 \lambda_1^4}{12R^2(1-\nu^2)\phi_1^2} \right]}{\frac{\lambda_1^2}{2} + n^2}$$

This formula is based on the assumption that the boundary conditions do not affect the prebuckling deformations. The Von Mises pressures will, in general, be less than those given by Equation [42], except where $a_1(1 + 8\phi_1^2) > 1$. The two solutions are identical for $\beta \gg 1$, where η_∞ approaches zero, but are not accurate in this range. For such a case, the Von Mises formula [6] of Reference 29 should be used.

A comparable solution is that of Von Sanden and Tölke¹² which, for the case of simple support, can be written

$$p_n = \frac{-\frac{Eh}{R} \left[\phi_1^2 + \frac{h^2 \lambda_1^4}{12R^2(1-\nu^2)\phi_1^2} \right]}{\frac{\lambda_1^2}{2} + n^2 \left[\frac{3(2-\nu)}{4} \left(1 - \frac{\eta_\infty}{\eta'_\infty} \right) + \frac{\nu}{2} \right]}$$

$$\eta'_\infty = \frac{4}{\beta} \left[\frac{\cosh \frac{\beta}{2} - \cos \frac{\beta}{2}}{\sinh \frac{\beta}{2} + \sin \frac{\beta}{2}} \right]$$

In deriving this formula, Von Sanden and Tölke took into account the effect of the boundary conditions on the prebuckling deformations. However, because they did not use the exact Fourier coefficients for \bar{w} , their equation is not identical with Equation [42] of the present analysis.

$$\phi_1^4 = \frac{\pi^4}{4\beta^4} \left\{ \frac{\left[1 - \frac{y}{2}(1 - a_1)\right] \left(\frac{1}{\phi_1} - 2\right) + 4ya_1\phi_1(3 - 4\phi_1) + 1}{\left[1 - \frac{y}{2}(1 - a_1)\right] \left(\frac{3}{\phi_1} - 2\right) + 4ya_1\phi_1 + 1} \right\} \quad [43]$$

where y is $(2 - \nu)\eta_\infty$ and $\frac{h^2\lambda_1^4}{12R^2(1 - \nu^2)}$ has been replaced by $\frac{\pi^4}{4\beta^4}$. Equations [42] and [43] can be combined in such a way that the following result is obtained:

$$\frac{p_c}{E} \left(\frac{R}{h}\right)^2 = - \frac{\pi^2}{\beta^2 \phi_1^2 \sqrt{3(1 - \nu^2)}} \left\{ \frac{1}{\left[1 - \frac{y}{2}(1 - a_1)\right] \left(\frac{3}{\phi_1} - 2\right) + 4ya_1\phi_1 + 1} \right\} \quad [44]$$

where p_c is the critical buckling pressure. The quantity $\frac{p_c}{E} \left(\frac{R}{h}\right)^2$ is thus represented as a function of β only, as ϕ_1 assumes its critical value defined in terms of β by Equation [43]. Since this equation cannot be solved explicitly for ϕ_1 , a system of plotting was used to obtain ϕ_1 as a graphical function of β , shown in Figure 7. A plot of $\frac{nL_f}{\pi R}$ versus β ,

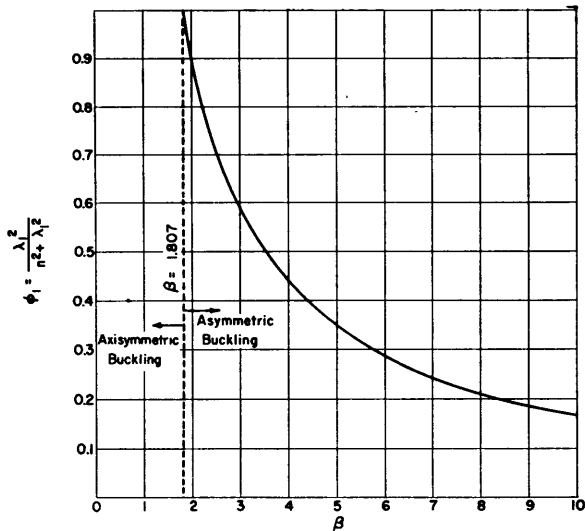


Figure 7 - ϕ_1 as a Function of β for Simple Support ($\nu = 0.3$)

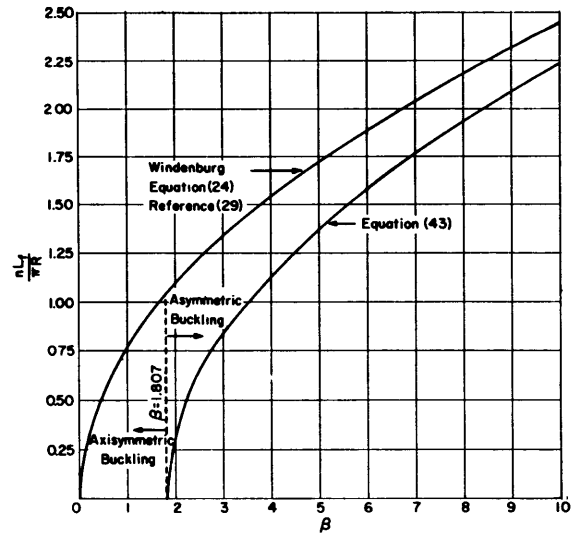


Figure 8 - n as a Function of β for Simple Support ($\nu = 0.3$)

obtained directly from Figure 7, is shown in Figure 8 together with a comparable curve obtained from Windenburg's Equation [24]* of Reference 29, based on the Von Mises solution. It should be noted that according to Equation [43], the condition for axisymmetric buckling ($\phi_1 = 1$, or $n = 0$) occurs where the value of β is approximately 1.807. In cases where β is less than 1.807, Equation [43] has no physical significance, n being zero for all such cases. The plot of Equation [43] in Figure 8 shows that as β is reduced, n does not increase indefinitely. Evidently, it attains some limiting value after which it decreases until the axisymmetric condition is reached.

With appropriate values of ϕ_1 determined from Figure 7, a plot of Equation [44] was obtained and is shown as the solid curve of Figure 9

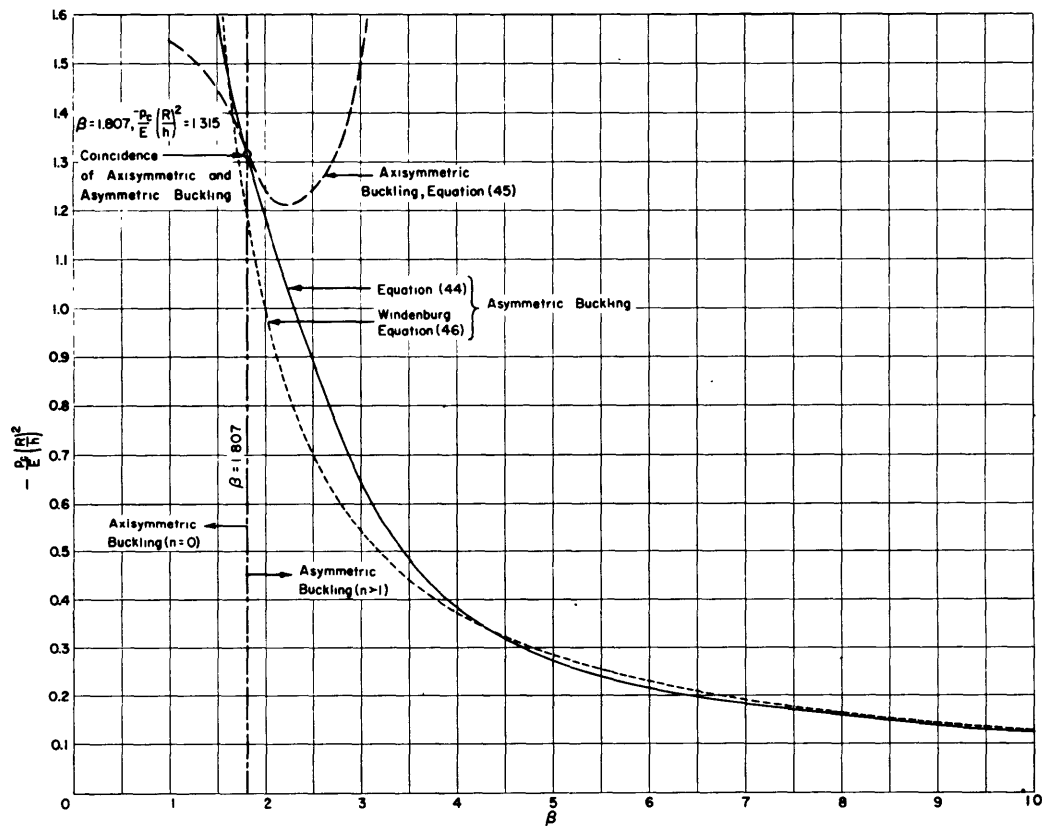


Figure 9 - Buckling Pressure as a Function of β for Simple Support ($\nu = 0.3$)

$$* \frac{nL_f}{\pi R} = 0.770 \sqrt{\beta}$$

where $\frac{P_c}{E} \left(\frac{R}{h}\right)^2$ is plotted as a function of β . Also shown is a curve for axisymmetric buckling representing the well-known equation

$$\frac{P_c}{E} \left(\frac{R}{h}\right)^2 = - \frac{1}{\sqrt{3(1-\nu^2)}} \left(\frac{2\beta^2}{\pi^2} + \frac{\pi^2}{2\beta^2} \right) \quad [45]$$

for $\beta < \pi$. This equation is readily obtained from Equation [42] if n is set equal to zero and is the same as that for the buckling of a cylinder under end thrust³⁴ where the length of a full longitudinal wave is equal to $2L_f$. It will be seen that the two curves intersect at the point $\beta = 1.807$, $\frac{P_c}{E} \left(\frac{R}{h}\right)^2 = -1.315$. Since Equation [45] is not applicable for $\beta > 1.807$, the curve is shown dashed in that region. Similarly, the curve of Equation [44] is shown dashed where $\beta < 1.807$. Figure 9 also includes a plot of the familiar equation of Windenburg²⁹ (shown dotted), often referred to as "EMB Formula [10]." This is an approximate representation of the Von Mises solution (see earlier footnote) in minimized form which, in the terminology of this report, can be expressed by*

$$\frac{P_c}{E} \left(\frac{R}{h}\right)^2 = - \frac{1.180}{\beta - 0.8175} \quad [46]$$

This equation and all three curves of Figure 9 are based on a value of ν of 0.3. Equation [46] is more conservative than Equation [44] in the low- β end of the asymmetric-buckling range because, as was pointed out in a previous footnote, the Von Mises analysis neglects the effect of boundary conditions on the initial (prebuckling) deformations.

It should be mentioned that the "beam-column" effect represented by the factor p/p_m appearing in a_m was found to have a negligible influence

*The formula is better known in its original form:

$$P_c = - \frac{2.60 \left(\frac{h}{2R}\right)^{5/2}}{\frac{L}{2R} - 0.45 \left(\frac{h}{2R}\right)^{1/2}}$$

on the curves of Figures 7, 8, and 9. The approximate form of Equation [40] is, therefore, sufficiently accurate, and was used in the construction of the curves.

RINGS OF INFINITE RIGIDITY (CLAMPED SUPPORT CONDITIONS)

Another special case of some interest is that of a shell having infinitely rigid rings. As indicated previously, a solution for this case cannot be obtained from the equations for finite rings by letting the frame rigidities become infinite. This is because the use of the stress function approximation has imposed certain constraints upon u and v which can give rise to serious errors when the frame parameters become very large. It is preferable instead to proceed from the more general Equation [5], allowing full variability of u and v (consistent with the boundary conditions) as well as of w . Since the shell is now fully clamped at regular intervals against any deformations, the boundary conditions are*

$$\bar{w} = w = v = w_x = u_\theta = 0 \quad \text{at} \quad x = 0, L_f \quad [47]$$

As in the case of simple support, the condition on \bar{w} requires that

$$\begin{aligned} \eta = \eta_\infty &= \frac{1}{\sum_{m=-\infty}^{\infty} a_m} \\ &= \frac{2}{\beta} \left(\frac{\cosh \beta - \cos \beta}{\sinh \beta + \sin \beta} \right), \quad \text{if pressure term in } a_m \text{ can be} \\ &\quad \text{neglected} \end{aligned}$$

The effect of imposing the conditions of Equation [47] is to cause all frame integrals in Equation [5] to vanish. If it is assumed as before that the bending energy ΔU_b involving the initial deflections can be neglected, Equation [5] becomes

*These conditions permit axisymmetric translation at the boundaries.

$$\begin{aligned}
\Delta U_T = & \frac{EhR}{2(1-\nu^2)} \int_0^{2L_f} \int_0^{2\pi} \left[u_x^2 + \left(\frac{w+v_\theta}{R} \right)^2 + 2\nu u_x \left(\frac{w+v_\theta}{R} \right) + \left(\frac{1-\nu}{2} \right) \left(v_x + \frac{u_\theta}{R} \right)^2 \right] dx d\theta \\
& + \frac{Eh^3}{24R(1-\nu^2)} \int_0^{2L_f} \int_0^{2\pi} \left[R^2 w_{xx}^2 + \left(\frac{w_{\theta\theta} + v_\theta}{R} \right)^2 + 2\nu w_{xx} (w_{\theta\theta} + v_\theta) \right. \\
& \quad \left. + \left(\frac{1-\nu}{2} \right) (2w_{x\theta} + v_x)^2 \right] dx d\theta \\
& + \frac{EhR}{2(1-\nu^2)} \int_0^{2L_f} \int_0^{2\pi} \left\{ \bar{w} \left[\frac{u_\theta^2}{R^2} + \left(\frac{w_{\theta\theta} + v_\theta}{R} \right)^2 + \nu (w_x^2 + v_x^2) - (1-\nu) \frac{u_\theta}{R} \left(v_x + \frac{u_\theta}{R} \right) \right] \right. \\
& \quad \left. + \bar{w}_x \left[2\nu w_x \left(\frac{w+v_\theta}{R} \right) + (1-\nu) \left(\frac{w_{\theta\theta} + v_\theta}{R} \right) \left(v_x + \frac{u_\theta}{R} \right) + 2u_x w_x \right] \right. \\
& \quad \left. + \bar{u}_x \left[v_x^2 + w_x^2 + \nu \left(\frac{u_\theta^2}{R^2} \right) + \nu \left(\frac{w_{\theta\theta} + v_\theta}{R} \right)^2 - (1-\nu) v_x \left(v_x + \frac{u_\theta}{R} \right) \right] \right\} dx d\theta \\
& - \frac{pR^2}{2} \int_0^{2L_f} \int_0^{2\pi} \left[\frac{2w}{R} + u_x \left(\frac{2w+v_\theta}{R} \right) + \frac{w^2+v^2}{R^2} + u_x \right] dx d\theta
\end{aligned} \tag{48}$$

It will be assumed that the buckling displacements can be represented by Equation [10]:

$$\begin{aligned}
u &= \cos n\theta \sum_{m=1}^{\infty} u_m \cos \left(\frac{\lambda_m x}{R} \right) \\
v &= \sin n\theta \sum_{m=1}^{\infty} v_m \sin \left(\frac{\lambda_m x}{R} \right) \\
w &= \cos n\theta \sum_{m=1}^{\infty} w_m \sin \left(\frac{\lambda_m x}{R} \right)
\end{aligned} \tag{10}$$

Before proceeding with the integration, a few assumptions can be made which simplify the results considerably. These are as follows:

$$\begin{aligned}
 w_\theta &>> v \\
 \int_0^{2\pi} w_\theta^2 d\theta &>> \int_0^{2\pi} u_\theta^2 d\theta, \int_0^{2\pi} R u_\theta v_x d\theta \\
 \int_0^{2\pi} w_x^2 d\theta &>> \int_0^{2\pi} v_x^2 d\theta, \int_0^{2\pi} \frac{u_\theta v_x}{R} d\theta \\
 \int_0^{2\pi} w^2 d\theta &>> \int_0^{2\pi} v^2 d\theta
 \end{aligned} \tag{49}$$

The basis for these conditions is the assumption that the relative orders of magnitude of u_m , v_m , and w_m can be estimated from the results of the stress function approximation (Equations [12]). The assumptions in Equation [49] are consistent with those made in Equations [17] and [25] through [27], and are based on the fact that unity is negligible compared with n^2 and λ_m^2 for short shells. If the small quantities in Equation [49] are neglected, Equation [48] is reduced to

$$\begin{aligned}
 \Delta U_T &= \frac{EhR}{2(1-\nu^2)} \int_0^{2L_f} \int_0^{2\pi} \left[u_x^2 + \left(\frac{w+v_\theta}{R} \right)^2 + 2\nu u_x \left(\frac{w+v_\theta}{R} \right) + \left(\frac{1-\nu}{2} \right) \left(v_x + \frac{u_\theta}{R} \right)^2 \right] dx d\theta \\
 &+ \frac{Eh^3}{24R(1-\nu^2)} \int_0^{2L_f} \int_0^{2\pi} \left[R^2 w_{xx}^2 + \frac{w_{\theta\theta}^2}{R^2} + 2\nu w_{xx} w_{\theta\theta} + 2(1-\nu) w_{x\theta}^2 \right] dx d\theta \\
 &+ \frac{EhR}{2(1-\nu^2)} \int_0^{2L_f} \int_0^{2\pi} \left\{ \frac{\bar{w}}{R} \left[\frac{w_\theta^2}{R^2} + \nu w_x^2 \right] + \bar{u}_x \left[\frac{\nu w_\theta^2}{R^2} + w_x^2 \right] \right. \\
 &\quad \left. + \bar{w}_x \left[2\nu w_x \left(\frac{w+v_\theta}{R} \right) + 2u_x w_x + (1-\nu) \frac{w_\theta}{R} \left(v_x + \frac{u_\theta}{R} \right) \right] \right\} dx d\theta \\
 &- \frac{pR^2}{2} \int_0^{2L_f} \int_0^{2\pi} \left[\frac{2w}{R} + u_x \left(\frac{2w+v_\theta}{R} \right) + \frac{w^2}{R^2} + u_x \right] dx d\theta \tag{50}
 \end{aligned}$$

When the series expressions, Equations [6] and [10], are substituted into Equation [50] and the integrations are performed, the result is

$$\begin{aligned}
\frac{R(1-\nu^2)}{Eh\pi L_f} \Delta U_T = & \frac{1}{2} \sum_{m=1}^{\infty} \left[u_m^2 \lambda_m^2 - 2\nu u_m \lambda_m (w_m + \nu v_m) + \left(\frac{1-\nu}{2} \right) (v_m \lambda_m - \nu u_m)^2 \right. \\
& \left. + (\nu v_m + w_m)^2 \right] + \frac{h^2}{24R^2} \sum_{m=1}^{\infty} \frac{w_m^2 \lambda_m^4}{\phi_m^2} \\
& + \frac{\psi(1-\nu^2)}{2} \sum_{m=1}^{\infty} \left[w_m^2 \left(n^2 + \frac{\lambda_m^2}{2} - 1 \right) + \lambda_m u_m (2w_m + \nu v_m) \right] \\
& + \frac{\psi(2-\nu)}{4} \eta_{\infty} \sum_{i=1}^{\infty} \sum_{j=1}^{\infty} \left\{ w_i w_j n^2 \left(a_{\frac{1}{2}(i+j)} - a_{\frac{1}{2}(i-j)} \right) (1-\nu^2) \right. \\
& \left. + [(\lambda_i + \lambda_j) a_{\frac{1}{2}(i+j)} + (\lambda_i - \lambda_j) a_{\frac{1}{2}(i-j)}] [2\nu \lambda_j w_j (\nu v_i + w_i) \right. \\
& \left. - 2w_j u_i \lambda_i \lambda_j - n(1-\nu) w_i (\lambda_j v_j - \nu u_j)] \right\} \quad [51]
\end{aligned}$$

where, for convenience, the equation has been divided by $\frac{Eh\pi L_f}{(1-\nu^2)R}$.

The boundary conditions (Equation [47]) on w and v are automatically satisfied by Equations [10]; the conditions on w_x and u_{θ} require

$$\begin{aligned}
\sum_{m=1}^{\infty} u_m &= \sum_{m=1}^{\infty} (u_m)(-1)^m = 0 \\
\sum_{m=1}^{\infty} w_m \lambda_m &= \sum_{m=1}^{\infty} w_m \lambda_m (-1)^m = 0
\end{aligned} \quad [52]$$

or

$$\sum_{m=1}^{\infty} u_{2m} = \sum_{m=1}^{\infty} u_{2m-1} = 0$$

$$\sum_{m=1}^{\infty} w_{2m} \lambda_{2m} = \sum_{m=1}^{\infty} w_{2m-1} \lambda_{2m-1} = 0 \quad [53]$$

Thus summations of the odd and the even terms must vanish separately.

The problem now is to arrive at a stationary value of the change in total potential, Equation [51], while at the same time satisfying the four conditions of constraint, Equation [53]. This can be done through the use of the Lagrange multiplier method which requires that the expression

$$U' = \frac{R(1-v^2)}{Eh\pi L_f} \Delta U_T + \alpha_1 \sum_{m=1}^{\infty} u_{2m-1} + \alpha_2 \sum_{m=1}^{\infty} w_{2m-1} \lambda_{2m-1}$$

$$+ \alpha_3 \sum_{m=1}^{\infty} u_{2m} + \alpha_4 \sum_{m=1}^{\infty} w_{2m} \lambda_{2m} \quad [54]$$

be stationary, where the α 's are the unknown multipliers. The requirement gives rise to the equations

$$\frac{\partial U'}{\partial u_j} = \frac{\partial U'}{\partial v_j} = \frac{\partial U'}{\partial w_j} = 0 \quad [55]$$

which can be written explicitly as follows:*

$$A_j u_j + B_j v_j + C_j w_j + \sum_{i=1}^{\infty} c_{ji} w_i + \frac{\alpha_1}{2} [1 - (-1)^j] + \frac{\alpha_3}{2} [1 + (-1)^j] = 0 \quad [56]$$

*The quantities designated by A_j , B_j , C_j , etc., should not be confused with other quantities appearing earlier in this report which bear the same notation.

$$B_j u_j + D_j v_j + E_j w_j + \sum_{i=1}^{\infty} e_{ji} w_i = 0$$

$$C_j u_j + E_j v_j + F_j w_j + \sum_{i=1}^{\infty} c_{ij} u_i + \sum_{i=1}^{\infty} e_{ij} v_i + \sum_{i=1}^{\infty} f_{ij} w_i \\ + \lambda_j \left\{ \frac{\alpha_2}{2} [1 - (-1)^j] + \frac{\alpha_4}{2} [1 + (-1)^j] \right\} = 0$$

where

$$A_j = \lambda_j^2 + \frac{n^2}{2} (1 - \nu)$$

$$B_j = -\frac{n\lambda_j}{2} [1 + \nu - \psi(1 - \nu^2)]$$

$$C_j = -\lambda_j [\nu - \psi(1 - \nu^2)]$$

$$D_j = \left(\frac{1 - \nu}{2} \right) \lambda_j^2 + n^2$$

$$E_j = n$$

$$F_j = 1 + \frac{h^2}{12R^2} (n^2 + \lambda_j^2)^2 + \psi(1 - \nu^2) \left[n^2 + \frac{\lambda_j^2}{2} - 1 \right]$$

$$c_{ji} = \frac{\psi(2 - \nu)}{4} \eta_{\infty} \left\{ a_{\frac{1}{2}(i+j)} (\lambda_i + \lambda_j) [n^2(1 - \nu) - 2\lambda_i \lambda_j] \right. \\ \left. + a_{\frac{1}{2}(i-j)} (\lambda_i - \lambda_j) [n^2(1 - \nu) + 2\lambda_i \lambda_j] \right\}$$

$$e_{ji} = \frac{\psi(2 - \nu)}{4} \eta_{\infty} \left\{ a_{\frac{1}{2}(i+j)} (\lambda_i + \lambda_j) [2\nu n \lambda_i - n(1 - \nu)\lambda_j] \right. \\ \left. - a_{\frac{1}{2}(i-j)} (\lambda_i - \lambda_j) [2\nu n \lambda_i + n(1 - \nu)\lambda_j] \right\}$$

$$f_{ij} = \frac{\psi(2 - \nu)}{2} \eta_{\infty} \left\{ n^2(1 - \nu^2) [a_{\frac{1}{2}(i+j)} - a_{\frac{1}{2}(i-j)}] \right. \\ \left. + \nu [a_{\frac{1}{2}(i+j)} (\lambda_i + \lambda_j)^2 - a_{\frac{1}{2}(i-j)} (\lambda_i - \lambda_j)^2] \right\}$$

It will be seen that once again the coupling conditions on the odd and the even modes are in effect because of the coefficients multiplying the α 's and the definition of a_m . Thus Equation [56] represents two systems of equations corresponding to all odd and all even values of j and i . As before, only the odd-valued system is of practical interest. If j and i are given an upper limit J , the complete set of equations for this system is

$$\begin{aligned}
A_j u_j + B_j v_j + C_j w_j + \sum_{i=1}^J c_{ji} w_i + \alpha_1 &= 0 \\
B_j u_j + D_j v_j + E_j w_j + \sum_{i=1}^J e_{ji} w_i &= 0 \\
C_j u_j + E_j v_j + F_j w_j + \sum_{i=1}^J (c_{ij} u_i + e_{ij} v_i + f_{ij} w_i) + \alpha_2 \lambda_j &= 0 \\
\sum_{i=1}^J u_i &= 0 \\
\sum_{i=1}^J \lambda_i w_i &= 0
\end{aligned} \tag{57}$$

$i, j = 1, 3, 5 \dots J$

the last two equations representing the two constraints. There are thus $2 + \frac{3(J+1)}{2}$ equations and, including α_1 and α_2 , $2 + \frac{3(J+1)}{2}$ unknowns. The system can be solved in the same manner as Equation [32]. However, it is highly complicated; moreover, because c_{ji} and e_{ji} are not generally invariant when i and j are interchanged, the matrix of the coefficients is not symmetric.

This situation can be greatly simplified if, as in the case of Equation [34], we neglect all c_{ji} , e_{ji} , and f_{ji} for which j and i are unequal. Further simplifications can also be made by neglecting the small quantity $\psi(1 - v^2)$ appearing in the coefficients B_j and C_j , and -1 in the second term of F_j . Equations [57] then reduce to

$$A_j u_j + B_j v_j + \bar{C}_j w_j + \alpha_1 = 0$$

$$B_j u_j + D_j v_j + \bar{E}_j w_j = 0$$

$$\bar{C}_j u_j + \bar{E}_j v_j + \bar{F}_j w_j + \alpha_2 \lambda_j = 0$$

$$\sum_{j=1}^{J_1} u_j = 0 \quad [58]$$

$$\sum_{j=1}^J \lambda_j w_j = 0 \quad j = 1, 3, 5 \dots J$$

where

$$A_j = \lambda_j^2 + \left(\frac{1-\nu}{2}\right) n^2$$

$$B_j = -\frac{n\lambda_j}{2} (1+\nu)$$

$$\bar{C}_j = -\nu\lambda_j + \psi\left(\frac{2-\nu}{2}\right) \eta_\infty a_j \lambda_j [n^2(1-\nu) - 2\lambda_j^2]$$

$$D_j = \left(\frac{1-\nu}{2}\right) \lambda_j^2 + n^2$$

$$\bar{E}_j = n - \psi\left(\frac{2-\nu}{2}\right) \eta_\infty a_j \lambda_j^2 n (1-3\nu)$$

$$\begin{aligned} \bar{F}_j = 1 + \frac{h^2}{12R^2} (n^2 + \lambda_j^2)^2 + \psi(1-\nu^2) \left(n^2 + \frac{\lambda_j^2}{2}\right) \\ + \psi\left(\frac{2-\nu}{2}\right) \eta_\infty [n^2(1-\nu^2)(a_j-1) + 4\nu a_j \lambda_j^2] \end{aligned}$$

The equations can be solved in a manner similar to that followed in the solution of Equations [35]. From the first three equations, v_j is eliminated and the expressions

$$\begin{aligned}
u_j &= \frac{\alpha_1 (\bar{E}_j^2 - \bar{F}_j D_j)}{G_j} + \frac{\alpha_2 \lambda_j (\bar{C}_j D_j - B_j \bar{E}_j)}{G_j} \\
w_j &= \frac{\alpha_1 (\bar{C}_j D_j - B_j \bar{E}_j)}{G_j} + \frac{\alpha_2 \lambda_j (B_j^2 - A_j D_j)}{G_j}
\end{aligned} \tag{59}$$

$$G_j = \bar{C}_j (B_j \bar{E}_j - \bar{C}_j D_j) + \bar{E}_j (B_j \bar{C}_j - A_j \bar{E}_j) + \bar{F}_j (A_j D_j - B_j^2) \neq 0$$

are obtained. When these are substituted into the last two of Equations [58] and α_1 and α_2 are eliminated, the resulting buckling equation is

$$\left[\sum_{j=1}^J \frac{\lambda_j (\bar{C}_j D_j - B_j \bar{E}_j)}{G_j} \right]^2 - \left[\sum_{j=1}^J \frac{\lambda_j^2 (B_j^2 - A_j D_j)}{G_j} \right] \left[\sum_{j=1}^J \frac{\bar{E}_j^2 - D_j \bar{F}_j}{G_j} \right] = 0$$

$j = 1, 3, 5 \dots J$ [60]

By neglecting the small terms involving ψ^2 , the complexity of the expressions is greatly reduced, and after some rearrangement, the equation takes the form

$$\left[\sum_{j=1}^J \frac{R_j}{Q_j} \right]^2 - \left[\sum_{j=1}^J \frac{S_j}{Q_j} \right] \left[\sum_{j=1}^J \frac{T_j}{Q_j} \right] = 0$$

$j = 1, 3, 5 \dots J$ [61]

in which

$$Q_j = \frac{h^2 \lambda_j^4 (1+k_j)^4}{12R^2(1-\nu^2)} + \psi \lambda_j^2 \left[\frac{(1+k_j)^2}{2} \left\{ k_j [2 - y(1-a_j)] + 1 \right\} + 4y k_j a_j \right] + 1$$

$$R_j = k_j - \nu$$

$$S_j = \lambda_j^2 (1+k_j)^2$$

$$T_j = \frac{1}{\lambda_j^2} + \frac{h^2}{12R^2} \lambda_j^2 (1+k_j)^2 \left(1 + \frac{2k_j}{1-\nu}\right) + \psi \left\{ [k_j(2-y) + 1] \left(\frac{1-\nu}{2} + k_j\right) (1+\nu) + y a_j \left[k_j \left(\frac{5-\nu^2}{2}\right) + k_j^2 (1+\nu) + 2\nu \right] \right\}$$

$$k_j = \frac{n^2}{\lambda_j^2}$$

The solution of Equation [61] can be accomplished graphically with the same procedure described for Equation [39]. Once again the lowest root should occur between the first two asymptotes where Q_1 and Q_3 vanish. The accuracy of the result will depend, as before, on the size of J .

NUMERICAL EXAMPLE

The example to be used for numerical study is the test of the machined cylinder BR-4B having external rectangular stiffeners and which is considered in the section on experimental work. Its dimensions in inches are as follows:

$$\begin{aligned} R &= 8.048 \\ h &= 0.081 \\ L_f &= 4.266 \\ d \text{ (frame depth)} &= 0.570 \\ b \text{ (frame width)} &= 0.138 \\ \beta &= 6.80 \end{aligned}$$

The value of β (6.80) is considerably larger than that usually encountered in pressure-vessel design.

Rings of Finite Rigidity

As a preliminary to the calculations, Table 1 shows the first 11 coefficients (a_m) of the initial deflections (\bar{w} and \bar{u}) as calculated by Equation [8]; m is written with the absolute value sign since both positive and negative values are permitted. Despite the relatively large value of β ,

Table 1

Coefficients of the Initial Deflections
for Cylinder BR-4B

$ m $	a_m Equation [8]
0	1.00000
1	0.84590
2	0.25538
3	0.06345
4	0.02099
5	0.00870
6	0.00422
7	0.00228
8	0.00134
9	0.00084
10	0.00055
11	0.00037

Table 2

Comparison of Approximate and
Matrix Solutions for Cylinder
BR-4B with Finite Rings

J	Buckling Pressure, psi	
	Matrix Equation [33]	Approximate Equation [39]
1	693.1*	693**
3	657.1	668
5	646.3	654
7	641.4	648
9	638.7	645
11	636.9	642
13	635.7	*Calculations performed on IBM-7090 computer
15	634.8	
17	634.1	
19	633.5	
21	633.1	**Slide rule calculations
Pressures for $n=11$, $E=28.9 \times 10^6$ psi		

the convergence of $\sum_{m=-\infty}^{\infty} a_m$ is quite rapid. For purposes of calculation, only the first four or five values are significant. As previously indicated, the convergence will be more rapid for smaller values of β .

It is of some interest to compare results of the matrix solution, Equation [33], and the simplified solution, Equation [39]. The critical buckling mode for both equations was found to be 11.* Table 2 shows the buckling pressures according to these two solutions for successive values of J. Since Equation [33] was solved using an IBM-7090 computer, results were readily obtainable for large values of J (an arbitrary limit of 21 was imposed). Solutions of Equation [39] were obtained

*Before the calculations were begun, a preliminary estimate of the critical value of n was obtained from Figure 8 for the case of simple support.

by slide rule up to $J = 11$; it did not appear worthwhile to continue beyond this.

The information in Table 2 is also shown graphically in Figure 10. It is evident that the convergence of both solutions is fairly rapid so that little accuracy is gained in proceeding beyond, say, $J = 7$. Such a conclusion, however, cannot be stated generally. If the frames had been larger, the solutions would probably have converged more slowly. For this example it also appears that Equation [39] is a reasonably accurate approximation to Equation

[33].* Furthermore, since the accuracy of the approximation depends only on the rapidity of convergence of $\sum_{m=-\infty}^{\infty} a_m$, one should expect closer agreement for smaller values of β .

Equation [33] also permits the determination of the relative amplitudes w_j of the buckling modes. Table 3 lists the ratios w_j/w_1 for $n = 11$ and $J = 21$. It will be noted that the components are of successively decreasing magnitude and the first is much larger and of opposite sign from all the rest. The rotation of a frame $w_1 \lambda_1/R$ produced by the first component is thus partially reduced by the sum of the succeeding components.

Simple Support Conditions

Results of calculations for Cylinder BR-4B ($\beta = 6.80$) with simple supports replacing the rings are given in Table 4. The pressure and mode obtained from the minimized curves of Figures 8 and 9, representing Equations [43] and [44], compare well with the results for the unminimized

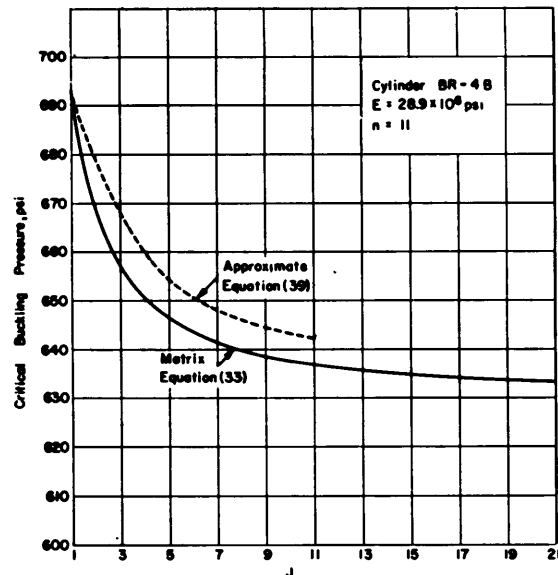


Figure 10 - Variation in Approximate and Matrix Solutions with J for Cylinder BR-4B

*Since Equation [39] does not contain the approximation in the linear case, the results of both equations should be identical for $J = 1$.

Equation [42]. Corresponding results for the Von Mises solution, also obtained from Figures 8 and 9, show a slightly higher pressure and different mode. This difference reflects the influence of the boundary conditions on the initial deformations. Although for this case, the inclusion of this effect gives rise to a lower pressure, Figure 9 shows that the pressures will be higher for $\beta < 4.35$.

Rings of Infinite Rigidity

Using Equation [61], it should be possible to approach as closely as desired the exact solution to the problem of fixed support, consistent with the approximations made in the derivation of the equation. It may be surprising, then, to consider the results of calculations for Cylinder BR-4B given in Table 5. Equation [61], carried out to the eleventh degree

Table 3
Relative Amplitudes of Buckling Modes for Cylinder BR-4B with Finite Rings

j	w_j/w_1 Equation [33] n = 11 J = 21
1	1.00000
3	- 0.06654
5	- 0.01962
7	- 0.00773
9	- 0.00378
11	- 0.00211
13	- 0.00129
15	- 0.00085
17	- 0.00058
19	- 0.00042
21	- 0.00031

Table 4
Buckling Pressures for Cylinder BR-4B with Simple Supports

Solution	P_c	n
Equation [42]	550	11
Minimized Form (Figures 8 and 9)	551	11
Minimized Von Mises Solution ²⁹ (Figures 8 and 9)	580	12
Shell length assumed to be center-to-center frame spacing ($L_f = 4.266$ in.)		

Table 5
Buckling Pressures for Cylinder BR-4B
with Infinitely Rigid Rings

Effect of Boundary Conditions on Initial Deflections	Theory	P _c psi	n
Included $\left[a_m = \frac{1}{1 + 4 \left(\frac{m\pi}{\beta} \right)^4} \right]$	Equation [61] (J = 21)	811	11
Neglected (a _m = 0)	Equation [61] (J = 21)	810	11
	Nash ³⁵	804	12
In all cases, shell length was taken to be the center-to-center frame spacing (L _f = 4.266 in.)			

(J = 21), gave a buckling pressure of 811 psi for n = 11, while the far simpler equation* of Nash³⁵ gave 804 psi for n = 12. This latter equation is almost identical with that obtained by Galletly and Bart²³ and is in good agreement with other more complicated solutions also obtained by Nash.¹⁶ The fundamental characteristic of all of these solutions is that they are based on the assumed buckling configuration

$$w = w_o \left[1 - \cos \left(\frac{\lambda_2 x}{R} \right) \right] \quad [62]$$

*

$$P_c = \frac{-\frac{Eh}{R} \left\{ \frac{h^2}{12R^2(1-\nu^2)} \left[8\lambda_1^4 + \frac{3n^4}{2} + 4\lambda_1^2 n^2 \right] + \frac{8\lambda_1^4}{(4\lambda_1^2 + n^2)^2} \right\}}{\frac{3}{2}(n^2 - 1) + \lambda_1^2}$$

In all calculations, the distance between supports was taken to be the center-to-center frame spacing (L_f = 4.266 in.). Frequently, when formulas of this type are applied to ring-stiffened cylinders, the inner or unsupported distance between frames is used.

This function will not, in general, satisfy the differential equations of equilibrium. Rather it has been chosen somewhat arbitrarily because it satisfies the boundary conditions and is conveniently used with the energy method. When applied to ring-stiffened cylinders, the solutions based on this function have often predicted pressures much higher than those observed experimentally. Consequently, one natural conclusion is that the use of a different function could lead to lower pressures. While the results in Table 5 are too limited to warrant a general conclusion, they indicate that the configuration of Equation [62] may in fact be nearly correct and that the difficulty actually lies in the assumption that full fixity can be provided by rings of practical size.

It is also worth noting that the convergence of Equation [61] was much slower than for the other two cases previously discussed. This was caused by the slow convergence of $\sum_{j=1}^J \frac{S_j}{Q_j}$ which necessitated carrying the calculations out to $J = 21$. From this it may be concluded that the sine series (Equation [10]) is not well suited to the boundary conditions for fixed supports and that the use of some other set of functions, similar, for example, to Equation [62], would probably result in more rapid convergence.

Table 5 also shows that for the geometry in question, the influence of the boundary conditions on the initial deflections had a negligible effect on the collapse pressure. When this influence is neglected ($a_m = 0$), the initial deflections are those for an infinitely long cylinder, the condition assumed by Nash, and the buckling pressure is 810 psi. That the pressure (804 psi) given by the Nash equation is lower than this can probably be explained by the fact that the buckling configuration assumed by Nash does not completely satisfy the boundary conditions of Equation [47]. Because of certain approximations arising from the use of a stress function of the Donnell type, the circumferential buckling strain e_θ does not vanish at the boundaries.*

*Following the procedure indicated in Appendix E, Nash eliminates u and v through the use of a stress function. Because w for this case is of the form of Equation [62], the resulting stress function is

In view of these results, it might be of interest to compare the buckling configuration employed in the present analysis with that represented by Equation [62] for this example on a quantitative basis. By suitable rearrangement of Equations [58] through [61], an equation expressing the relative magnitude of the corresponding buckling coefficients w_j is obtained:

$$\frac{w_i}{w_j} = \frac{1}{j} \left(\frac{\Gamma_i}{\Gamma_j} \right) \quad [63]$$

where

$$\Gamma_k = \frac{R_k}{Q_k} \sum_{j=1}^J \frac{R_j}{Q_j} - \frac{S_k}{Q_k} \sum_{j=1}^J \frac{T_j}{Q_j} \quad j, k = 1, 3, 5 \dots J$$

*(Footnote continued from preceding page)

$$F = - \frac{ER\lambda_2^2}{n^2 + \lambda_2^2} w_0 \cos n\theta \cos \left(\frac{\lambda_2 x}{R} \right)$$

in the notation of this report, and the circumferential strain,

$$e_\theta = \frac{1}{E} \left(\frac{\partial^2 F}{\partial x^2} - \frac{\nu \partial^2 F}{R^2 \partial \theta^2} \right)$$

does not vanish at $x = 0$ and $x = L_f$. However, if Equations [122] of Appendix E are modified so that

$$\sigma_x = \frac{\partial^2 F}{R^2 \partial \theta^2} + f(\theta)$$

$$\sigma_\theta = \frac{\partial^2 F}{\partial x^2} + g(\theta)$$

$$\sigma_{x\theta} = - \frac{\partial^2 F}{R \partial x \partial \theta}$$

it is then possible to satisfy the condition on e_θ by proper adjustment of the functions $f(\theta)$ and $g(\theta)$. The resulting buckling pressure is slightly higher than that given by Nash.

and all quantities retain the definitions of Equation [61]. An equivalent of Equation [63] can be obtained for the buckling configuration of Nash by expanding the function*

$$\begin{aligned} w &= w_0 \left(1 - \cos \frac{\lambda_2 x}{R} \right) & 0 \leq x \leq L_f \\ w &= -w_0 \left(1 - \cos \frac{\lambda_2 x}{R} \right) & L_f \leq x \leq 2L_f \end{aligned} \quad [64]$$

in a Fourier series. The result is

$$\begin{aligned} w &= \sum_{j=1}^J w_j \sin \frac{\lambda_j x}{R} \\ w_j &= -\frac{16w_0}{\pi j(j^2 - 4)} \quad j = 1, 3, 5 \dots J \end{aligned} \quad [65]$$

In order to compare these results, calculations were carried out with the aid of Equation [63] for the numerical example where $a_m = 0$, $J = 21$, and $p_c = 810$ psi. The results appear in Table 6 in the form of w_j/w_1 , together with the corresponding values from Equation [65]. Ratios beyond $j = 11$ were not calculated. It will be seen that there is considerable difference in the individual coefficients. Apparently their total effect is such that the difference in buckling pressures is insignificant.

SUMMARY AND CONCLUSIONS

1. An analysis for the elastic buckling of ring-supported cylindrical shells has been developed which considers the influence of the rings on deformations before and during buckling.

2. The bending stresses associated with the prebuckling deformations have a negligible effect on the theoretical buckling strength.

*The function in Equation [64] is periodic in the interval $0 \leq x \leq 2L_f$ while Equation [62] repeats itself in each bay. However, their corresponding buckling pressures are identical.

Table 6
 Comparison of Buckling Configurations for Cylinder
 BR-4B with Infinitely Rigid Rings

j	w_j/w_1	
	Equation [63]*	Equation [65] (Nash ³⁵)
1	1.0000	1.0000
3	-0.1492	-0.2000
5	-0.0387	-0.0286
7	-0.0173	-0.0095
9	-0.0085	-0.0045
11	-0.0047	-0.0023
* $a_m = 0$; $J = 21$; $n = 11$; $p_c = 810$ psi.		

3. The buckling equations for a shell with finite rings represented by the stability determinant, Equation [33], can be approximated with good accuracy by the single Equation [39].

4. A special result of the general analysis is the buckling equation for a shell with simple supports. This differs from the buckling equation of Von Mises since it accounts for the effect of the boundary conditions on the prebuckling deformations.

5. Another special case is that for a shell with fully fixed edges. It appears possible from numerical results that the use of the simplified form $1 - \cos \frac{2\pi x}{L_f}$ to represent the longitudinal buckling profile may be a reasonable approximation for this case.

6. The energy approach has been used to obtain the trigonometric series equivalent of the solution of Pulos and Salerno for the initial axisymmetric deformations of a ring-stiffened cylinder. This form has certain mathematical advantages, particularly when employed in the solution of buckling problems.

PART II - EXPERIMENT

EARLIER TESTS

Following the early work of Windenburg,²⁹ later experimental studies at the Model Basin were directed toward the evaluation of classical buckling theory for short shells. Tests of ring-stiffened cylinders, designated BR-1³⁰ and BR-5³¹, which were fabricated from steel plate by welding and not stress relieving, resulted in collapse pressures well below theoretical expectations. It was suspected that these discrepancies could be attributed to weakening effects of imperfect circularity and residual rolling and welding stresses. To investigate this suspicion further, two additional cylinders, BR-4³⁶ and BR-4A³⁷, were tested. These were identical in geometry and in material properties, but BR-4 was rolled and welded while BR-4A was machined from a stress-relieved thick cylinder. The results of the tests were striking. Both failures were inelastic with lobes appearing between stiffeners. However, BR-4 collapsed at 390 psi whereas BR-4A collapsed at 550 psi.

With the weakening effects of imperfections so clearly demonstrated, it was evident that further attempts to obtain elastic buckling data with imperfect, fabricated cylinders would be fruitless. A better alternative appeared to be the study of machined and initially stress-free cylinders. This approach had already proven successful in experimental studies of general instability.^{4,5,6} Accordingly, a third test cylinder, designated BR-4B, was manufactured. Geometrically, this was a smaller scale version of BR-4 and BR-4A, but it was machined from tubing of higher yield strength. With this combination of properties, it was expected that collapse would be initiated by elastic buckling.

DESCRIPTION OF TEST CYLINDER

BR-4B, whose dimensions were given as a numerical example earlier in this report, was a 6/10-scale model of BR-4A. As shown in Figure 11, it consisted of four central full-length bays and a short bay at each end terminated by a heavy bulkhead ring. One ring had evenly spaced holes to accept bolts for a flat closure head. The four-bay arrangement

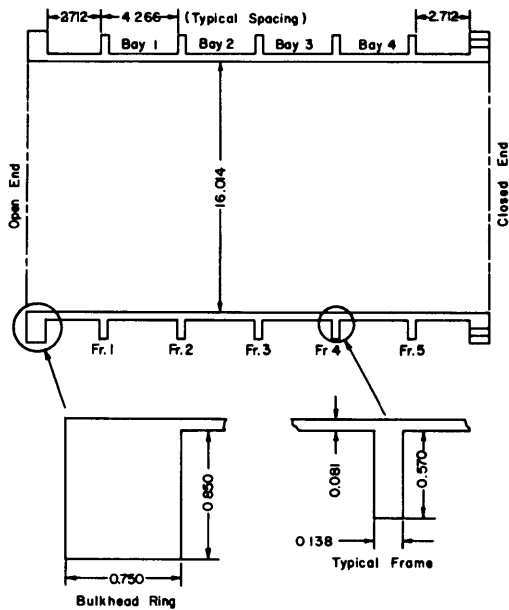


Figure 11 - Test Cylinder BR-4B
All dimensions in inches

For this purpose, a ring specimen was taken from one of the bulkhead rings at the conclusion of the tests. Measurements of the deflections of the ring under diametral point loading were used to establish a modulus of 28.9×10^6 psi. This procedure is described in Appendix F.

PRELIMINARY TEST

One of the objectives of the investigation was to determine whether any region in the area of failure had been stressed beyond the elastic limit prior to collapse. Ideally this would indicate extensive strain-gage instrumentation of this critical area, but to locate such an area prior to testing is an impossibility. On the other hand, it was not practical to provide each bay with such extensive strain-gage instrumentation that adequate coverage of any area would be insured. Consequently, it was decided that a preliminary test should be carried out in an effort to determine in which bay buckling would initiate. If this could be accomplished, the critical bay would then be liberally instrumented and a second test carried out in which the cylinder would be taken to collapse. An additional possibility was that

was intended to provide a central test section free of end effects. The cylinder was machined from a thick, forged-steel tube which had been part of a gun barrel liner. Compression tests of specimens taken from the tube prior to machining indicated a yield strength of 82,500 psi (based on an offset strain of 0.002) compared with 50,000 psi for BR-4 and BR-4A. The elastic limit was found to be 74,400 psi. Since the elastic buckling strength of the cylinder would be directly proportional to the modulus of elasticity of the material, it was important that this quantity be determined accurately.

nonlinear elastic strains would appear during the preliminary tests, and would be of such a magnitude that the buckling pressure could be predetermined by means of the Southwell method. This procedure had been used with considerable success in tests of cylinders collapsing by general instability,³⁸ but as yet had not been tried in the case of shell instability. Since nonlinear strains were not observed in the test of BR-4A, it was not expected that they would appear at pressures below 540 psi, the highest pressure at which strains were measured during that test.

The exterior of the cylinder was instrumented with electrical resistance strain gages located circumferentially at intervals of 10 deg in the middle of each of the four typical bays and extending completely around the circumference. Temperature compensation was provided by "dummy" gages. The test chamber was a 2500-psi pressure tank, 20 in. in diameter, and oil was used as the pressurizing fluid. Prior to the actual test, the cylinder was immersed in the tank in a free-flooding condition. The pressure was then raised in increments to 500 psi and strains measured to detect gages that were undesirably "pressure-sensitive." Those which exhibited a sensitivity of 5 $\mu\text{in.}/\text{in.}$ or more for 100 psi were considered unsatisfactory. These gages were then checked by observing the strain induced when local pressure was applied to the gage. It was found that this procedure was an adequate substitute for the pressurizing method, and it was used subsequently as gages were successively replaced and checked until all were satisfactory.

The cylinder was then placed in the tank with one end closed by a flat, circular plate and the other sealed against the tank top, which had an opening to permit access to the interior of the cylinder. While strains were read with automatic strain recorders, the pressure was applied in small increments up to 570 psi. All strains were still linear at this pressure, and it appeared that proceeding to a higher pressure would only increase the risk that the cylinder would collapse before more extensive instrumentation could be installed. The pressure was, therefore, reduced in increments back to zero.

It was apparent from the strain plots that no yielding had taken place. The largest apparent permanent set for all operating gages was 45 $\mu\text{in.}/\text{in.}$ which was considered insignificant in a total strain of 1500 to 1800 $\mu\text{in.}/\text{in.}$,

Table 7
Circumferential Strain Sensitivities (Exterior)
at Midbay, Preliminary Test

Bay	Compressive Strain Sensitivity in micro-inches per inch per psi		
	Maximum	Minimum	Average of All Gages
1	2.91	2.52	2.74
2	2.96	2.40	2.83
3	3.15	2.72	2.97
4	3.12	2.79	2.92
Theory of Reference 33: Sensitivity = 3.03			

and probably due to the overall effect of pressure sensitivity and drift in the measuring system. The strain sensitivities in micro-inches per inch per pound per square inch observed during the tests are summarized in Table 7. The average sensitivity was highest (2.97) in Bay 3 and next highest (2.92) in Bay 4. The maximum individual sensitivity was observed at 90 deg in Bay 3. On the basis of these measurements, it appeared that Bay 3 would be critical, but that Bay 4 would also deserve close attention. Final instrumentation of the cylinder, carried out on the basis of these observations, is described in the next section.

FINAL TEST

Instrumentation and Test Procedure

Gage locations for the final test are shown in Figure 12. This time, interior as well as exterior gages were installed, the total number being limited to the capacity of the available automatic recorders. Most of the gages were concentrated in Bays 3 and 4 with major emphasis on Bay 3. The pairs of circumferential and longitudinal gages were so arranged that stresses could be measured at the two locations (outside at midbay and

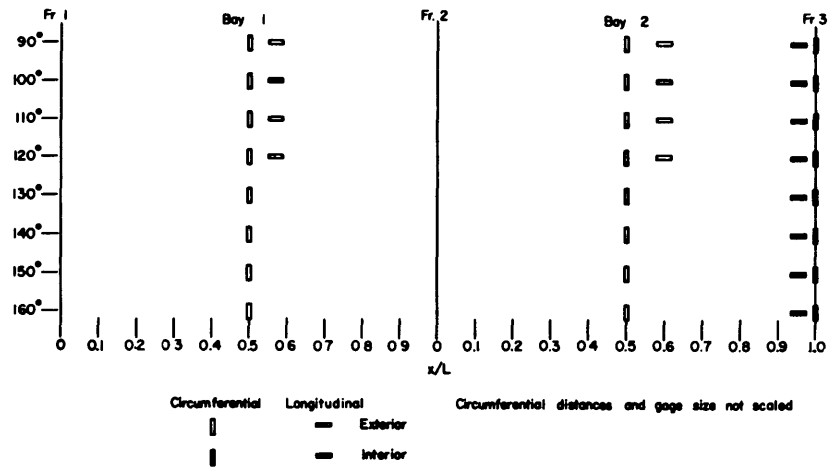


Figure 12a - Bays 1 and 2

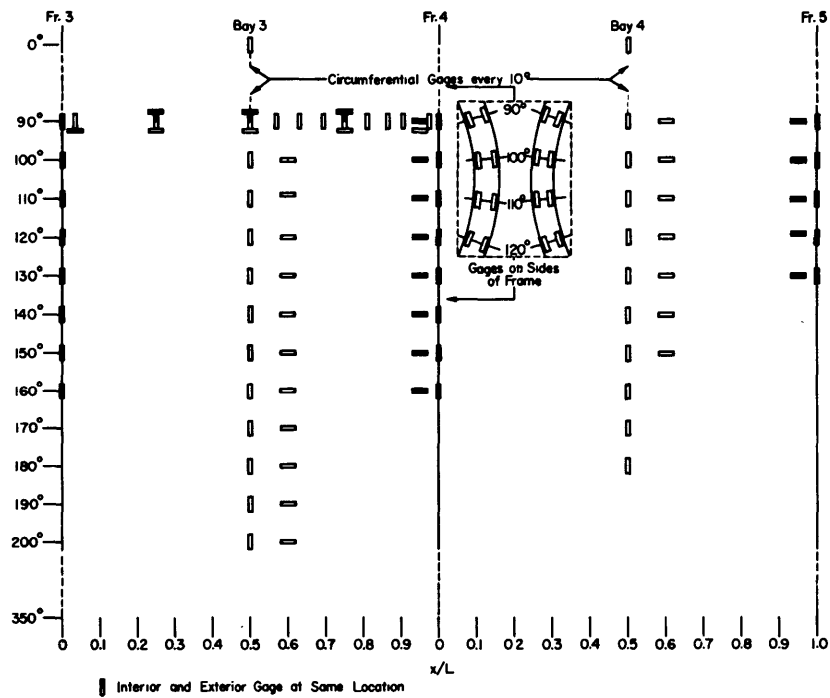


Figure 12b - Bays 3 and 4

Figure 12 - Gage Locations for Final Test

Table 8
Loading Schedule for Final Test

Pressures (psi) at which Strains Were Measured			
First Run		Second Run	
0	570	0	610
50	580	100	620
100	590	200	630
200	600	300	Failure
300	610	400	(633)
400	570	500	377
500	500	540	(Residual)
520	300	560	
540	100	580	0
560	0	600	

inside at a frame) where they are normally highest. The midbay arrays of circumferential gages were located in the four typical bays for the purpose of detecting lobe patterns should they appear prior to collapse. These measurements would be utilized in determining the elastic buckling pressure by means of the Southwell method.³⁸ The exterior circumferential gages located in Bay 3 along the 90-deg generator were intended to give an indication of the longitudinal profile of a lobe in the event one appeared. Since the highest strain in the preliminary test was meas-

ured at 90 deg in Bay 3, this appeared to be a likely location for the development of a lobe trough. Gages were also mounted on the sides of Frame 4 to provide a measure of any twisting and bending that might take place prior to collapse. All exterior gages were examined for pressure sensitivity and replaced in accordance with the procedure followed for the preliminary test.

Two pressure runs were made during the final test, as indicated in Table 8. On the first run, a maximum pressure of 610 psi was attained. During the second run, collapse occurred suddenly at 633 psi, the last strain readings having been made at 630 psi, and the pressure immediately dropped to a residual value of 377 psi.

Results and Discussion

Visible damage to the cylinder, as shown in Figure 13, was confined to Bays 3 and 4 where a typical lobar pattern developed in the area of heaviest instrumentation. While the lobes did not completely encircle the circumference, a close examination indicated that a complete pattern would have contained 11 lobes.



Figure 13a - Exterior View

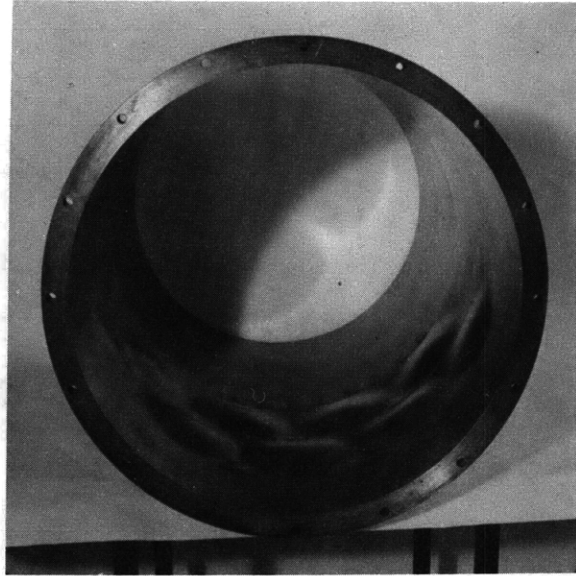


Figure 13b - Interior View

Figure 13 - Views of Collapsed Cylinder BR-4B

During the first run, the strains were generally linear with pressure up to about 590 psi. Small deviations from linearity appeared at 600 psi, and became more noticeable when 610 psi was reached. On the unloading portion of the run, the strain-pressure plots obtained during loading were in most cases retraced. At the conclusion of the run, the maximum zero shift was approximately 50 $\mu\text{in.}/\text{in.}$ There appeared to be no correlation in general between zero shifts and departures from linearity observed during the pressure run. As in the preliminary run, the shifts can be attributed to error in the measuring system rather than to a significant yielding of the material.

On the second run, the deviations from linearity again appeared at 600 psi and grew with pressure until, at 630 psi, a pronounced lobar pattern was evident. Such patterns have often been observed in stiffened cylinders prior to collapse by general instability.³⁸ They are produced by initial imperfections which, even though minute in machined cylinders, have a decided effect near the point of buckling. Figure 14 shows some examples of the strain-pressure plots for both runs. The circumferential

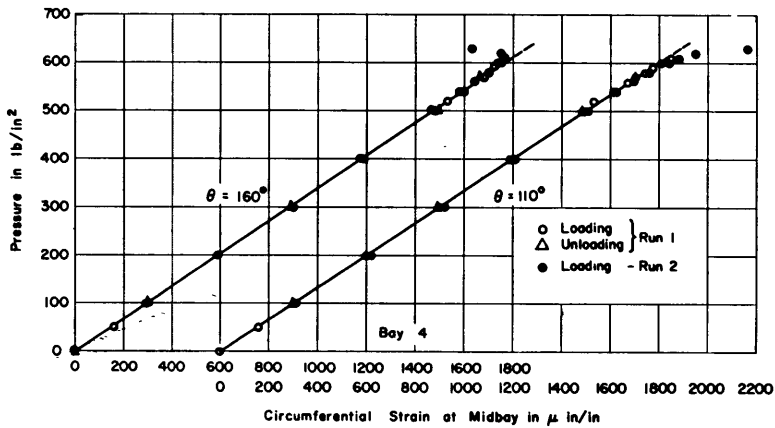
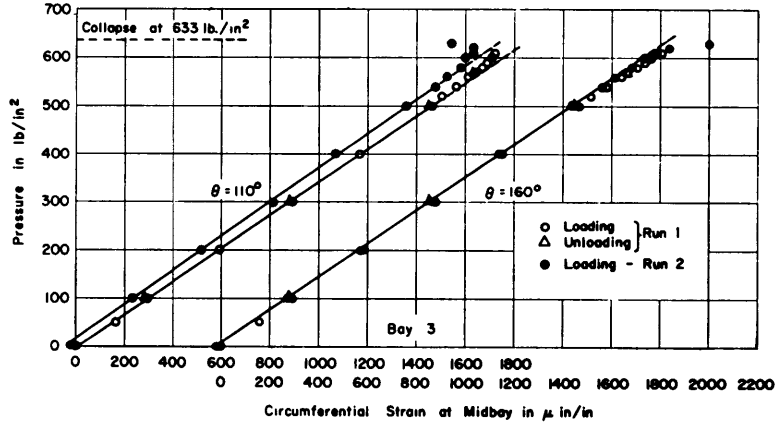


Figure 14 - Typical Plots of Circumferential Strains at Midbay versus Pressure (Final Test)

lobar strain patterns in Bays 3 and 4 at 630 psi are shown in Figure 15. For contrast, the strains at 500 psi are also shown. It will be seen that the patterns in the two bays are staggered, just as are the final deformations in Figure 13. Although the strain patterns are not complete because of a few gage failures, close inspection of both patterns indicates the existence of 11 lobes. It can also be seen that, as anticipated, a lobe trough developed at or near the 90-deg generator of Bay 3.

From strain data of the type shown in Figure 14, it was possible to obtain Southwell plots of fairly good quality. Plots for the gages of Figure 14 appear in Figure 16. With this method, the nonlinear component (ϵ^*)

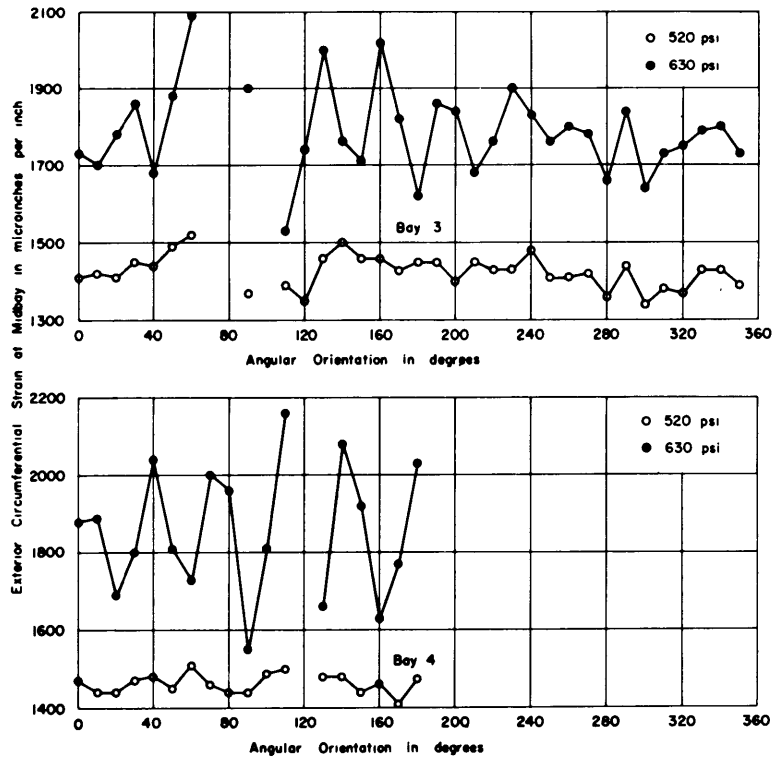


Figure 15 - Circumferential Strain Patterns
(Run 2, Final Test)

of the total strain is determined and plotted against the ratio $\frac{\epsilon^*}{p}$.[†] The elastic buckling pressure is then obtained from the slope of the resulting straight line plot. This was done for a number of midbay circumferential gages located externally in Bays 3 and 4. The gages were selected on the basis of data quality from those showing the largest deviations from linearity. Table 9 gives a summary of these results. It can be seen that the pressures are all in good agreement. Furthermore, the average buckling pressure of 637 psi is very close to the experimental collapse pressure

[†]Since ϵ^* is positive or negative depending on the gage orientation, $|\epsilon^*|$ and $|\frac{\epsilon^*}{p}|$ were used in Figure 16 so that all points would lie in the first quadrant.

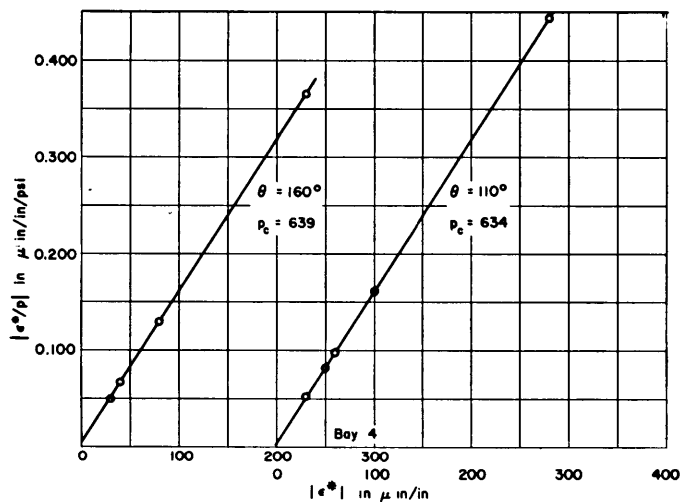
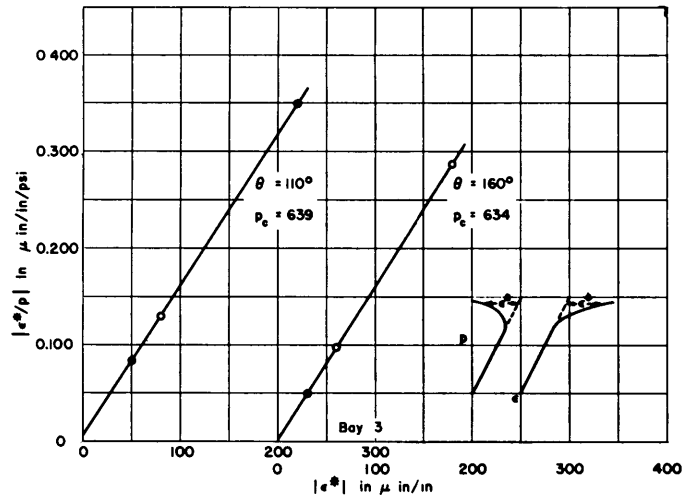


Figure 16 - Typical Southwell Plots for Exterior Circumferential Strains at Midbay (Run 2, Final Test)

Table 9

Southwell Results from Circumferential Strains at Midbay (Run 2, Final Test)

Bay	Angular Location	P_c psi
3	110°	639
	130°	636
	160°	634
	180°	643
4	40°	638
	60°	636
	90°	638
	110°	634
	160°	639
	180°	636
Average $p_c = 637$		
Gages selected on basis of data quality from those showing largest nonlinear strains.		

of 633 psi.* However, it should be noted that accurate data could be obtained only at pressures within 95 percent of collapse.

These results are of some interest as they relate to the problem of "snap-through" in thin cylindrical shells. The Southwell method is based

*In practice the Southwell method, when applicable, predicts a buckling load slightly higher than that actually attained. This is to be expected since the method gives the elastic buckling load for a geometrically perfect structure.

Table 10
 Maximum Stresses Measured during Final Run
 (Bay 4 at 110 deg, 630 psi)

x/L	Stress Orientation	Stress in psi	
		Measured	Pulos-Salerno Theory
1.000	Long. Interior	-	72,900
0.943*	Long. Interior	52,100	47,500
0.500	Circ. Exterior	74,100	64,800
Elastic Limit = 74,400 psi			
*Longitudinal gage located as close to frame as possible.			

on small deflection theory and predicts the buckling load for the geometrically perfect structure. Hence, it should not give accurate results for imperfect structures where the buckling strength can only be explained on the basis of large deflection theory. In such cases, "snap-through" occurs at some load less than the load predicted by small deflection theory. The Southwell results, therefore, indicate that if "snap-through" took place, it did not significantly affect the buckling strength.

It is also apparent that the failure, if not initially elastic, was so nearly so that the collapse pressure was not seriously affected by inelastic behavior. Had this not been the case, the Southwell plots would have been nonlinear and the elastic buckling pressure, though possibly obtainable from strains in the elastic region, would not have agreed well with the experimental collapse pressure.

In this regard, it is useful to examine the stresses determined from strains measured in critical areas. The maximum stresses were observed in Bay 4 at 110 deg and are listed in Table 10 along with the corresponding values from the theory of Pulos and Salerno.³³ All stresses are for a pressure of 630 psi. The differences between the measurements and the calculations can be attributed to additional bending stresses which accompanied the lobar deformations. It will be seen that none of the measured stresses

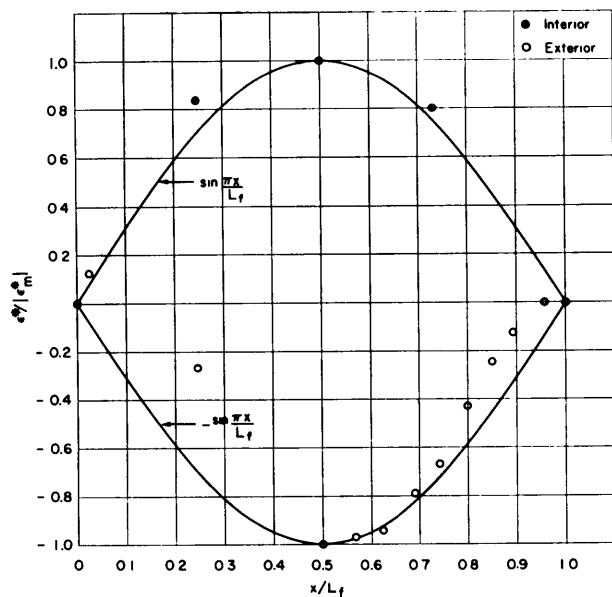


Figure 17 - Distribution of Nonlinear Circumferential Strain for Bay 3 at 630 psi along 90-deg Generator

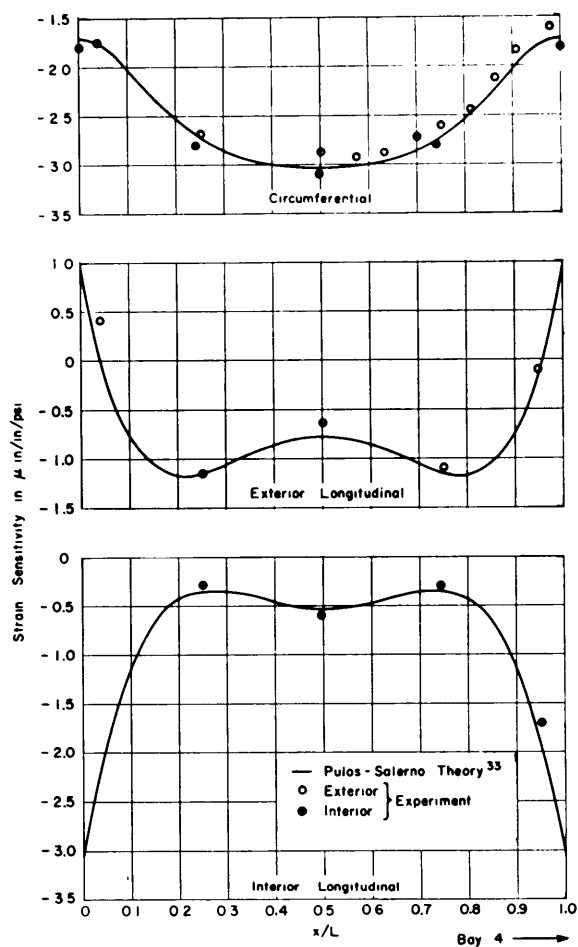


Figure 18 - Theoretical and Experimental Distribution of Linear Strain for Bay 3 (Run 2, Final Test)

reached the elastic limit. However, it should be pointed out that the interior longitudinal stress exactly at the juncture of frame and shell could not be measured because the longitudinal gages were necessarily displaced slightly ($0.057L$) from the juncture to allow for the length of a gage element. The maximum stress measured at this neighboring point and the theoretical values for this region (Table 10) indicate that the elastic limit may have been exceeded by the interior longitudinal stress in Bay 4 at 110 deg immediately adjacent to Frame 5. Because of the high stress gradient in this region, a precise estimate of this stress was not possible. In any event, it appears that whatever yielding may have occurred was very

slight and highly localized.

The circumferential gages in Bay 3, located along the 90-deg generator, provide some information regarding the longitudinal profile of a lobe. Figure 17 shows a nondimensional plot $\epsilon^*/|\epsilon_m^*|$ versus x/L_f for a pressure of 630 psi. As explained previously, ϵ^* is the nonlinear or lobar component of the total strain, ϵ_m^* is the value of ϵ^* at midbay, and x is the distance measured from the center of Frame 3. Also shown is a sine-wave distribution such as would exist in the case of simple support. The departure of the experimental points from this sine wave indicates to some extent the influence of the rotational restraint on the buckling configuration. Undoubtedly, experimental error is responsible for some of the deviations. Strains measured on Frame 4 in this region showed some evidence of asymmetric deformations, but the strain variations were not large enough for the determination of a well-defined pattern.

Strains measured in Bay 3 also provided an opportunity for further evaluation of the axisymmetric stress analysis of Pulos and Salerno³³ in the linear range. Figure 18 compares the theoretical distribution with the distribution of circumferential and longitudinal strain sensitivities measured across Bay 3 at 90 deg. Agreement between theory and experiment, it will be seen, was generally good.

COMPARISON WITH PREVIOUS TESTS

Table 11 summarizes the test results of Cylinder BR-4B and the earlier results for Cylinders BR-4 and BR-4A. The cylinders were geometrically similar but differed in their yield strengths. The table includes pressures given by Formula [92A] of Von Sanden and Günther,³² at which the exterior circumferential stress at midbay reaches the yield value. Since this pressure for BR-4 and BR-4A was less than the elastic buckling pressure given by Equation [33], it is clear that both of these failures were initially inelastic. Use of much higher strength steel in the case of BR-4B resulted in a yield pressure well above the elastic buckling pressure and in a mode of collapse which appears to have been initially elastic.

Table 11

Experimental Results Compared with Previous Tests

Cylinder Number		BR-4	BR-4A	BR-4B
Fabrication		Welded	Machined	Machined
σ_y , psi*		50,000	50,000	82,500
Collapse Pressure, psi	Von Sanden and Günther Formula [92A] ³²	494	494	815
	Equation [33]	633(11)**		
	Experiment	390(10)	550(10-11)	633(11)
<p>*Based on an offset strain of 0.002 .</p> <p>**Number of lobes in parantheses.</p> <p>Dimensions and Young's Modulus (28.9×10^6 psi) assumed identical for the three cylinders.</p>				

SUMMARY AND CONCLUSIONS

1. The test Cylinder BR-4B collapsed at 633 psi in an asymmetric shell buckling mode characterized by 11 circumferential lobes. On the basis of strain measurements, it is concluded that the collapse was initiated by elastic buckling.

2. The Southwell method can be an effective means of determining nondestructively the elastic buckling strength of short shells. It is likely to be accurate only where imperfections and residual stresses are small, as in the case of machined cylinders, and only where it is possible to approach very closely the elastic buckling pressure. Hence, its practicality as a nondestructive technique may be rather limited for this mode of buckling.

PART III - EVALUATION OF BUCKLING THEORY

COMPARISON OF THEORY WITH EXPERIMENT

According to the theory developed in this report (Equation [33]), buckling for Cylinder BR-4B occurs at 633 psi in a configuration of 11 circumferential lobes, which is in exact agreement with the test results. Such agreement is, of course, better than one has any right to expect, even for the most rigorous theory imaginable. The present theory makes use of several approximations; moreover, its accuracy depends on the uniformity of the test cylinder and the accuracy with which its properties can be determined. The shell thickness, for example, must necessarily be represented by an average of many measurements, all subject to error. The determination of Young's modulus required a separate test which utilized the response of a ring to diametral loading. While this method is believed reliable, it is still subject to experimental error, and no claim is made that it is the best that could have been used. Other techniques, for example, the use of optical strain gages to measure the response of a specimen under direct stress, are highly regarded. Because perfect isotropy is never achieved, methods which employ different conditions of stress cannot be expected to yield identical results.

In view of these uncertainties, the degree of correlation of theory with experiment can be regarded with some suspicion, but the results are, nevertheless, substantial evidence of the validity of the theory.

The test of BR-4B is considered successful as a demonstration of the phenomenon of elastic buckling, but it is not an ideal example of the influence of stiffening rings on shell buckling strength. The buckling pressure was only slightly greater than that (600 psi*) given by the theory of Von Mises (Equation [46]) for the case of simple supports. This is a

*This figure is obtained on the basis that buckling is confined to the unsupported length (L) of shell plating. If the full frame spacing (L_f) is used, the resulting pressure is 580 psi, as indicated in Table 4. Still less is the pressure (550 psi) given by Equation [42], which includes the effect of the boundary conditions on the initial deflections.

natural consequence of the large value of β (6.80) used in an effort to obtain an elastic failure. Nevertheless, the test did demonstrate that the Von Mises pressure can be exceeded.

Fortunately, since the test of BR-4B, other results have become available that provide better data regarding the influence of stiffening rings. These have been selected from tests of a number of machined steel cylinders, 8 in. in diameter, most of which were recently reported.³⁹ The cylinders in many cases had more typical bays than did BR-4B, but there is no indication that the extra length had any influence on collapse other than to isolate the central bays from end effects. In all cases, failures were of the interframe variety, but in only a few was there evidence of elastic buckling. Since none of them was instrumented for the specific purpose of detecting an elastic failure, the cases cited here were selected by comparing p_c , the critical buckling pressure according to Equation [33], with an estimated yield pressure p_y , given by Von Sanden and Günther Formula [92A].³² The pressure p_y is that at which the exterior circumferential stress at midbay reaches the yield value defined at an offset strain of 0.002. When p_y exceeds p_c , the possibility of elastic buckling exists. If p_c exceeds p_y , the failure must be inelastic. On this basis, three of the cylinders were in the elastic category. Their properties and those of BR-4B are listed in Table 12. Since modulus measurements for the small cylinders were not available, a nominal value of 30×10^6 psi was assumed. The collapse pressures, both experimental and theoretical, for the four cylinders appear in Table 13.

The influence of the frames is clearly seen by comparing the Von Mises pressures in the table with the experimental results. The additional strength provided by the frames (as much as 22 percent) results primarily from the fact that for each of the small cylinders, β was considerably less than for BR-4B. Evidently the present theory adequately accounts for this effect. In each case, the pressure given by Equation [33] agrees well with the experimental pressure. These results are also presented graphically in Figure 19. The abscissa is p_c/p_y and the ordinate is the ratio of p_f , the experimental failure pressure, to p_y . The 45-deg line drawn on the figure represents perfect agreement between theory and experiment. If p_c/p_y is less than unity (indicated by the dotted line),

Table 12

Properties of Steel Test Cylinders

Cylinder Number	BR-4B	U-73	U-56	U-23(1)
β	6.800	5.264	4.744	4.124
h/R	1.007×10^{-2}	0.6728×10^{-2}	0.8268×10^{-2}	0.7608×10^{-2}
L_f/R	0.5301	0.3359	0.3356	0.2798
b/R	1.714×10^{-2}	1.915×10^{-2}	1.546×10^{-2}	1.497×10^{-2}
d/R	7.083×10^{-2}	7.661×10^{-2}	6.158×10^{-2}	5.939×10^{-2}
E in psi	28.9×10^6 *	30.0×10^6	30.0×10^6	30.0×10^6
σ_y in psi**	82,500	103,200	103,700	108,600
Number of Typical Bays	4	7	6	10
<p>All cylinders machined with external rectangular frames. Poisson's Ratio assumed to be 0.3 for all cases. $\beta = [3(1 - \nu^2)]^{\frac{1}{4}} L_f / \sqrt{Rh}$; b = Frame Width; d = Frame Height.</p>				
<p>*Measured value for other cylinders assumed. **Compressive yield stress based on offset strain of 0.002.</p>				

Table 13

Comparison of Theory and Experiment

Cylinder Number	Experimental Collapse Pressure psi	Theoretical Collapse Pressure, psi				Yield Von Sanden and Günther Formula [92A] ³²
		Elastic Instability				
		Equation [33]	Von Mises (Fig. 8 & 9)	Von Sanden and Tölke ¹²	Nash ³⁵ (Fixed Ends)	
BR-4B	633(11)*	633(11)	600(10)	599(11)	845(11)	815
U-73	475(14)	460(14)	387(14)	386(16)	560(15)	644
U-56	725(13)	744(13)	654(14)	665(14)	965(15)	820
U-23(1)	803(14)	811(14)	665(15)	693(16)	1031(17)	815

*Numbers in parentheses indicate number of circumferential lobes.

In applying the formulas of Von Mises and Nash, the effective length of the shell is taken to be the unsupported distance (L) between frames. In Equation [33] and in the Von Sanden and Tölke equation, the full frame spacing (L_f) is used.

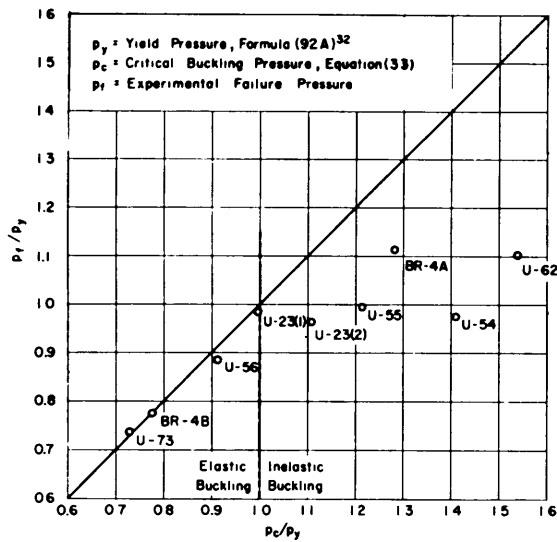


Figure 19 - Experimental and Theoretical Results

using small-deflection theory, and are consistent with earlier remarks regarding the application of the Southwell method for the case of BR-4B. This does not necessarily indicate that the observed failures were not, in fact, precipitated by a "snap-through" mode of instability. That this phenomenon can occur in cylindrical shells under hydrostatic pressure has been demonstrated experimentally by Kirstein and Wenk,²¹ and theoretically by the large deflection analyses of Donnell,^{17,18} Langhaar and Boresi,¹⁹ and Kempner and Crouzet-Pascal,²⁰ among others. However, these studies have also shown that the pressure at which "snap-through" takes place is not much less than the pressure given by small-deflection theory even in the presence of imperfections.* For machined shells, this pressure difference might be too small to be detectable.

Table 13 also shows that according to the solution of Von Sanden and Tölke,¹² the pressures reflect some strengthening due to the presence of the frames, but still fall short of experiment. This is to be expected since

elastic buckling is expected. It will be seen that the four cases of Table 13 all fall within this region and the plotted points all lie close to the 45-deg line. Some of the other tests reported in Reference 39 are also plotted in the figure along with the test of BR-4A. In all of these cases, p_c/p_y exceeds unity, so that the points are outside the elastic region and, as expected, all lie below the 45-deg line.

These results indicate that the performances of the four cylinders have been satisfactorily explained

*This is in marked contrast to the behavior of cylindrical shells under axial compression or torsion where the pressure difference can be very large.

the analysis considers the effect of the frames on the prebuckling deformations but fails to account for the restraint which they provide during buckling. On the other hand, the Nash solution for a shell with full fixity³⁵ greatly overestimates the strength actually realized in each case, as the table indicates. This should be interpreted not as a refutation of the solution, but rather as evidence of its inapplicability for the cases considered. It is possible, as has already been indicated, that the analysis may be quite accurate in cases where complete fixity is actually attained.

Finally, it should be said that the experimental results reported here, though meager, are all of which the author is aware. Unfortunately, there are no data for internally framed cylinders, and none are apt to be forthcoming because of the machining problems presented by internal frames.

While no future studies in the area of elastic shell instability are contemplated, should additional experimental data become available, they will be examined with interest.

CONCLUSIONS

1. The small deflection theory of this report predicts with accuracy the elastic buckling of cylindrical shells supported by closely spaced ring stiffeners, at least where stiffeners are external and β is greater than 4.0. Because of the restraint provided by the rings, the buckling strength can be considerably greater than that expected for a shell with simple support.

2. The solution of Von Sanden and Tölke is conservative in all cases because it accounts only partially for the strengthening influence of the stiffeners.

3. The fact that the Nash analysis for a shell with clamped edges greatly overestimates the buckling strength of ring-supported shells does not necessarily indicate the use of an unrealistic buckling shape in the analysis. It is more likely that the disparity exists chiefly because frames of practical size do not provide restraint comparable to complete fixity.

4. Since the Von Mises analysis is based on the assumptions that the

shell is unsupported prior to buckling and simply supported during buckling, it can be highly inaccurate in predicting buckling pressures for ring-stiffened shells. Nevertheless, it is probably the most practical means for estimating elastic buckling strength because it is always conservative and can be represented in a very simple form.

ACKNOWLEDGMENTS

Many members of the Structural Mechanics Laboratory have made contributions to this study. Particular recognition should go to Mr. Arthur F. Kirstein, whose careful planning and preparation were responsible for the successful execution of the tests of Cylinder BR-4B, and to Mr. William F. Blumenberg who collaborated during the tests and reduced much of the data. The author also gratefully acknowledges the additional data supplied by Messrs. Kenneth Hom, John E. Buhl, Jr. and William P. Couch.

Special recognition is due Dr. Robert Bart and Mr. Hom for preparing the computer program.

**INTENTIONALLY
BLANK**

APPENDIX A

STRAIN ENERGY OF THE SHELL

In the development which follows, basic strain-displacement relations are obtained with accuracy preserved through quadratic terms in the displacements. The strain energy integral of the shell is then formulated with displacement terms maintained through the third order.

We consider an element situated within the thickness of the shell at a radius r and having axial and angular coordinates x and θ . The element undergoes displacements u' , v' , and w' in the axial, tangential, and radial directions, respectively, with w' taken as positive outward. We will assume that the strain in the radial direction is negligible so that only deformations within the plane of the element need be considered. Novozhilov⁴⁰ describes these deformations in terms of strain components which will be designated ϵ_{xx} , $\epsilon_{\theta\theta}$, and $\epsilon_{x\theta}$ for cylindrical coordinates. They are related to the displacements as follows:

$$\begin{aligned}\epsilon_{xx} &= u'_x + \frac{1}{2}(u'_x{}^2 + v'_x{}^2 + w'_x{}^2) \\ \epsilon_{\theta\theta} &= \frac{v'_\theta + w'}{r} + \frac{1}{2} \left[\left(\frac{u'_\theta}{r} \right)^2 + \left(\frac{v'_\theta + w'}{r} \right)^2 + \left(\frac{w'_\theta - v'}{r} \right)^2 \right] \\ \epsilon_{x\theta} &= v'_x + \frac{u'_\theta}{r} + u'_x \left(\frac{u'_\theta}{r} \right) + v'_x \left(\frac{v'_\theta + w'}{r} \right) + w'_x \left(\frac{w'_\theta - v'}{r} \right)\end{aligned}\tag{66}$$

where the subscripts on u' , v' , and w' indicate differentiation. In order to calculate strain energy, it is necessary to consider strains of line elements that lie along mutually perpendicular axes - in this case the x and θ coordinate lines. These strains, according to Novozhilov,⁴⁰ can be expressed in terms of the strain components by

$$\begin{aligned}e_x &= \sqrt{1 + 2\epsilon_{xx}} - 1 \\ e_\theta &= \sqrt{1 + 2\epsilon_{\theta\theta}} - 1\end{aligned}\tag{67}$$

$$e_{x\theta} = \frac{\sin^{-1} \epsilon_{x\theta}}{\sqrt{(1 + 2 \epsilon_{xx})(1 + 2 \epsilon_{\theta\theta})}} \quad [67] \quad \text{continued}$$

where e_x and e_θ are unit strains in the x and θ directions and $e_{x\theta}$ is the shear strain expressing the change in the angle between the coordinate lines. By combining Equations [66] and [67] and discarding all displacement terms of order higher than quadratic, one obtains

$$\begin{aligned} e_x &= u'_x + \frac{1}{2} (v'_x{}^2 + w'_x{}^2) \\ e_\theta &= \frac{v'_\theta + w'}{r} + \frac{1}{2} \left[\left(\frac{u'_\theta}{r} \right)^2 + \left(\frac{w'_\theta - v'}{r} \right)^2 \right] \\ e_{x\theta} &= v'_x + \frac{u'_\theta}{r} + w'_x \left(\frac{w'_\theta - v'}{r} \right) - u'_x v'_x - \frac{u'_\theta}{r} \left(\frac{v'_\theta + w'}{r} \right) \end{aligned} \quad [68]$$

It may be surprising to note that retention of only linear terms in the strain components, as was apparently done by Langhaar and Boresi,¹⁹ leads to a slightly more complicated result.*

To relate the displacements u' , v' , w' at any point to the displacements u , v , w at the middle surface of the shell, it is useful to employ relations developed by Langhaar and Boresi.

$$\begin{aligned} u' &= u + z\xi \\ v' &= v + z\omega \\ w' &= w + z\gamma \end{aligned} \quad [69]$$

*In that case, the strains are identical with the corresponding strain components. However, the difference between Equations [66] and [68] is probably of little practical significance.

where

$$\begin{aligned}\xi &= -w_x + v_x \left(\frac{w_\theta - v}{R} \right) + u_x w_x \\ \omega &= - \left(\frac{w_\theta - v}{R} \right) + \frac{u_\theta w_x}{R} + \left(\frac{v_\theta + w}{R} \right) \left(\frac{w_\theta - v}{R} \right) \\ \gamma &= - \frac{w_x^2}{2} - \left(\frac{w_\theta - v}{R} \right)^2\end{aligned}$$

where R is the radius to the middle surface of the shell and z is the thickness coordinate measured positive outward from the middle surface of the shell. Equations [69] are based on the assumption of Kirchoff that normals to the undeformed middle surface remain normal, straight, and unextended after deformation. By combining Equations [68] and [69] after suitable differentiation, the resulting equations are

$$\begin{aligned}e_x &= u_x - z w_{xx} + \frac{1}{2} (v_x^2 + w_x^2) + z (N v_{xx} + u_{xx} w_x + u_x w_{xx}) + \frac{z^2 N_x^2}{2} \\ e_\theta &= M - \frac{z N_\theta}{R} + \frac{1}{2} \left(\frac{u_\theta^2}{R^2} + N^2 \right) + \frac{z}{R} \left(\frac{u_{\theta\theta} w_x}{R} + M_\theta N + M N_\theta \right. \\ &\quad \left. - \frac{w_x^2}{2} + \frac{N^2}{2} \right) + \frac{z^2}{2R^2} (w_{x\theta}^2 + N^2) \quad [70] \\ e_{x\theta} &= v_x + \frac{u_\theta}{R} - \frac{z}{R} (R N_x + w_{x\theta}) + w_x N - u_x v_x - \frac{u_\theta M}{R} + \frac{z}{R} \left(2 u_{x\theta} w_x \right. \\ &\quad \left. + u_\theta w_{xx} + u_x w_{x\theta} + R M_x N + R M N_x + N_\theta v_x + N v_{x\theta} + w_x N \right. \\ &\quad \left. + R u_x N_x + \frac{u_\theta N_\theta}{R} + w_{x\theta} M \right) - \frac{z^2}{R^2} (R^2 w_{xx} N_x + w_{x\theta} N_\theta)\end{aligned}$$

where

$$M = \frac{v_\theta + w}{R}$$

$$N = \frac{w_\theta - v}{R}$$

In obtaining Equations [70], it was assumed that r could be replaced by R with negligible loss of accuracy. A further simplification can be made in $e_{x\theta}$ by neglecting z/R in comparison to unity. Then

$$e_{x\theta} = v_x + \frac{u_\theta}{R} - \frac{z}{R} (R N_x + w_{x\theta}) + w_x N - u_x v_x - \frac{u_\theta M}{R} \quad [71]$$

$$+ \frac{z}{R} \left(2 u_{x\theta} w_x + u_\theta w_{xx} + u_x w_{x\theta} + R M_x N + R M N_x + N_\theta v_x \right.$$

$$\left. + N v_{x\theta} + R u_x N_x + \frac{u_\theta N_\theta}{R} + w_{x\theta} M \right) - \frac{z^2}{R^2} (R^2 w_{xx} N_x + w_{x\theta} N_\theta)$$

In formulating the expression for the strain energy of the shell, it will be assumed that the stress in the radial direction is zero. According to Langhaar and Boresi,¹⁹ the shell energy U_s can then be expressed by

$$U_s = \frac{E}{2(1-\nu^2)} \int_{x_1}^{x_2} \int_0^{2\pi} \int_{-\frac{h}{2}}^{\frac{h}{2}} \left[e_x^2 + e_\theta^2 + 2\nu e_x e_\theta + \left(\frac{1-\nu}{2}\right) e_{x\theta}^2 \right] R dx d\theta dz \quad [72]$$

where E is Young's modulus and h is the shell thickness. After combining Equations [70] and [71] with Equation [72], performing the integration on z and discarding terms higher than the third order, one obtains:

$$U_s = \frac{EhR}{2(1-\nu^2)} \int_{x_1}^{x_2} \int_0^{2\pi} \left\{ u_x^2 + u_x (v_x^2 + w_x^2) + M^2 + M \left(\frac{u_\theta^2}{R^2} + N^2 \right) \right.$$

$$\left. + 2\nu \left[u_x M + \frac{u_x}{2} \left(\frac{u_\theta^2}{R^2} + N^2 \right) + \frac{M}{2} (v_x^2 + w_x^2) \right] \right. \quad [73]$$

$$\left. + \left(\frac{1-\nu}{2} \right) \left[\left(v_x + \frac{u_\theta}{R} \right)^2 + 2 \left(v_x + \frac{u_\theta}{R} \right) \left(w_x N - u_x v_x - \frac{u_\theta M}{R} \right) \right] \right\} dx d\theta$$

$$\begin{aligned}
& + \frac{Eh^3}{24R(1-\nu^2)} \int_{x_1}^{x_2} \int_0^{2\pi} \left\{ R^2 \left[w_{xx}^2 + u_x N_x^2 - 2w_{xx}(N v_{xx} + u_{xx} w_x \right. \right. \\
& \quad \left. \left. + u_x w_{xx}) \right] + N_\theta^2 + M w_{x\theta}^2 - 2N_\theta \left(\frac{u_{\theta\theta} w_x}{R} + M_\theta N + M N_\theta - \frac{w_x^2}{2} \right) \right. \\
& \quad \left. + 2\nu \left[R w_{xx} N_\theta + \frac{u_\theta w_{x\theta}^2}{2} - R w_{xx} \left(\frac{u_{\theta\theta} w_x}{R} + M_\theta N + M N_\theta - \frac{w_x^2}{2} \right) \right. \right. \\
& \quad \left. \left. - R N_\theta (N v_{xx} + u_{xx} w_x + u_x w_{xx}) + \frac{R^2 N_x^2 M}{2} \right] + \frac{1-\nu}{2} \left[(R N_x + w_{x\theta})^2 \right. \right. \\
& \quad \left. \left. - 2 \left(v_x + \frac{u_\theta}{R} \right) (R^2 w_{xx} N_x + w_{x\theta} N_\theta) - 2(R N_x + w_{x\theta}) \left(2 u_{x\theta} w_x \right. \right. \right. \\
& \quad \left. \left. + u_\theta w_{xx} + u_x w_{x\theta} + R M_x N + R M N_x + R v_x w_{xx} + N_\theta v_x \right. \right. \\
& \quad \left. \left. \left. + N v_{x\theta} + R u_x N_x + \frac{u_\theta N_\theta}{R} + w_{x\theta} M \right) \right] \right\} dx d\theta \quad [73] \\
& \hspace{15em} \text{continued}
\end{aligned}$$

**INTENTIONALLY
BLANK**

APPENDIX B

STRAIN ENERGY OF RINGS

The strain energy of a ring will be considered as the sum of three quantities: U_{IP} , the energy due to deformations in the plane of curvature; U_{OP} , the energy of deformations perpendicular to the plane of curvature; and U_{TOR} , the energy due to torsion about an axis parallel to the θ -coordinate line. Thus, the strain energy of a ring is

$$U_f = U_{IP} + U_{OP} + U_{TOR} \quad [74]$$

In this equation, the energy associated with restricted warping as well as that due to extensions of the ring in the z and x directions has been neglected.

U_{IP} is simply the energy associated with the circumferential strain, or

$$U_{IP} = \frac{E}{2} \int_{A_f} \int_0^{2\pi} (e_\theta^2)_{x=iL_f} (R+e) dA_f d\theta \quad [75]$$

where A_f is the cross-sectional area of a ring situated at a distance iL_f from the origin. From Appendix A, Equation [68] is

$$e_\theta = \frac{v'_\theta + w'}{R+e} + \frac{1}{2} \left[\left(\frac{u'_\theta}{R+e} \right)^2 + \left(\frac{w'_\theta - v'}{R+e} \right)^2 \right] \quad [76]$$

when the approximation is made that r can be replaced by $R+e$. Referring to Figure 3, e is the distance between the middle surface of the shell and the center of gravity of the ring cross section. When substitutions from Equation [69] of Appendix A are made, Equation [76] becomes

$$e_\theta = \frac{R}{R+e} \left\{ M - \frac{z}{R} N_\theta + \frac{R}{2(R+e)} \left(\frac{u_\theta^2}{R^2} + N^2 \right) + \frac{z}{R} \left[\frac{u_{\theta\theta} w_x}{R} + \frac{u_\theta w_{x\theta}}{R} \left(\frac{e}{R+e} \right) \right. \right. \\ \left. \left. + M_\theta N + MN_\theta - \frac{w_x^2}{2} + \frac{N^2}{2} \left(\frac{R-e}{R+e} \right) \right] + \frac{R}{R+e} \left(\frac{z}{R} \right)^2 (w_{x\theta}^2 + N^2) \right\} \quad [77]$$

After this expression is substituted in Equation [75] and terms higher than the third order are discarded, one obtains

$$\begin{aligned}
U_{IP} = & \frac{ER^2}{2(R+e)} \int_{A_f} \int_0^{2\pi} \left[M^2 + \frac{RM}{R+e} \left(\frac{u_\theta^2}{R^2} + N^2 \right) + \frac{z^2}{R^2} N_\theta^2 \right. \\
& + \frac{z}{R} \left\{ 2M \left[-N_\theta + \frac{u_{\theta\theta} w_x}{R} + \frac{e}{R(R+e)} u_\theta w_{x\theta} + M_\theta N + MN_\theta - \frac{w_x^2}{2} \right. \right. \\
& + \left. \left. \frac{N^2}{2} \left(\frac{R-e}{R+e} \right) \right] - \frac{RN_\theta}{R+e} \left(\frac{u_\theta^2}{R^2} + N^2 \right) \right\} + \frac{z^2}{R^2} \left\{ \frac{RM}{R+e} (w_{x\theta}^2 + N^2) \right. \\
& - 2N_\theta \left[\frac{u_{\theta\theta} w_x}{R} + \frac{e}{R(R+e)} u_\theta w_{x\theta} + M_\theta N + MN_\theta - \frac{w_x^2}{2} \right. \\
& \left. \left. + \frac{N^2}{2} \left(\frac{R-e}{R+e} \right) \right] \right\} \right] dA_f d\theta \tag{78}
\end{aligned}$$

Before integrating over the area A_f , it is helpful to make use of the following definitions:

$$\begin{aligned}
\int_{A_f} z dA_f &= e A_f \\
\int_{A_f} z^2 dA_f &= I_{xG} + A_f e^2
\end{aligned} \tag{79}$$

I_{xG} is the moment of inertia about an axis normal to the area A_f at its center of gravity. U_{IP} can then be written:

$$\begin{aligned}
U_{IP} = & \frac{ER^2 A_f}{2(R+e)} \int_0^{2\pi} \left[M^2 + \frac{M}{1 + \frac{e}{R}} \left(\frac{u_\theta^2}{R^2} + N^2 \right) + \frac{e}{R} \left\{ 2M \left[-N_\theta + \frac{u_{\theta\theta} w_x}{R} \right. \right. \right. \\
& + \left. \left. \frac{e}{R(R+e)} u_\theta w_{x\theta} + M_\theta N + MN_\theta - \frac{w_x^2}{2} + \frac{N^2}{2} \left(\frac{R-e}{R+e} \right) \right] - \frac{RN_\theta}{R+e} \left(\frac{u_\theta^2}{R^2} + N^2 \right) \right\} \\
& + \left(\frac{I_{xG}}{A_f R^2} + \frac{e^2}{R^2} \right) \left\{ N_\theta^2 + \frac{RM}{R+e} (w_{x\theta}^2 + N^2) - 2N_\theta \left[\frac{u_{\theta\theta} w_x}{R} \right. \right. \\
& \left. \left. + \frac{e}{R(R+e)} u_\theta w_{x\theta} + M_\theta N + MN_\theta - \frac{w_x^2}{2} + \frac{N^2}{2} \left(\frac{R-e}{R+e} \right) \right] \right\} \right] d\theta \tag{80}
\end{aligned}$$

According to fundamental beam theory, the out-of-plane bending energy is

$$U_{OP} = \frac{EI_{zG}}{2} \int_0^{2\pi} \chi^2 (R+e) d\theta \quad [81]$$

where I_{zG} is the moment of inertia of the ring about an axis parallel to the z-coordinate through its center of gravity and, according to Reference 34,

$$\chi = -\frac{1}{R+e} \left[(\xi)_{x=iL_f} + \frac{u_{G\theta\theta}}{R+e} \right] \quad [82]$$

u_G is the axial displacement of the centroid of the ring; ξ is the rotation of the ring in the x-z plane as defined in Equation [69] of Appendix A. Because each ring is assumed to undergo no strain in the axial direction,

$$(\xi)_{x=iL_f} = \left[-w_x + v_x \left(\frac{w_\theta - v}{R} \right) \right]_{x=iL_f} \quad [83]$$

With z replaced by e in Equation [69] of Appendix A, it follows that

$$\begin{aligned} u_{G\theta\theta} &= \left[u_{\theta\theta} + e(-w_{x\theta\theta} + v_{x\theta\theta} N + 2v_{x\theta} N_\theta + v_x N_{\theta\theta}) \right]_{x=iL_f} \\ \chi &= -\frac{1}{R+e} \left\{ -w_x + v_x N + \frac{1}{R+e} \left[u_{\theta\theta} + e(-w_{x\theta\theta} + v_{x\theta\theta} N \right. \right. \\ &\quad \left. \left. + 2v_{x\theta} N_\theta + v_x N_{\theta\theta}) \right] \right\}_{x=iL_f} \end{aligned} \quad [84]$$

Combining Equations [81] and [84] and discarding terms higher than the third order, one obtains

$$\begin{aligned} U_{OP} &= \frac{EI_{zG}}{2(R+e)} \int_0^{2\pi} \left\{ \left[w_x - \frac{u_{\theta\theta}}{R+e} + \left(\frac{e}{R+e} \right) w_{x\theta\theta} \right]^2 - 2 \left[w_x - \frac{u_{\theta\theta}}{R+e} \right. \right. \\ &\quad \left. \left. + \left(\frac{e}{R+e} \right) w_{x\theta\theta} \right] \left[v_x N + \frac{e}{R+e} (v_{x\theta\theta} N + 2v_{x\theta} N_\theta + v_x N_{\theta\theta}) \right] \right\}_{x=iL_f} d\theta \end{aligned} \quad [85]$$

According to Reference 34, the torsional energy is expressed by

$$U_{\text{TOR}} = \frac{EK}{4(1+\nu)} \int_0^{2\pi} \Phi^2 (R+e) d\theta \quad [86]$$

where Φ is the angle of twist per unit of circumference and K is the torsion constant. For example, in the case of a rectangular ring where the depth d is much greater than the width b , K is given by $\frac{1}{3}db^3$. When an open section is comprised of several narrow rectangles, K for the section is given approximately by the sum of the values K for each part.⁴¹ Reference 42 gives values of K for rectangles where d does not greatly exceed b . Reference 34 defines the angle of twist as

$$\Phi = \frac{1}{R+e} \left[(\xi_\theta)_{x=iL_f} - \frac{u_{G\theta}}{R+e} \right] \quad [87]$$

After appropriate substitution this becomes

$$\Phi = \frac{1}{(R+e)^2} \left[R(-w_{x\theta} + v_{x\theta}N + v_x N_\theta) - u_\theta \right]_{x=iL_f} \quad [88]$$

and the torsional energy is

$$U_{\text{TOR}} = \frac{EK}{4(1+\nu)(R+e)^3} \int_0^{2\pi} \left[(Rw_{x\theta} + u_\theta)^2 - 2R(Rw_{x\theta} + u_\theta)(v_{x\theta}N + v_x N_\theta) \right]_{x=iL_f} d\theta \quad [89]$$

with terms above third order discarded.

APPENDIX C
POTENTIAL OF THE EXTERNAL LOADS

The work done by the external loads is defined as the product of the pressure and the change in volume undergone by the cylinder during deformation, or

$$W = p(V' - V) \quad [90]$$

where V and V' are the volumes before and after deformation, respectively. The volume bounded by an element of the deformed shell is defined

$$dV' = dA' dl' \quad [91]$$

where A' is the area enclosed by the median surface of the shell in the $R - \theta$ plane, and dl' is the length of the element measured in the x -direction. Referring to Figure 20,

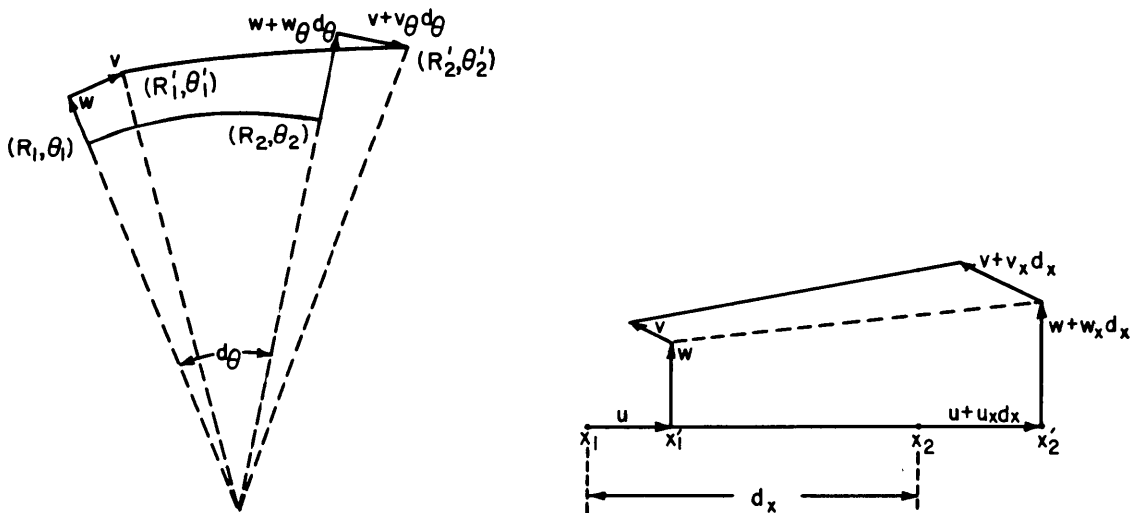


Figure 20 - Deflected Element of Shell

$$dA' = \frac{R'_1 R'_2}{2} (\theta'_2 - \theta'_1) \quad [92]$$

$$dl' = x'_2 - x'_1$$

The coordinates can be expressed as follows:

$$\begin{aligned} R'_1 &= [(R + w)^2 + v^2]^{\frac{1}{2}} \\ R'_2 &= [(R + w + w_\theta d\theta)^2 + (v + v_\theta d\theta)^2]^{\frac{1}{2}} \\ \theta'_1 &= \theta_1 + \frac{v}{R'_1} \\ \theta'_2 &= \theta_1 + d\theta + \frac{v + v_\theta d\theta}{R'_2} \\ dl' &= (1 + u_x) dx \end{aligned} \quad [93]$$

When quantities above the second order are neglected,

$$dA' = \frac{1}{2} [(R + w)^2 + v_\theta (R + w) + v(v + w_\theta)] \quad [94]$$

and

$$\begin{aligned} W &= \frac{pR}{2} \int_{x_1}^{x_2} \int_0^{2\pi} \left[v_\theta + 2w + R u_x + 2w u_x + v_\theta u_x \right. \\ &\quad \left. + \frac{1}{R} (w^2 + v_\theta w + v^2 + v w_\theta) \right] dx d\theta \end{aligned} \quad [95]$$

But, since $\int_0^{2\pi} \left[v_\theta + \frac{1}{R} (v_\theta w + v w_\theta) \right] d\theta$ vanishes because of continuity, therefore

$$W = \frac{pR}{2} \int_{x_1}^{x_2} \int_0^{2\pi} \left(2w + R u_x + 2w u_x + v_\theta u_x + \frac{w^2 + v^2}{R} \right) dx d\theta \quad [96]$$

APPENDIX D

INFINITE SERIES FORMULATION OF THE INITIAL DEFLECTIONS

The axisymmetric elastic deformations of a ring-stiffened cylindrical shell under external pressure were first analyzed by Von Sanden and Günther.³² This work was later extended by Pulos and Salerno³³ to include the nonlinear or "beam-column" effect of the axial load. To express the deflections in the form of a trigonometric series it would, therefore, be possible to perform a straightforward Fourier expansion of either of these closed form solutions. An alternative approach, however, is favored here since it leads quite simply to the desired result directly from the equations of equilibrium with no dependence upon prior solutions.

The axisymmetric deformations of the cylinder are described as follows:

$$\begin{aligned}\bar{u} &= \bar{u}(x) \\ \bar{v} &= 0 \\ \bar{w} &= \bar{w}(x)\end{aligned}\tag{97}$$

with the added condition that \bar{w}_x vanishes at a frame. Referring to Equation [2] then, we have for the initial total potential,

$$\begin{aligned}\bar{U}_T &= \frac{EhR}{2(1-\nu^2)} \int_0^{L_f} \int_0^{2\pi} \left(\bar{u}_x^2 + \frac{\bar{w}^2}{R^2} + 2\nu \bar{u}_x \frac{\bar{w}}{R} + \bar{u}_x \bar{w}_x^2 + \frac{\bar{w} \bar{w}_x^2}{2R} \right) dx d\theta \\ &+ \frac{Eh^3}{24R(1-\nu^2)} \int_0^{L_f} \int_0^{2\pi} R^2 \bar{w}_{xx}^2 dx d\theta + \frac{EA_f}{2(R+e)} \int_0^{2\pi} (\bar{w}^2)_{x=0} d\theta \\ &- \frac{pR}{2} \int_0^{L_f} \int_0^{2\pi} \left(2\bar{w} + R\bar{u}_x + 2\bar{u}_x \bar{w} + \frac{\bar{w}^2}{R} \right) dx d\theta.\end{aligned}\tag{98}$$

Products of h^3 with third-order terms in the displacements have been neglected in this equation. Because deformations in each bay are identical, it is only necessary to carry out the integration on x from 0 to L_f .

Integration with respect to θ can, of course, be eliminated because of axial symmetry.

If we consider the dependent variables to be \bar{u}_x and $\frac{\bar{w}}{R}$, then one of the equations which results from equating the first variation of \bar{U}_T to zero is

$$\bar{u}_x = \frac{pR(1-\nu^2)}{2Eh} + \frac{\bar{w}}{R} \left[\frac{pR(1-\nu^2)}{Eh} - \nu \right] - \bar{w}_x^2 \quad [99]$$

By making this substitution in Equation [98], retaining only linear and quadratic terms in \bar{w} and its derivatives, and neglecting products of p^2 with \bar{w} , one obtains

$$\begin{aligned} \frac{\bar{U}_T}{2\pi} = & \frac{EhR}{2} \int_0^{L_f} \frac{\bar{w}^2}{R^2} dx + \frac{Eh^3R}{24(1-\nu^2)} \int_0^{L_f} \bar{w}_{xx}^2 dx + \frac{EA_f}{2(R+e)} (\bar{w}^2)_{x=0} \\ & - \frac{pR^2}{2} \int_0^{L_f} \left[\frac{\bar{w}}{R} (2-\nu) + \frac{\bar{w}^2}{R^2} (1-2\nu) - \frac{\bar{w}_x^2}{2} \right] dx + \frac{p^2R^3}{8Eh} (1-\nu^2) L_f \end{aligned} \quad [100]$$

\bar{w} is now taken to be

$$\bar{w} = \sum_{m=-\infty}^{\infty} \bar{w}_m \cos\left(\frac{2\lambda_m x}{R}\right) = \bar{w}_0 + 2 \sum_{m=1}^{\infty} \bar{w}_m \cos\left(\frac{2\lambda_m x}{R}\right) \quad [101]$$

where λ_m is $\frac{m\pi R}{L_f}$. When this series is substituted into Equation [100] and the integration is performed

$$\begin{aligned} \frac{\bar{U}_T}{2\pi} = & \frac{EhL_f}{2R} \sum_{m=-\infty}^{\infty} \bar{w}_m^2 \left[1 + \frac{h^2(2\lambda_m)^4}{12R^2(1-\nu^2)} \right] + \frac{EA_f}{2(R+e)} \left[\sum_{m=-\infty}^{\infty} \bar{w}_m \right]^2 \\ & - \frac{pRL_f}{2} (2-\nu) \bar{w}_0 - pL_f \sum_{m=-\infty}^{\infty} \bar{w}_m^2 \left(\frac{1}{2} - \nu - \lambda_m^2 \right) + \frac{p^2R^3}{8Eh} (1-\nu^2) L_f \end{aligned} \quad [102]$$

The equations of equilibrium are obtained by minimizing with respect to the \bar{w}_m 's:

$$\frac{\partial \bar{U}_T}{\partial \bar{w}_0} = \frac{EhL_f}{R} \bar{w}_0 + \frac{EA_f}{R+e} \sum_{m=-\infty}^{\infty} \bar{w}_m - \frac{pRL_f}{2} (2-\nu) - pL_f (1-2\nu) \bar{w}_0 = 0 \quad [103]$$

$$\frac{\partial \bar{U}_T}{\partial \bar{w}_j} = \frac{EhL_f}{R} \bar{w}_j \left[1 + 4 \left(\frac{j\pi}{\beta} \right)^4 \right] + \frac{EA_f}{R+e} \sum_{m=-\infty}^{\infty} \bar{w}_m + pL_f \bar{w}_j (2\lambda_j^2 - 1 + 2\nu) = 0 \quad j \neq 0 \quad [104]$$

where β^4 is $\frac{3(1-\nu^2)L_f^4}{R^2 h^2}$. Subtracting Equation [104] from Equation [103] yields

$$\bar{w}_j = \frac{\bar{w}_0 \left[1 - \frac{pR}{Eh} (1-2\nu) \right] - \frac{pR^2}{2Eh} (2-\nu)}{1 + 4 \left(\frac{j\pi}{\beta} \right)^4 + \frac{pR}{Eh} (2\lambda_j^2 - 1 + 2\nu)} \quad j \neq 0 \quad [105]$$

$$\approx \frac{\bar{w}_0 - \frac{pR^2}{2Eh} (2-\nu)}{1 + 4 \left(\frac{j\pi}{\beta} \right)^4 + \frac{2pR}{Eh} \lambda_j^2}$$

when $\frac{pR}{Eh}$ is negligible compared with unity and $2\lambda_j^2 \gg 1-2\nu$. Summing the \bar{w}_j 's we obtain:

$$\sum_{m=-\infty}^{\infty} \bar{w}_m = \left[\bar{w}_0 - \frac{pR^2}{2Eh} (2-\nu) \right] \sum_{m=-\infty}^{\infty} \frac{1}{1 + 4 \left(\frac{m\pi}{\beta} \right)^4 + \frac{2pR}{Eh} \lambda_m^2} + \frac{pR^2}{2Eh} (2-\nu) \quad [106]$$

\bar{w}_0 is then determined by combining Equations [103] and [106].

$$\bar{w}_0 = \frac{pR^2}{2Eh} (2 - \nu)(1 - \eta)$$

$$\eta = \frac{1}{\frac{L_f h}{A_f} \left(1 + \frac{e}{R}\right) + \sum_{m=-\infty}^{\infty} a_m} \quad [107]$$

$$a_m = \frac{1}{1 + 4 \left(\frac{m\pi}{\beta}\right)^4 + \frac{2pR}{Eh} \lambda_m^2}$$

a_m can be put in a more convenient form as follows: If an unstiffened cylinder were to buckle in the axisymmetric configuration $\bar{w} = a_m \cos\left(\frac{2\lambda_m x}{R}\right)$, the corresponding buckling pressure p_m would be given by

$$p_m = \frac{2E \left(\frac{h}{R}\right)^2}{\sqrt{3(1 - \nu^2)}} \left[\frac{\beta^2}{4m^2 \pi^2} + \frac{m^2 \pi^2}{\beta^2} \right] \quad [108]$$

This equation also applies in the case of a long cylinder under end thrust where the length of a complete axial buckling wave is equal to L_f/m . If Equations [107] and [108] are combined, we find that

$$a_m = \frac{1}{\left[1 + 4 \left(\frac{m\pi}{\beta}\right)^4\right] \left(1 - \frac{p}{p_m}\right)} \quad [109]$$

From Equations [105] and [107], we have

$$\bar{w}_j = -a_j \frac{pR^2}{2Eh} (2 - \nu) \eta$$

$$\bar{w} = \frac{pR^2}{2Eh} (2 - \nu) \left[1 - \eta - 2\eta \sum_{m=1}^{\infty} a_m \cos\left(\frac{2\lambda_m x}{R}\right)\right] \quad [110]$$

$$\bar{w} = \frac{pR^2}{2Eh} (2 - \nu) \left[1 - \eta \sum_{m=-\infty}^{\infty} a_m \cos \left(\frac{2\lambda_m x}{R} \right) \right] \quad [110] \text{ continued}$$

since a_0 equals unity. The combination of Equations [110] and [99] gives

$$\bar{u}_x = \frac{pR}{2Eh} \left[1 - 2\nu + \nu(2 - \nu)\eta \sum_{m=-\infty}^{\infty} a_m \cos \left(\frac{2\lambda_m x}{R} \right) \right] \quad [111]$$

if quadratic terms in p are neglected.

One consequence of Equation [110] is a condition for axisymmetric buckling. It can be seen that \bar{w} will increase without limit should $1/\eta$ approach zero. The governing condition then is

$$\frac{L_f h}{A_f} \left(1 + \frac{e}{R} \right) + \sum_{m=-\infty}^{\infty} \frac{1}{\left[1 + 4 \left(\frac{m\pi}{\beta} \right)^4 \right] \left(1 - \frac{p}{P_m} \right)} = 0 \quad [112]$$

So long as $A_f > 0$, this condition can be met only when $p > p_m$ for one or more values of m . If $A_f = 0$, Equation [112] is satisfied when $p = p_m$. This is to be expected since Equation [108] holds only for buckling of an unstiffened cylinder.* In that case the expression in Equation [110] for \bar{w} becomes indeterminate.

For purposes of comparison, the closed-form solution of Pulos and Salerno³³ for \bar{w} can be written as follows:

$$\bar{w} = \frac{pR^2}{2Eh} (2 - \nu) \left\{ 1 - \frac{f(x)}{f(0) \left[1 + \frac{Lh}{A_f} \left(1 + \frac{e}{R} \right) \left(\frac{b}{L} + G \right) \right]} \right\} \quad [113]$$

*It should be emphasized that the buckling configurations mentioned here are all of a single class characterized by symmetry about a frame and need not correspond to the minimum buckling pressure. Configurations of the nonsymmetric class, permitting frame rotation, can result in lower pressures, depending on the geometry of the cylinder.

where

$$f(x) = \mu_1 [\cosh K_1 x \sin K_2 (L - x) + \cosh K_1 (L - x) \sin K_2 x] \\ + \mu_2 [\sinh K_1 x \cos K_2 (L - x) + \sinh K_1 (L - x) \cos K_2 x]$$

$$G = \frac{2\mu_1 \mu_2 L_f}{\beta L} \left[\frac{\cosh K_1 L - \cos K_2 L}{\mu_2 \sinh K_1 L + \mu_1 \sin K_2 L} \right]$$

$$K_1 = \frac{\mu_1 \beta}{L_f} ; \quad K_2 = \frac{\mu_2 \beta}{L_f}$$

$$\mu_1 = \sqrt{1 - \frac{p}{p^*}} ; \quad \mu_2 = \sqrt{1 + \frac{p}{p^*}}$$

$$p^* = \frac{2E \left(\frac{h}{R} \right)^2}{\sqrt{3(1 - \nu^2)}}$$

where L is the inner, or unsupported, frame spacing and b is the faying width of a frame. If b is neglected, L equals L_f and Equations [110] and [113] should be equivalent. Equating these two expressions at $x = 0$, we find that

$$\sum_{m=-\infty}^{\infty} a_m = \sum_{m=-\infty}^{\infty} \frac{1}{\left[1 + 4 \left(\frac{m\pi}{\beta} \right)^4 \right] \left(1 - \frac{p}{p_m} \right)} = \frac{1}{G} \quad [114] \\ = \frac{\beta}{2\mu_1 \mu_2} \left[\frac{\mu_2 \sinh \mu_1 \beta + \mu_1 \sin \mu_2 \beta}{\cosh \mu_1 \beta - \cos \mu_2 \beta} \right]$$

and

$$\bar{w} = \frac{pR^2}{2Eh} \left\{ 1 - \frac{\sum_{m=-\infty}^{\infty} a_m \cos \left(\frac{2\lambda_m x}{R} \right)}{\frac{L_f h}{A_f} \left(1 + \frac{e}{R} \right) + \frac{1}{G}} \right\} \quad [115]$$

Combining Equations [113] and [115] yields the additional result:

$$f(x) = \frac{2\mu_1\mu_2}{\beta} (\cosh\mu_1\beta - \cos\mu_2\beta) \sum_{m=-\infty}^{\infty} a_m \cos\left(\frac{2\lambda_m x}{R}\right) \quad [116]$$

The principal reason for introducing the Pulos and Salerno solution was to provide the alternative means (Equation [114]) when needed for computing $\sum_{m=-\infty}^{\infty} a_m$. Graphs of the function G can be found in Reference 33 where it is designated F_1 for $p < p^*$ and F_5 for $p > p^*$. In cases where $p \ll p^*$, it follows from Equation [108] that $p \ll p_m$. Then Equation [114] reduces to

$$\sum_{m=-\infty}^{\infty} a_m = \sum_{m=-\infty}^{\infty} \frac{1}{1 + 4\left(\frac{m\pi}{\beta}\right)^4} = \frac{\beta}{2} \left[\frac{\sinh\beta + \sin\beta}{\cosh\beta - \cos\beta} \right] \quad [117]$$

For purposes of buckling calculations, this latter equation is usually sufficient. Furthermore, it is often as simple to work with the series form since, except for large values of β , convergence is quite rapid.[†] Usually only three or four terms will provide good accuracy.

[†]Using a comparison test with the convergent series $\sum_{m=1}^{\infty} \frac{1}{m^2}$, one can easily show that the series (Equation [117]) converges for all finite values of β .

**INTENTIONALLY
BLANK**

APPENDIX E
STRESS FUNCTION

The energy expression in Equation [5] is extremely unwieldy as it stands. It can be greatly simplified if u and v can be somehow eliminated. To do this, use will be made of a stress function following the method of Donnell.⁴³

The strain-displacement relations with only linear terms retained are

$$\begin{aligned} e_x &= \frac{\partial u}{\partial x} \\ e_\theta &= \frac{1}{R} \left(w + \frac{\partial v}{\partial \theta} \right) \\ e_{x\theta} &= \frac{\partial v}{\partial x} + \frac{1}{R} \frac{\partial u}{\partial \theta} \end{aligned} \quad [118]$$

It then follows that

$$\frac{\partial^2 e_\theta}{\partial x^2} + \frac{\partial^2 e_x}{R^2 \partial \theta^2} - \frac{\partial^2 e_{x\theta}}{R \partial x \partial \theta} - \frac{\partial^2 w}{\partial x^2} = 0 \quad [119]$$

But, from the fundamental definitions of plane strain

$$\begin{aligned} e_x &= \frac{1}{E} (\sigma_x - \nu \sigma_\theta) \\ e_\theta &= \frac{1}{E} (\sigma_\theta - \nu \sigma_x) \\ e_{x\theta} &= \frac{2(1+\nu)}{E} \sigma_{x\theta} \end{aligned} \quad [120]$$

where σ_x , σ_θ and $\sigma_{x\theta}$ are, respectively, the axial, circumferential, and shear stresses. Combining Equations [119] and [120] we find

$$\left[\frac{\partial^2}{\partial x^2} - \nu \frac{\partial^2}{R^2 \partial \theta^2} \right] \sigma_\theta + \left[\frac{\partial^2}{R^2 \partial \theta^2} - \nu \frac{\partial^2}{\partial x^2} \right] \sigma_x - \frac{2(1+\nu)}{R} \frac{\partial^2 \sigma_{x\theta}}{\partial x \partial \theta} - \frac{E}{R} \frac{\partial^2 w}{\partial x^2} = 0 \quad [121]$$

The stress function F is defined as follows:

$$\begin{aligned}\sigma_x &= \frac{\partial^2 F}{R^2 \partial \theta^2} \\ \sigma_\theta &= \frac{\partial^2 F}{\partial x^2} \\ \sigma_{x\theta} &= -\frac{\partial^2 F}{R \partial x \partial \theta}\end{aligned}\quad [122]$$

Equation [121] now becomes

$$\nabla^4 F - \frac{E}{R} \frac{\partial^2 w}{\partial x^2} = 0 \quad [123]$$

where ∇^4 indicates the operator $\frac{\partial^4}{\partial x^4} + \frac{2\partial^4}{R^2 \partial \theta^2 \partial x^2} + \frac{\partial^4}{R^4 \partial \theta^4}$

Once w has been specified, F is determined from Equation [123], and u and v are obtained from

$$\begin{aligned}\frac{\partial u}{\partial x} &= \frac{1}{E} \left(\frac{\partial^2 F}{R^2 \partial \theta^2} - \nu \frac{\partial^2 F}{\partial x^2} \right) \\ \frac{\partial v}{\partial \theta} &= \frac{R}{E} \left(\frac{\partial^2 F}{\partial x^2} - \nu \frac{\partial^2 F}{R^2 \partial \theta^2} \right) - w\end{aligned}\quad [124]$$

APPENDIX F

DETERMINATION OF THE MODULUS OF ELASTICITY FOR CYLINDER BR-4B

Young's modulus for the test cylinder was determined by measuring the deflections under concentrated loading of a ring taken from one end of the cylinder. Although not in common practice, this method has certain advantages. One is that relatively large elastic deflections can be produced which are easier to measure accurately than, for example, strains in an axially stressed rod. Another advantage is that a larger, and therefore more representative, specimen of the cylinder can be used.

After the test of BR-4B had been completed, the bulkhead ring nearest the damaged portion (Figure 13) was cut from the cylinder and machined to the following dimensions:

$$\begin{aligned} \text{Mean radius (R)} &= 8.196 \text{ in.} \\ \text{Depth (d)} &= 0.3585 \text{ in.} \\ \text{Width (b)} &= 0.7494 \text{ in.} \end{aligned}$$

The ring was placed vertically between the heads of a universal testing machine and was set in position by an initial compressive load of 50 lb. The load was then increased in 50-lb increments up to 350 lb while the shortening of the vertical diameter of the ring was measured with a dial indicator. The ring was unloaded in the same manner. Two such runs were made and, in each case, measurements during loading and unloading agreed within 0.002 in. The results of the test are shown graphically in Figure 21.

According to Reference 44, for a ring of rectangular cross section, the change Δ in the diameter produced by the load P can be expressed as follows:

$$\Delta = \frac{PR^2}{Ebdc} \left\{ \left(1 - \frac{c}{R}\right) \left[\frac{\pi}{4} - \frac{2}{\pi} \left(1 - \frac{c}{R}\right) \right] + \frac{3\pi}{4} (1+\nu) \frac{c}{R} \right\} \quad [125]$$

$$c = \frac{d^2}{12R} \left[1 + \frac{1}{15} \left(\frac{d}{R}\right)^2 \right]$$

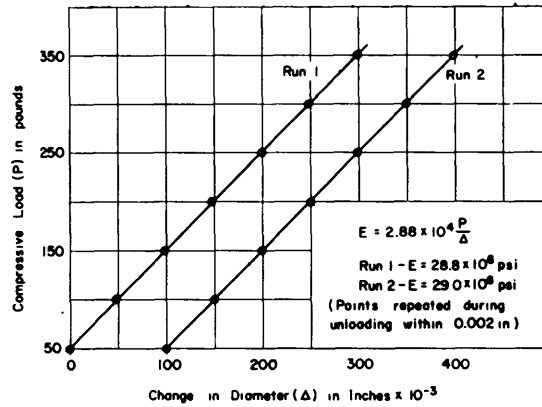


Figure 21 - Determination of Young's Modulus for BR-4B
(Response of Ring to Diametral Loading)

The equation is applicable to thick rings and accounts for direct and shear stresses as well as bending effects. For the ring in question, the result is

$$E = 2.88 \times 10^4 \frac{P}{\Delta} \quad [126]$$

From the slopes of the plots of Figure 21, the values for E in pounds per square inch were 28.8×10^6 and 29.0×10^6 . An average value of 28.9×10^6 psi was thereby determined.

REFERENCES

1. Kendrick, S., "The Buckling under External Pressure of Circular Cylindrical Shells with Evenly Spaced, Equal Strength Circular Ring Frames - Part I," Naval Construction Research Establishment Report NCRE/R.211 (Feb 1953).
2. Kendrick, S., "The Buckling under External Pressure of Circular Cylindrical Shells with Evenly Spaced, Equal Strength Circular Ring Frames - Part II," Naval Construction Research Establishment Report NCRE/R.243 (Sep 1953).
3. Kendrick, S., "The Buckling under External Pressure of Circular Cylindrical Shells with Evenly Spaced, Equal Strength Circular Ring Frames - Part III," Naval Construction Research Establishment Report NCRE/R.244 (Sep 1953).
4. Galletly, G.D., et al., "General Instability of Ring-Stiffened Cylindrical Shells Subject to External Hydrostatic Pressure - A Comparison of Theory and Experiment," Journal of Applied Mechanics, Vol. 25; Transactions, American Society of Mechanical Engineers, Vol. 80 (Jun 1958) pp. 259-266.
5. Reynolds, T.E., "General Instability of Ring-Stiffened Cylindrical Shells Subject to External Hydrostatic Pressure," David Taylor Model Basin Report C-841 (Jun 1957) CONFIDENTIAL.
6. Reynolds, T.E. and Blumenberg, W.F., "General Instability of Ring-Stiffened Cylindrical Shells Subject to External Hydrostatic Pressure," David Taylor Model Basin Report 1324 (Jun 1959).
7. Salerno, V.L. and Levine, B., "General Instability of Reinforced Shells under Hydrostatic Pressure," Polytechnic Institute of Brooklyn Report No. 189 (Sep 1951).
8. Southwell, R.V., "On the Collapse of Tubes by External Pressure," Philosophical Magazine, Part I, Vol. 25 (May 1913), pp. 687-698; Part II, Vol. 26 (Sep 1913), pp. 502-511; Part III, Vol. 29 (Jan 1915), pp. 66-67.
9. Von Mises, R., "The Critical External Pressure of Cylindrical

Tubes" (Der kritische Aussendruck zylindrischer Rohre), VDI-Zeitschrift, Vol. 58, No. 19 (1914), pp. 750-755; David Taylor Model Basin Translation 5 (Aug 1931).

10. Von Mises, R., "The Critical External Pressure of Cylindrical Tubes under Uniform Radial and Axial Load" (Der kritische Aussendruck für allseits belastete zylindrische Rohre), Stodolas Feschrift, Zurich (1929), pp. 418-430; David Taylor Model Basin Translation 6 (Aug 1933).

11. Tokugawa, T., "Model Experiments on the Elastic Stability of Closed and Cross-Stiffened Circular Cylinders under Uniform External Pressure," Proceedings World Engineering Congress, Tokyo, Vol. 29 (1929), pp. 249-279.

12. Von Sanden, K. and Tölke, F., "On Stability Problems in Thin Cylindrical Shells" (Über Stabilitätsprobleme dünner, Kreiszyklindrischer Schalen), Ingenieur-Archiv, Vol. 3 (1932), pp. 24-66; David Taylor Model Basin Translation 33 (Dec 1949).

13. Salerno, V.L. and Levine, B., "Buckling of Circular Cylindrical Shells with Evenly Spaced, Equal Strength Circular Ring Frames, Part I," Polytechnic Institute of Brooklyn Report No. 167 (1950).

14. Salerno, V.L. and Levine, B., "Buckling of Circular Cylindrical Shells with Evenly Spaced, Equal Strength Circular Ring Frames, Part II," Polytechnic Institute of Brooklyn Report No. 169 (1950).

15. Sturm, R.G., "A Study of the Collapsing Pressure of Thin-Walled Cylinders," University of Illinois Engineering Experiment Station Bulletin No. 329 (1941).

16. Nash, W.A., "Buckling of Multi-Bay Ring-Reinforced Cylindrical Shells Subject to Hydrostatic Pressure," Journal of Applied Mechanics, Vol. 20, No. 4 (Dec 1953), pp. 469-474. Also David Taylor Model Basin Report 785 (Apr 1954).

17. Donnell, L.H., "Effect of Imperfections on Buckling of Thin Cylinders under External Pressure," Journal of Applied Mechanics, Vol. 23 (Dec 1956), p. 569.

18. Donnell, L.H., "Effect of Imperfections on Buckling of Thin Cylinders under External Pressure," Final Report on Second Phase of Contract No. Nonr-1406(01), Illinois Institute of Technology (Feb 1957).

19. Langhaar, H.L. and Boresi, A.P., "Buckling and Post-Buckling Behavior of a Cylindrical Shell Subjected to External Pressure," University of Illinois, T. & A.M. Report No. 93 (Apr 1956).

20. Kempner, J. and Crouzet-Pascal, J., "Post-Buckling Behavior of Circular Cylindrical Shells under Hydrostatic Pressure," Polytechnic Institute of Brooklyn Report No. 343 (Jan 1956).

21. Kirstein, A.F. and Wenk, E., Jr., "Observations of Snap-Through Action in Thin Cylindrical Shells under External Pressure," David Taylor Model Basin Report 1062 (Nov 1956).

22. Bodner, S.R. and Berks, W., "The Effect of Imperfections on the Stresses in a Circular Cylindrical Shell under Hydrostatic Pressure," Polytechnic Institute of Brooklyn Report No. 210 (Dec 1952).

23. Galletly, G.D. and Bart, R., "Effects of Boundary Conditions and Initial Out-of-Roundness on the Strength of Thin-Walled Cylinders Subject to External Hydrostatic Pressure," David Taylor Model Basin Report 1066 (Nov 1957).

24. Gerard, G., "Compressive and Torsional Buckling of Thin-Wall Cylinders in Yield Region," National Advisory Committee for Aeronautics Technical Note 3726 (Aug 1956).

25. Gerard, G., "Plastic Stability Theory of Stiffened Cylinders under Hydrostatic Pressure," New York University Technical Report SM 61-13 (Oct 1961).

26. Lurchick, M.E., "Plastic Axisymmetric Buckling of Ring-Stiffened Cylindrical Shells Fabricated from Strain-Hardening Materials and Subjected to External Hydrostatic Pressure," David Taylor Model Basin Report 1393 (Jan 1961).

27. Nott, J.A., "Investigation on the Influence of Stiffener Size on the Buckling Pressures of Circular Cylindrical Shells under Hydrostatic Pressure," David Taylor Model Basin Report 1600 (Dec 1961).

28. Reynolds, T.E., "Inelastic Lobar Buckling of Cylindrical Shells under External Hydrostatic Pressure," David Taylor Model Basin Report 1392 (Aug 1960).

29. Windenburg, D.F. and Trilling, C., "Collapse by Instability of Thin Cylindrical Shells under External Pressure," Transactions, American Society of Mechanical Engineers, Vol. 56, No. 11 (1934). Also Experimental Model Basin Report 385 (Jul 1934).

30. Nash, W.A. and Wenk, E., Jr., "Tests of the Elastic Stability of a Ring-Stiffened Cylindrical Shell, Model BR-1 ($\lambda = 1.82$), Subjected to Hydrostatic Pressure," David Taylor Model Basin Report C-439 (Feb 1953) CONFIDENTIAL.

31. Slankard, R.C. and Nash, W.A., "Tests of the Elastic Stability of a Ring-Stiffened Cylindrical Shell, Model BR-5 ($\lambda = 1.705$), Subjected to Hydrostatic Pressure," David Taylor Model Basin Report 822 (May 1953).

32. Von Sanden, K. and Günther, K., "The Strength of Cylindrical Shells, Stiffened by Frames and Bulkheads, under Uniform External Pressure on All Sides" (Über das Festigkeitsproblem Guerversteifter Hohlzylinder unter Allseitig Gleichmässigem Aussendruck), Werft und Reederei, Vol. 1 (1920), No. 8, pp. 163-168, No. 9, pp. 189-198, No. 10, pp. 216-221; Vol. 2, No. 17 (1921), pp. 505-510; David Taylor Model Basin Translation 38 (Mar 1952).

33. Pulos, J.G. and Salerno, V.L., "Axisymmetric Elastic Deformations and Stresses in a Ring-Stiffened, Perfectly Circular Cylindrical Shell under External Hydrostatic Pressure," David Taylor Model Basin Report 1497 (Sep 1961).

34. Timoshenko, S., "Theory of Elastic Stability," McGraw-Hill Book Company, Inc., New York, N.Y. (1936).

35. Nash, W.A., "Buckling of Thin Cylindrical Shells Subject to Hydrostatic Pressure," Journal of the Aeronautical Sciences, Vol. 21 (May 1954), p. 354.

36. Slankard, R.C., "Test of the Elastic Stability of a Ring-Stiffened Cylindrical Shell, Model BR-4 ($\lambda = 1.103$) Subjected to Hydrostatic

Pressure," David Taylor Model Basin Report 876 (Feb 1955).

37. Kirstein, A.F. and Slankard, R.C., "An Experimental Investigation of the Shell-Instability Strength of a Machined, Ring-Stiffened Cylindrical Shell under Hydrostatic Pressure (Model BR-4A)," David Taylor Model Basin Report 997 (Apr 1956).

38. Galletly, G.D. and Reynolds, T.E., "A Simple Extension of Southwell's Method for Determining the Elastic General Instability Pressure of Ring-Stiffened Cylinders Subject to External Hydrostatic Pressure," Proceedings for the Society of Experimental Stress Analysis, Vol. XIII, No. 2 (1956), p. 141. Also David Taylor Model Basin Report 1191 (Feb 1958).

39. Hom, K. and Couch, W.P., "Hydrostatic Tests of Inelastic and Elastic Stability of Ring-Stiffened Cylindrical Shells Machined from Strain-Hardening Steel," David Taylor Model Basin Report 1501 (Dec 1961).

40. Novozhilov, S., "Foundations of the Nonlinear Theory of Elasticity," Graylock Press, Rochester, N.Y. (1953), p. 12.

41. Bleich, F., "Buckling Strength of Metal Structures," McGraw-Hill Book Company, Inc., New York, N.Y. (1952), p. 111.

42. Timoshenko, S., "Theory of Elasticity," McGraw-Hill Book Company, Inc., New York, N.Y. (1934), p. 248.

43. Donnell, L.H., "A New Theory for the Buckling of Thin Cylinders under Axial Compression and Bending," Transactions, American Society of Mechanical Engineers, Vol. 56 (1934), p. 795.

44. Timoshenko, S., "Strength of Materials - Part II," D. van Nostrand Company, Inc., New York, N.Y. (1941), p. 88.

**INTENTIONALLY
BLANK**

INITIAL DISTRIBUTION

Copies	Copies
<p>14 CHBUSHIPS</p> <ul style="list-style-type: none"> 1 Lab Mgt (Code 320) 3 Tech Info (Code 335) 1 Struc Mech, Hull Matl, & Fab (Code 341A) 1 Prelim Des Br (Code 420) 1 Prelim Des Sec (Code 421) 1 Ship Protec (Code 423) 1 Hull Des (Code 440) 1 Struc (Code 443) 2 Sub (Code 525) 1 Hull Arr, Struc, & Preserv (Code 633) 1 Press Ves (Code 651F) <p>2 CHONR</p> <ul style="list-style-type: none"> 1 Struc Mech (Code 439) 1 USW (Code 466) <p>4 CNO</p> <ul style="list-style-type: none"> 1 (Op 07T) 1 (Op 311) 1 (Op 713) 1 (Op 725) <p>10 CDR, ASTIA</p> <ul style="list-style-type: none"> 1 CO & DIR, USNEES 1 CDR, USNRL (2027) 1 CO & DIR, USNUSL 1 CO & DIR, USNEL 1 CDR, USNOTS, China Lake 1 CO, USNUOS 2 NAVSHIPYD PTSMH 2 NAVSHIPYD MARE 1 NAVSHIPYD CHASN 1 SUPSHIP, Groton 1 EB Div, Gen Dyn Corp 1 SUPSHIP, Newport News 1 NNSB & DD Co 1 SUPSHIP, Pascagoula 1 Ingalls Shipbldg Corp 1 SUPSHIP, Camden 1 NY Shipbldg Corp 	<ul style="list-style-type: none"> 1 SUPSHIP, Quincy 1 DIR, DEF R and E, Attn: Tech Lib 1 CO, USNROTC & NAVADMINU, MIT 1 O in C, PGSCOL, Webb 1 DIR, APL, Univ of Washington, Seattle 1 NAS, Attn: Comm on Undersea Warfare 1 Prof J. Kempner, Polytech Inst of Bklyn 1 Prof G. Gerard, N.Y. Univ 1 Dr. E. Wenk, Jr, The White House 1 Dr. R. DeHart, SRI 1 Mr. L.P. Zick, Chic, Bridge & Iron Co, Chicago 1 Dean V.L. Salerno, Fairleigh Dickinson Univ 1 Prof E.O. Waters, Yale Univ 1 Mr. C.F. Larson, Sec'y, Welding Research Council 1 Mr. A.F. Kirstein, NBS 1 Dr. W.A. Nash, Univ of Florida 1 Prof H.L. Langhaar, Univ of Illinois 1 Prof P.P. Bijlaard, Cornell Univ 1 Dr. R.G. Sturm, 1245 Scott Ave, Chicago Heights, Ill 1 Dr. J. Walsh, WHOI

ERRATA

for

David Taylor Model Basin Report 1614, September 1962



Page 38, Equation [48]. Change six signs marked with arrow from plus (+) to minus (-).

$$\begin{aligned}
 \Delta U_T = & \frac{EhR}{2(1-\nu^2)} \int_0^{2L_f} \int_0^{2\pi} \left[u_x^2 + \left(\frac{w+v_\theta}{R} \right)^2 + 2\nu u_x \left(\frac{w+v_\theta}{R} \right) + \left(\frac{1-\nu}{2} \right) \left(v_x + \frac{u_\theta}{R} \right)^2 \right] dx d\theta \\
 & + \frac{Eh^3}{24R(1-\nu^2)} \int_0^{2L_f} \int_0^{2\pi} \left[R^2 w_{xx}^2 + \left(\frac{w_{\theta\theta} + v_\theta}{R} \right)^2 + 2\nu w_{xx} (w_{\theta\theta} + v_\theta) \right. \\
 & \quad \left. + \left(\frac{1-\nu}{2} \right) (2w_{x\theta} + v_x)^2 \right] dx d\theta \\
 & + \frac{EhR}{2(1-\nu^2)} \int_0^{2L_f} \int_0^{2\pi} \left\{ \bar{w} \left[\frac{u_\theta^2}{R^2} + \left(\frac{w_\theta + v}{R} \right)^2 + \nu (w_x^2 + v_x^2) - (1-\nu) \frac{u_\theta}{R} \left(v_x + \frac{u_\theta}{R} \right) \right] \right. \\
 & \quad \left. + \bar{w}_x \left[2\nu w_x \left(\frac{w+v_\theta}{R} \right) + (1-\nu) \left(\frac{w_\theta + v}{R} \right) \left(v_x + \frac{u_\theta}{R} \right) + 2u_x w_x \right] \right. \\
 & \quad \left. + \bar{u}_x \left[v_x^2 + w_x^2 + \nu \left(\frac{u_\theta^2}{R^2} \right) + \nu \left(\frac{w_\theta + v}{R} \right)^2 - (1-\nu) v_x \left(v_x + \frac{u_\theta}{R} \right) \right] \right\} dx d\theta \\
 & - \frac{pR^2}{2} \int_0^{2L_f} \int_0^{2\pi} \left[\frac{2w}{R} + u_x \left(\frac{2w+v_\theta}{R} \right) + \frac{w^2 + v^2}{R^2} + u_x \right] dx d\theta
 \end{aligned}$$

[48]

Corrections made 12/3/63
G. S. D.

Date Due

JAN 25 2006

Lib-26-67

MAR 15 197

APR 27 1977

MAY 5 1981

MAY 7 1982

OCT 7 1986

JAN 7 1987